

Phenomenological Implications of an $SU(5) \times S_4 \times U(1)$ SUSY GUT of Flavour

Maria Dimou^{* a}, Stephen F. King^{† a}, Christoph Luhn^{‡ b}

^a *School of Physics and Astronomy, University of Southampton,
Southampton, SO17 1BJ, United Kingdom*

^b *Theoretische Physik 1, Naturwissenschaftlich-Technische Fakultät,
Universität Siegen, Walter-Flex-Straße 3, 57068 Siegen, Germany*

Abstract

We discuss the characteristic low energy phenomenological implications of an $SU(5)$ Supersymmetric Grand Unified Theory (SUSY GUT) whose flavour structure is controlled by the family symmetry $S_4 \times U(1)$, which provides a good description of all quark and lepton masses, mixings as well as CP violation. Although the model closely mimics Minimal Flavour Violation (MFV) as shown in [1], here we focus on the differences. We first present numerical estimates of the low energy mass insertion parameters, including canonical normalisation and renormalisation group running, for well-defined ranges of SUSY parameters and compare the naive model expectations to the numerical scans and the experimental bounds. Our results are then used to estimate the model-specific predictions for Electric Dipole Moments (EDMs), Lepton Flavour Violation (LFV), B and K meson mixing as well as rare B decays. The largest observable deviations from MFV come from the LFV process $\mu \rightarrow e\gamma$ and the electron EDM.

^{*}E-mail: md1e10@soton.ac.uk

[†]E-mail: king@soton.ac.uk

[‡]E-mail: christoph.luhn@uni-siegen.de

Contents

1	Introduction	1
2	Yukawa matrices and SUSY breaking parameters	4
2.1	Yukawa sector	4
2.2	Soft SUSY breaking sector	6
2.3	Mass insertion parameters	7
3	Numerical analysis	8
3.1	Parameter range	8
3.2	Estimates of the low energy mass insertion parameters	13
3.2.1	Up-type quark sector	13
3.2.2	Down-type quark sector	17
3.2.3	Charged lepton sector	21
4	Phenomenological implications	24
4.1	Electron EDM	25
4.2	$BR(\mu \rightarrow e\gamma)$	28
4.3	Meson mixing	32
4.3.1	$B_q - \bar{B}_q$	33
4.3.2	$K - \bar{K}$	39
4.4	$BR(b \rightarrow s\gamma)$	43
4.5	$BR(B_{s,d} \rightarrow \mu^+ \mu^-)$	43
4.6	Neutron and ^{199}Hg EDMs	45
5	Conclusions	48
A	Low energy mass insertion parameters	50
B	Loop functions	57

1 Introduction

The flavour problem has been around for a long time, but only relatively recently has new information been provided in the form of neutrino mass and lepton mixing. Subsequently, a lot of effort has been put into trying to formulate a theory of flavour (for reviews see e.g. [2]) which can account for the observed pattern of fermion masses and mixing, while

providing more accurate predictions for the less well measured (or unmeasured) flavour parameters in the neutrino sector, see e.g. [3].

A possible additional source of experimental information which could shed light on the flavour puzzle would be the observation of rare flavour changing processes at rates beyond that predicted by the Standard Model (SM). Such observations could in principle provide insight into the nature of the theory of flavour beyond the SM. So far, experiment has unfortunately not measured any flavour or CP violation beyond SM expectations. Indeed all data are consistent with the concept of Minimal Flavour Violation (MFV) [4], in which all flavour and CP-violating transitions are governed by the CKM matrix and the only relevant local operators are the ones that are relevant in the SM. Although the formulation of MFV in an effective field theory, involving an approximate $SU(3)^5$ symmetry¹ broken by the Yukawa matrices, allows some new operators which can in principle give significant contributions [8, 9], in all cases, MFV predicts very SM-like flavour and CP violation consistent with observation.

The absence of flavour violation is consistent with the absence of any new physics beyond the SM, such as Supersymmetry (SUSY) which, if softly broken at the TeV scale, would in general imply large deviations from SM flavour and CP violation [10]. For example, SUSY models involve one-loop diagrams that induce Flavour Changing Neutral Current (FCNC) processes such as $b \rightarrow s\gamma$ and $\mu \rightarrow e\gamma$ at rates which are proportional to the mass insertion parameters, i.e. the off-diagonal elements of the scalar mass matrices in the super-CKM (SCKM) basis where the Yukawa matrices are diagonal [10, 11]. Such SUSY contributions are very small in the the Constrained Minimal Supersymmetric Standard Model (CMSSM) where the squark and slepton mass squared matrices are proportional to the unit matrix at the high energy scale and the trilinear A -terms are aligned with the Yukawa matrices, resulting in an (approximate) MFV-like structure at low energy [10]. But there is no convincing theoretical basis for either the CMSSM or MFV. Moreover, in SUSY GUTs, the CMSSM framework while providing suppressed flavour violation, cannot easily control CP violation in the form of Electric Dipole Moments (EDMs) which remains a challenge [10]. However, the real challenge is to justify the assumptions of MFV or the CMSSM, while at the same time providing a realistic explanation of quark and lepton (including neutrino) masses, mixing and CP violation.

Following the discovery of neutrino mass and mixing, there has been an impetus to revisit the flavour problem using a family symmetry of some kind, in particular discrete non-Abelian family symmetry [2]. It was realised that in such models, spontaneous CP and

¹In the framework of Grand Unified Theories (GUTs) it is not possible to implement $SU(3)^5$ symmetry at the GUT scale. However, in GUTs based on $SU(5)$ [5] or Pati-Salam [6], it is certainly possible to introduce an $SU(3)^2$ flavour symmetry, and this has been shown to be sufficient [7].

flavour violation could solve the CP and flavour problems of the SM [12, 13] without any *ad hoc* assumptions about MFV or the CMSSM. The family symmetry that is responsible for the structure of the Yukawa sector will automatically control the soft SUSY breaking sector as long as the SUSY breaking hidden sector respects the family symmetry. This is realised for instance in supergravity induced SUSY breaking.

Considering a SUSY framework, the choice of an $SU(3)$ family symmetry [13, 14] provides a benchmark scenario where flavour and CP violation is controlled by family symmetry. The spontaneous breaking of family and CP symmetry by Vacuum Expectation Values (VEVs) of the so-called flavon fields perturbs the SUSY breaking sector, thereby generating distinct deviations from MFV or the CMSSM. Unfortunately, these signatures which were expected to appear in Run 1 of the LHC [15] did not in fact materialise, and the allowed parameter space has been much reduced [16]. At leading order, the CMSSM is enforced by the $SU(3)$ family symmetry acting on the squark and slepton mass squared matrices. When $SU(3)$ is broken by flavon VEVs, to generate quark and lepton flavour, those flavons appearing in the Kähler potential give important contributions to the kinetic terms, requiring extra canonical normalisation [17]. Since SUSY breaking also originates from the Kähler potential, the flavons also modify the couplings of squarks and sleptons to the fields with SUSY breaking F -terms, where the corrections have a different form to the flavon corrections appearing in the superpotential. All of this occurs at the high scale. Additional flavour violation is generated by renormalisation group (RG) running down to low energy, taking into account the seesaw mechanism [18] and threshold corrections [19].

In this paper we discuss the characteristic low energy phenomenological implications of an $SU(5)$ Supersymmetric Grand Unified Theory (SUSY GUT) whose flavour structure is controlled by the family symmetry $S_4 \times U(1)$, which provides a good description of all quark and lepton masses, mixings as well as CP violation. In a recent paper we showed how MFV emerges approximately in this setup [1]. Assuming a SUSY breaking mechanism which respects the family symmetry, we calculated in full explicit detail the low energy mass insertion parameters in the SCKM basis, including the effects of canonical normalisation and renormalisation group running, showing that the peculiar flavour structure of the model, defined by the small family symmetry $S_4 \times U(1)$, is sufficient to approximately mimic MFV.² However there are important phenomenological differences which can provide tell-tale signatures of the model, and it is the main purpose of this paper to discuss these in detail. In other words, we exploit the low energy mass insertion parameters of the model calculated in [1] to analyse a panoply of rare and flavour changing processes as well as EDMs in both the lepton and quark sectors. The results are quite

²Depending on the implementation of a particular family symmetry, SUSY GUTs of flavour typically realise some approximation of MFV at high as well as low scales [20].

illuminating: while we find only small new effects in B physics, very large effects arise for Lepton Flavour Violation (LFV) and the electron EDM which are therefore predicted to be observed soon.

The layout of the remainder of the paper is as follows. In Section 2 we give a succinct summary of the analytic Yukawa matrices and mass insertion parameters calculated in [1]. In Section 3 we discuss numerical estimates of the low energy mass insertion parameters for ranges of SUSY parameters which are consistent with the bounds from direct searches for squarks and sleptons at LHC Run 1. We compare the naive model expectations to the numerical scans and the experimental bounds. In Section 4 these results are then used to estimate the predictions for EDMs, LFV, B and K meson mixing as well as rare B decays. The largest observable deviations from MFV come from the LFV process $\mu \rightarrow e\gamma$ and the electron EDM. Section 5 concludes the paper.

2 Yukawa matrices and SUSY breaking parameters

In this section, we briefly summarise the GUT scale Yukawa matrices and soft SUSY breaking parameters constructed within the framework of the family symmetry model in [1]. Working in a power expansion of the Wolfenstein parameter $\lambda \approx 0.225$ [21], we present all expressions to Leading Order (LO). The entries of the flavour matrices are generally complex, where the phases are given in terms of two free parameters θ_2^d , θ_3^d , with the exception of the soft trilinear terms whose phases are not identified with the corresponding Yukawa phases but are kept as free parameters, even though their flavour structure is the same as that of the Yukawas. Details on this aspect can be found in [1]. In the present work, we will comment on the consequences of this generalisation where relevant.

2.1 Yukawa sector

The fermion structure was already scrutinised in [22], and we have completed this analysis by including the effects of canonical normalisation. In the basis with canonical kinetic terms, that is after redefining the superfields such that the Kähler metrics are identified with the unit matrix, the Yukawa matrix for the up-type quarks reads

$$Y_{\text{GUT}}^u \approx \begin{pmatrix} y_u \lambda^8 & -\frac{1}{2}k_2 y_c \lambda^8 & -\frac{1}{2}k_4 y_t e^{i(\theta_3^d - \theta_2^d)} \lambda^6 \\ -\frac{1}{2}k_2 y_c \lambda^8 & y_c \lambda^4 & -\frac{1}{2}k_3 y_t e^{-i5\theta_2^d} \lambda^5 \\ -\frac{1}{2}k_4 y_t e^{-i(3\theta_2^d + 2\theta_3^d)} \lambda^6 & -\frac{1}{2}k_3 y_t e^{-i(7\theta_2^d + 3\theta_3^d)} \lambda^5 & y_t \end{pmatrix}, \quad (2.1)$$

where y_f and k_i are real order one coefficients, with the former stemming from the Yukawa part of the superpotential of the theory and the latter from the Kähler potential. In particular, k_2, k_3 and k_4 appear in the non-canonical Kähler metric of the $SU(5)$ **10**-plets, in the (12), (23) and (13) elements, respectively.

The Yukawa matrices for the down-type quarks and charged leptons take the form

$$Y_{\text{GUT}}^d \approx \begin{pmatrix} z_1^d e^{-i\theta_2^d} \lambda^8 & \tilde{x}_2 \lambda^5 & -\tilde{x}_2 e^{i(3\theta_2^d + 2\theta_3^d)} \lambda^5 \\ -\tilde{x}_2 \lambda^5 & y_s e^{-i\theta_2^d} \lambda^4 & -y_s e^{2i(\theta_2^d + \theta_3^d)} \lambda^4 \\ (z_3^d - \frac{K_3}{2} y_b) e^{-i(3\theta_2^d + 2\theta_3^d)} \lambda^6 & (z_2^d - \frac{K_3}{2} y_b) e^{-i(3\theta_2^d + 2\theta_3^d)} \lambda^6 & y_b \lambda^2 \end{pmatrix}, \quad (2.2)$$

$$Y_{\text{GUT}}^e \approx \begin{pmatrix} -3z_1^d e^{-i\theta_2^d} \lambda^8 & -\tilde{x}_2 \lambda^5 & (z_3^d - \frac{K_3}{2} y_b) \lambda^6 \\ \tilde{x}_2 \lambda^5 & -3e^{-i\theta_2^d} y_s \lambda^4 & (z_2^d - \frac{K_3}{2} y_b) \lambda^6 \\ -\tilde{x}_2 \lambda^5 & 3e^{-i\theta_2^d} y_s \lambda^4 & y_b \lambda^2 \end{pmatrix}. \quad (2.3)$$

Again, these expressions are given in the canonical basis and all coefficients are real and of order one. \tilde{x}_2, y_f and z_i^d arise from the superpotential operators and K_3 from the Kähler potential, where it enters symmetrically in all off-diagonal elements of the non-canonical Kähler metric of the $SU(5)$ **5**-plets.

Finally, the Dirac neutrino Yukawa matrix in the canonical basis is given by

$$Y^\nu \approx \begin{pmatrix} y_D & -\frac{y_D(K_3 + K_3^N)}{2} \lambda^4 & \left(z_1^D - \frac{y_D(K_3 + K_3^N)}{2}\right) \lambda^4 \\ -\frac{y_D(K_3 + K_3^N)}{2} \lambda^4 & \left(z_1^D - \frac{y_D(K_3 + K_3^N)}{2}\right) \lambda^4 & y_D \\ \left(z_1^D - \frac{y_D(K_3 + K_3^N)}{2}\right) \lambda^4 & y_D & -\frac{y_D(K_3 + K_3^N)}{2} \lambda^4 \end{pmatrix}, \quad (2.4)$$

which is real up to LO in λ . The parameters y_D and z_1^D originate from the superpotential, while K_3^N is associated to the Kähler metric of the right-handed neutrinos. Note that this metric is identical to that of the $SU(5)$ **5**-plets, up to renaming the order one coefficients, see [1] for details.

Transforming the left- and right-handed superfields $f_{L,R}$ by unitary matrices $U_{L,R}^f$, we obtain the canonically normalised diagonal and positive Yukawas in the SCKM basis

$$\tilde{Y}_{\text{GUT}}^u \approx \begin{pmatrix} y_u \lambda^8 & 0 & 0 \\ 0 & y_c \lambda^4 & 0 \\ 0 & 0 & y_t \end{pmatrix}, \quad \tilde{Y}_{\text{GUT}}^d \approx \begin{pmatrix} \frac{\tilde{x}_2^2}{y_s} \lambda^6 & 0 & 0 \\ 0 & y_s \lambda^4 & 0 \\ 0 & 0 & y_b \lambda^2 \end{pmatrix}, \quad (2.5)$$

$$\tilde{Y}_{\text{GUT}}^e \approx \begin{pmatrix} \frac{\tilde{x}_2^2}{3y_s} \lambda^6 & 0 & 0 \\ 0 & 3y_s \lambda^4 & 0 \\ 0 & 0 & y_b \lambda^2 \end{pmatrix}. \quad (2.6)$$

Up to phase convention, the CKM matrix is given by $V_{\text{CKM}_{\text{GUT}}} = (U_L^u)^T U_L^{d*}$, leading to the mixing angles

$$\sin(\theta_{13}^q)_{\text{GUT}} \approx \frac{\tilde{x}_2}{y_b} \lambda^3, \quad \tan(\theta_{23}^q)_{\text{GUT}} \approx \frac{y_s}{y_b} \lambda^2, \quad \tan(\theta_{12}^q)_{\text{GUT}} \approx \frac{\tilde{x}_2}{y_s} \lambda. \quad (2.7)$$

The mixing arises purely from the down-type quark sector and incorporates the Gatto-Sartori-Tonin relation [23] $\theta_{12}^q \approx \sqrt{m_d/m_s}$. The amount of CP violation is given by the Jarlskog invariant [24]

$$J_{\text{CP}_{\text{GUT}}}^q \approx \lambda^7 \frac{\tilde{x}_2^3}{y_b^2 y_s} \sin \theta_2^d. \quad (2.8)$$

These results are in agreement with the LO expressions derived in [22], where canonical normalisation effects were ignored. As discussed in [1], the LO results for the quark and charged lepton masses and mixing angles remain unaffected by the process of canonicalising the kinetic terms. We point out that these 13 observables of the charged fermion sector are given in terms of only 8 input parameters (λ , $y_{u,c,t}$, $y_{s,b}$, \tilde{x}_2 and θ_2^d) at LO.

2.2 Soft SUSY breaking sector

The soft trilinear A -terms and the Yukawa couplings originate in the same superpotential terms. Hence, they have a similar flavour structure and, in the basis of canonical kinetic terms, the soft flavour matrices A_{GUT}^f/A_0 , where A_0 denotes the scale of the trilinear terms, can be deduced from Eqs. (2.1-2.4) by simply replacing $y_u \rightarrow a_u e^{i(\theta_u^a - \theta_u^y)}$, $y_c \rightarrow a_c e^{i(\theta_c^a - \theta_c^y)}$, $y_t \rightarrow a_t$, $y_s \rightarrow a_s e^{i(\theta_s^a - \theta_s^y)}$, $y_b \rightarrow a_b e^{i(\theta_b^a - \theta_b^y)}$, $\tilde{x}_2 \rightarrow \tilde{x}_2^a e^{i(\theta_2^{\tilde{x}_a} - \theta_2^{\tilde{x}})}$, $z_i^f \rightarrow z_i^{fa} e^{i(\theta_i^{\tilde{z}fa} - \theta_i^{\tilde{z}f})}$ and $y_D \rightarrow \alpha_D$. Here, the Yukawa phases are all given in terms of θ_2^d , θ_3^d as follows: $\theta_u^y = \theta_c^y = \theta_s^y = \theta_1^{zd} = 2\theta_2^d + 3\theta_3^d$, $\theta_b^y = \theta_2^{zd} = \theta_3^{zd} = \theta_3^d$ and $\theta_2^{\tilde{x}} = 3(\theta_2^d + \theta_3^d)$. On the other hand, the trilinear phases θ_f^a , $\theta_2^{\tilde{x}_a}$, $\theta_i^{\tilde{z}fa}$ are kept free.

Turning to the soft scalar mass squared matrices in the canonical basis, we find

$$\frac{M_{T_{\text{GUT}}}^2}{m_0^2} \approx \begin{pmatrix} b_{01} & (b_2 - b_{01}k_2)\lambda^4 & e^{i(\theta_2^d - \theta_3^d)}(b_4 - \frac{k_4(b_{01}+b_{02})}{2})\lambda^6 \\ \cdot & b_{01} & e^{5i\theta_2^d}(b_3 - \frac{k_3(b_{01}+b_{02})}{2})\lambda^5 \\ \cdot & \cdot & b_{02} \end{pmatrix}, \quad (2.9)$$

for the $SU(5)$ **10**-plets as well as

$$\frac{M_{F(N)_{\text{GUT}}}^2}{m_0^2} \approx \begin{pmatrix} B_0^{(N)} & (B_3^{(N)} - K_3^{(N)})\lambda^4 & (B_3^{(N)} - K_3^{(N)})\lambda^4 \\ \cdot & B_0^{(N)} & (B_3^{(N)} - K_3^{(N)})\lambda^4 \\ \cdot & \cdot & B_0^{(N)} \end{pmatrix}, \quad (2.10)$$

for the $SU(5)$ **5**-plets and the right-handed neutrinos, with the latter being associated to the coefficients with index N . For convenience, we absorb the universal order one parameter B_0 on the diagonal into the soft SUSY breaking mass m_0 , so that the leading contribution to the diagonal entries of $M_{F_{\text{GUT}}}^2/m_0^2$ is one.

2.3 Mass insertion parameters

In order to study the phenomenological implications of the soft SUSY breaking sector, it is useful to rotate all quantities into the physical basis where the Yukawa matrices are diagonal and positive, i.e. the SCKM basis. Any misalignment between the fermion and sfermion flavour matrices constitutes a source of flavour violation, with the off-diagonal entries of the sfermionic mass matrices contributing to FCNCs. The sfermion mass matrices are given as

$$m_{\tilde{f}_{LL}}^2 = (\tilde{m}_f^2)_{LL} + \tilde{Y}_f \tilde{Y}_f^\dagger v_{u,d}^2, \quad m_{\tilde{f}_{RR}}^2 = (\tilde{m}_f^2)_{RR} + \tilde{Y}_f^\dagger \tilde{Y}_f v_{u,d}^2, \quad m_{\tilde{f}_{LR}}^2 = \tilde{A}_f v_{u,d} - \mu \tilde{Y}_f v_{d,u}, \quad (2.11)$$

where \tilde{m}_f^2 and \tilde{A}_f denote the soft flavour matrices in the SCKM basis, and \tilde{Y}_f are the diagonal Yukawa matrices. μ is the (real) higgsino mass parameter, and the VEVs of the two neutral Higgses are defined as

$$v_u = \frac{v}{\sqrt{1+t_\beta^2}} t_\beta, \quad v_d = \frac{v}{\sqrt{1+t_\beta^2}}, \quad (2.12)$$

where $t_\beta \equiv \tan \beta = \frac{v_u}{v_d}$ and $v = \sqrt{v_u^2 + v_d^2} = 174$ GeV. The indices L and R refer to the chirality of the corresponding SM fermions and $m_{\tilde{f}_{RL}}^2 \equiv (m_{\tilde{f}_{LR}}^2)^\dagger$. With these definitions, the amount of flavour violation can be measured in terms of the dimensionless mass insertion parameters [11]

$$(\delta_{LL}^f)_{ij} = \frac{(m_{\tilde{f}_{LL}}^2)_{ij}}{\langle m_{\tilde{f}}^2 \rangle_{LL}^2}, \quad (\delta_{RR}^f)_{ij} = \frac{(m_{\tilde{f}_{RR}}^2)_{ij}}{\langle m_{\tilde{f}}^2 \rangle_{RR}^2}, \quad (\delta_{LR}^f)_{ij} = \frac{(m_{\tilde{f}_{LR}}^2)_{ij}}{\langle m_{\tilde{f}}^2 \rangle_{LR}^2}, \quad (2.13)$$

where the average masses in the denominators are defined by

$$\langle m_{\tilde{f}}^2 \rangle_{AB}^2 = \sqrt{(m_{\tilde{f}_{AA}}^2)_{ii} (m_{\tilde{f}_{BB}}^2)_{jj}}. \quad (2.14)$$

We mention in passing that the phase structure of the mass insertion parameters depends on the choice of the phase conventions of the CKM and PMNS matrices. In [1], we have worked out the expressions in Eq. (2.13) explicitly for our model at the GUT scale,

choosing a phase convention in which V_{CKM} and U_{PMNS} take their standard form.

The effects of RG running down to the low energy scales where experiments are performed were also estimated, using the leading logarithmic approximation. Introducing the parameters

$$\eta = \frac{1}{16\pi^2} \ln \left(\frac{M_{\text{GUT}}}{M_{\text{low}}} \right), \quad \eta_N = \frac{1}{16\pi^2} \ln \left(\frac{M_{\text{GUT}}}{M_R} \right), \quad (2.15)$$

we performed a two-stage running (*i*) from M_{GUT} to M_R , where the right-handed neutrinos are integrated out, and (*ii*) from M_R to $M_{\text{SUSY}} \sim M_W \equiv M_{\text{low}}$. For $M_{\text{GUT}} \approx 2 \times 10^{16}$ GeV, $M_R \approx 10^{14}$ GeV and $M_{\text{low}} \approx 10^3$ GeV, $\eta \approx 0.19$ is of the order of our expansion parameter $\lambda \approx 0.22$ and $\eta_N \approx 0.03$. In terms of their λ -suppression, the resulting flavour structures of the low energy mass insertion parameters δ read

$$\delta_{LL}^u \sim \begin{pmatrix} 1 & \lambda^4 & \lambda^6 \\ \cdot & 1 & \lambda^5 \\ \cdot & \cdot & 1 \end{pmatrix}, \quad \delta_{RR}^u \sim \begin{pmatrix} 1 & \lambda^4 & \lambda^6 \\ \cdot & 1 & \lambda^5 \\ \cdot & \cdot & 1 \end{pmatrix}, \quad \delta_{LR}^u \sim \begin{pmatrix} \lambda^8 & 0 & \lambda^7 \\ 0 & \lambda^4 & \lambda^6 \\ 0 & \lambda^7 & 1 \end{pmatrix}, \quad (2.16)$$

$$\delta_{LL}^d \sim \begin{pmatrix} 1 & \lambda^3 & \lambda^4 \\ \cdot & 1 & \lambda^2 \\ \cdot & \cdot & 1 \end{pmatrix}, \quad \delta_{RR}^d \sim \begin{pmatrix} 1 & \lambda^4 & \lambda^4 \\ \cdot & 1 & \lambda^4 \\ \cdot & \cdot & 1 \end{pmatrix}, \quad \delta_{LR}^d \sim \begin{pmatrix} \lambda^6 & \lambda^5 & \lambda^5 \\ \lambda^5 & \lambda^4 & \lambda^4 \\ \lambda^6 & \lambda^6 & \lambda^2 \end{pmatrix}, \quad (2.17)$$

$$\delta_{LL}^e \sim \begin{pmatrix} 1 & \lambda^4 & \lambda^4 \\ \cdot & 1 & \lambda^4 \\ \cdot & \cdot & 1 \end{pmatrix}, \quad \delta_{RR}^e \sim \begin{pmatrix} 1 & \lambda^3 & \lambda^4 \\ \cdot & 1 & \lambda^2 \\ \cdot & \cdot & 1 \end{pmatrix}, \quad \delta_{LR}^e \sim \begin{pmatrix} \lambda^6 & \lambda^5 & \lambda^6 \\ \lambda^5 & \lambda^4 & \lambda^6 \\ \lambda^5 & \lambda^4 & \lambda^2 \end{pmatrix}. \quad (2.18)$$

Appendix A provides the explicit expressions for each entry in terms of the parameters of the model.

3 Numerical analysis

3.1 Parameter range

Numerical results for the running quark and charged lepton masses as well as for the quark mixing angles at the GUT scale can be found in [25]. The matching conditions from the SM to the Minimal Supersymmetric Standard Model (MSSM), imposed at the

SUSY scale, take the form

$$\begin{aligned}
y_{u,c,t}^{\text{SM}} &\approx y_{u,c,t}^{\text{MSSM}} \sin \bar{\beta}, \\
y_{d,s}^{\text{SM}} &\approx (1 + \bar{\eta}_q) y_{d,s}^{\text{MSSM}} \cos \bar{\beta}, \\
y_b^{\text{SM}} &\approx (1 + \bar{\eta}_b) y_b^{\text{MSSM}} \cos \bar{\beta}, \\
y_{e,\mu}^{\text{SM}} &\approx (1 + \bar{\eta}_l) y_{e,\mu}^{\text{MSSM}} \cos \bar{\beta}, \\
y_\tau^{\text{SM}} &\approx y_\tau^{\text{MSSM}} \cos \bar{\beta},
\end{aligned} \tag{3.1}$$

for the singular values of the Yukawa matrices. Similarly, we have for the CKM mixing

$$\theta_{i3}^{q,\text{SM}} \approx \frac{1 + \bar{\eta}_q}{1 + \bar{\eta}_b} \theta_{i3}^{q,\text{MSSM}}, \quad \theta_{12}^{q,\text{SM}} \approx \theta_{12}^{q,\text{MSSM}}, \quad \delta^{q,\text{SM}} \approx \delta^{q,\text{MSSM}}. \tag{3.2}$$

Here

$$\bar{\eta}_q = \eta_q - \eta'_l, \quad \bar{\eta}_b = \eta'_q + \eta_A - \eta'_l, \quad \bar{\eta}_l = \eta_l - \eta'_l, \tag{3.3}$$

represent SUSY radiative threshold corrections that are parametrised by $\eta_i = \epsilon_i \tan \beta$, with explicit expressions for ϵ_i available in [26]. The unprimed η parameters correspond to corrections to the first two generations, the primed ones to the third generation, and the one with index “A” to a correction due to the soft SUSY breaking trilinear terms. The parameter $\bar{\beta}$ follows from the absorption of η'_l into β ,

$$\cos \bar{\beta} \equiv (1 + \eta'_l) \cos \beta, \quad \sin \bar{\beta} \approx \sin \beta, \tag{3.4}$$

with the approximation being valid for $\tan \beta \gtrsim 5$. In the limit where threshold effects for the charged leptons are neglected, $\tan \bar{\beta}$ simply reduces to $\tan \beta$.

Our model predicts $\hat{y}_{b,\tau} = y_b \lambda^2$, where the hat indicates the diagonalised Yukawa sector at the GUT scale. As a consequence, very large values of $\tan \beta$ are excluded, and we only study the parameter space in which $\tan \beta \in [5, 25]$, keeping the value of y_b below four. In order to obtain viable ranges for our Yukawa input parameters, we plot $y_{u,c,t,b}$, $(\tilde{x}_2/y_s)^2$ and $(1 + \bar{\eta}_l)y_s$ against $\tan \bar{\beta}$ using the results for the diagonalised Yukawa sector at the GUT scale provided in [25]. We remark that y_b , y_s and \tilde{x}_2 are extracted from the lepton sector. We fit the resulting curves using the relative uncertainties $\sigma(y_u)/y_u = 31\%$, $\sigma(y_c)/y_c = 3.5\%$, $\sigma(y_t)/y_t = 10\%$, $\sigma(y_b)/y_b = 0.6\%$, see [25]. Concerning y_s and \tilde{x}_2 , we take $\sigma(y_s)/y_s = 10\%$ and $\sigma(\tilde{x}_2)/\tilde{x}_2 = 10\%$, allowing for higher order corrections to the

mass ratios that would reduce the discrepancy between the values of \tilde{x}_2/y_s predicted from the lepton and the quark sectors and maximise the GUT scale value of $(\hat{y}_\mu \hat{y}_d)/(\hat{y}_s \hat{y}_e)$. Due to the implementation of the Georgi-Jarlskog relation [27], it is equal to 9 in our model at LO, while its preferred range is $10.7^{+1.8}_{-0.8}$ [25], which is independent of threshold corrections and also not sensitive to a change of the SUSY scale.

We estimate the low energy Yukawa couplings using the leading logarithmic approximation as described in [1]. Clearly, the resulting low energy Yukawa matrices are only valid up to that approximation. Mindful of such limitations, we obtain

$$\tilde{Y}_{\text{low}}^u \approx \text{Diag} \left[(1 + R_u^y) y_u \lambda^8, (1 + R_u^y) y_c \lambda^4, (1 + R_t^y) y_t \right], \quad (3.5)$$

$$\tilde{Y}_{\text{low}}^d \approx \text{Diag} \left[(1 + R_d^y) \frac{\tilde{x}_2^2}{y_s} \lambda^6, (1 + R_d^y) y_s \lambda^4, (1 + R_b^y) y_b \lambda^2 \right], \quad (3.6)$$

$$\tilde{Y}_{\text{low}}^e \approx \text{Diag} \left[(1 + R_e^y) \frac{\tilde{x}_2^2}{3 y_s} \lambda^6, (1 + R_e^y) 3 y_s \lambda^4, (1 + R_e^y) y_b \lambda^2 \right], \quad (3.7)$$

where the corrections from the RG running are encoded in the parameters R_f^y

$$R_u^y = \eta \left(\frac{46}{5} g_U^2 - 3 y_t^2 \right) - 3 \eta_N y_D^2, \quad R_t^y = R_u^y - 3 \eta y_t^2, \quad (3.8)$$

$$R_d^y = \eta \frac{44}{5} g_U^2, \quad R_b^y = R_d^y - \eta y_t^2, \quad R_e^y = \eta \frac{24}{5} g_U^2 - \eta_N y_D^2. \quad (3.9)$$

Here, $g_U \approx \sqrt{0.52}$ denotes the universal gauge coupling constant at the GUT scale. Our scan produces the following values for the right-hand sides of Eq. (3.1)

$$\begin{aligned} \tilde{Y}_{\text{low}_{11}}^u \sin \bar{\beta} &\in [3.4, 6.9] \times 10^{-6}, \quad \tilde{Y}_{\text{low}_{22}}^u \sin \bar{\beta} \in [2.34, 2.65] \times 10^{-3}, \quad \tilde{Y}_{\text{low}_{33}}^u \sin \bar{\beta} \in [0.77, 0.89], \\ \tilde{Y}_{\text{low}_{11}}^d \cos \bar{\beta} (1 + \bar{\eta}_q) &\in [0.9, 1.6] \times 10^{-5}, \quad \tilde{Y}_{\text{low}_{22}}^d \cos \bar{\beta} (1 + \bar{\eta}_q) \in [2.2, 3.5] \times 10^{-4}, \\ \tilde{Y}_{\text{low}_{33}}^d \cos \bar{\beta} (1 + \bar{\eta}_b) &\in [1.17, 1.6] \times 10^{-2}, \\ \tilde{Y}_{\text{low}_{11}}^e \cos \bar{\beta} (1 + \bar{\eta}_l) &\in [2.4, 3.8] \times 10^{-6}, \quad \tilde{Y}_{\text{low}_{22}}^e \cos \bar{\beta} (1 + \bar{\eta}_l) \in [5.6, 7.7] \times 10^{-4}, \\ \tilde{Y}_{\text{low}_{33}}^e \cos \bar{\beta} &\in [1.06, 1.14] \times 10^{-2}, \end{aligned} \quad (3.10)$$

which have to be compared to the SM values, taken from Table 2 of [25],

$$\begin{aligned}
y_u^{\text{SM}} &\in [3.40, 7.60] \times 10^{-6}, & y_c^{\text{SM}} &\in [2.69, 3.20] \times 10^{-3}, & y_t^{\text{SM}} &\in [0.78, 0.88], \\
y_d^{\text{SM}} &\in [1.15, 1.56] \times 10^{-5}, & y_s^{\text{SM}} &\in [2.29, 2.84] \times 10^{-4}, & y_b^{\text{SM}} &\in [1.21, 1.42] \times 10^{-2}, \\
y_e^{\text{SM}} &\in [2.85, 2.88] \times 10^{-6}, & y_\mu^{\text{SM}} &\in [6.01, 6.08] \times 10^{-4}, & y_\tau^{\text{SM}} &\in [1.02, 1.03] \times 10^{-2}.
\end{aligned} \tag{3.11}$$

The corresponding ranges of the order one input parameters of the Yukawa sector are listed in the first five rows of the first column of Table 1. All other coefficients that are not fixed by this fit, are scanned over the interval $\pm[0.5, 2]$, with the following exceptions: we allow the absolute value of the Dirac neutrino Yukawa coupling y_D to be as small as 0.2 but not larger than 0.6, such that it does not exceed the maximum allowed value of y_t . We also relax the lower bounds on $|\tilde{x}_2^a|$, $|a_s|$ and $|a_u|$ and extend the upper bound on $|a_b|$, such that they are allowed to get the same values as the corresponding Yukawa coefficients. The coefficients c_{H_u} and c_{H_d} of the soft Higgs mass squares,

$$m_{H_{u\text{GUT}}}^2 = c_{H_u} m_0^2, \quad m_{H_{d\text{GUT}}}^2 = c_{H_d} m_0^2, \tag{3.12}$$

are taken to be positive, just like the coefficients b_{01} , b_{02} and $B_0^{(N)}$ of the leading order diagonal elements of the soft scalar mass squared matrices. Phases are generally allowed to take arbitrary values within $[0, 2\pi]$. As mentioned earlier, $\tan \beta$ is varied between 5 and 25. Concerning the CMSSM parameters, we define

$$\alpha_0 \equiv A_0/m_0, \quad x \equiv (M_{1/2}/m_0)^2, \tag{3.13}$$

and scan over $M_{1/2} \in [0.3, 5]$ TeV, $m_0 \in [0.05, 5]$ TeV as well as $\alpha_0 \in [-3, 3]$ in order to avoid charge and colour breaking minima.³

The μ parameter, which we take as real, is given at the electroweak scale by the relation⁴

$$\frac{M_Z^2}{2} = \frac{m_{H_d}^2 + \Sigma_d^d - (m_{H_u}^2 + \Sigma_u^u)t_\beta^2}{t_\beta^2 - 1} - \mu^2, \tag{3.14}$$

where M_Z denotes the Z boson mass [30]. Σ_u^u and Σ_d^d are radiative corrections, with the

³In our numerical scan, we have checked that the potentials are always bounded from below and that the corresponding minima do not break charge or colour [28].

⁴The lack of any evidence for low energy supersymmetry requires a certain amount of cancellation between the terms of Eq. (3.14), see e.g. [29].

Yukawa terms	Range	Soft trilinear terms	Range
\tilde{x}_2, y_s	$[0.2, 1.6]$	\tilde{x}_2^a, a_s	$\pm[0.2, 2]$
y_b	$[0.7, 3.8]$	a_b	$\pm[0.5, 4]$
y_u	$[0.3, 0.6]$	a_u	$\pm[0.3, 2]$
y_c	$[0.5, 0.6]$	a_c	$\pm[0.5, 2]$
y_t	$[0.46, 0.6]$	a_t	
y_D	$\pm[0.2, 0.6]$	α_D	
z_i^f	$\pm[0.5, 2]$	z_i^{fa}	
Kähler metric	Range	Soft mass terms	Range
$k_2, k_3, k_4, K_3^{(N)}$	$\pm[0.5, 2]$	$b_2, b_3, b_4, B_3^{(N)}$	$\pm[0.5, 2]$
		$b_{01}, b_{02}, B_0^{(N)}, c_{H_u}, c_{H_d}$	$[0.5, 2]$
SUSY masses	Range	SUSY ratios	Range
$M_{1/2}$	$[0.3, 5] \text{ TeV}$	$\tan \beta$	$[5, 25]$
m_0	$[0.05, 5] \text{ TeV}$	α_0	$[-3, 3]$

Table 1: Ranges of the input parameters used in our scan.

most important contributions coming from the stops

$$\Sigma_u^u(\tilde{t}_{1,2}) = \frac{3}{16\pi^2} F(m_{\tilde{t}_{1,2}}^2) \left(Y_t^2 - g_Z^2 \mp \frac{A_t^2 - 8g_Z^2 \left(\frac{1}{4} - \frac{2}{3}x_W \right) \Delta_t}{m_{\tilde{t}_2}^2 - m_{\tilde{t}_1}^2} \right), \quad (3.15)$$

$$\Sigma_d^d(\tilde{t}_{1,2}) = \frac{3}{16\pi^2} F(m_{\tilde{t}_{1,2}}^2) \left(g_Z^2 \mp \frac{Y_t^2 \mu^2 + 8g_Z^2 \left(\frac{1}{4} - \frac{2}{3}x_W \right) \Delta_t}{m_{\tilde{t}_2}^2 - m_{\tilde{t}_1}^2} \right). \quad (3.16)$$

In these expressions, Y_t , A_t and μ denote the low energy Yukawa and trilinear couplings and the low energy μ parameter, respectively. Moreover

$$m_{\tilde{t}_{1,2}}^2 = \frac{1}{2} \left(m_{\tilde{t}_{LL}}^2 + m_{\tilde{t}_{RR}}^2 \mp \sqrt{4m_{\tilde{t}_{LR}}^2 + (m_{\tilde{t}_{LL}}^2 - m_{\tilde{t}_{RR}}^2)^2} \right),$$

$$F(m^2) = m^2 \left(\log \left(\frac{m^2}{M_S^2} \right) - 1 \right), \quad \Delta_t = \frac{1}{2} \left(m_{\tilde{t}_{LL}}^2 - m_{\tilde{t}_{RR}}^2 \right) + M_Z^2 \cos(2\beta) \left(\frac{1}{4} - \frac{2}{3}x_W \right),$$

$$x_W = \sin^2 \theta_W, \quad g_Z^2 = \frac{M_Z^2}{4v^2}, \quad M_S = \sqrt{m_{\tilde{t}_1} m_{\tilde{t}_2}}, \quad (3.17)$$

with θ_W denoting the Weinberg angle. $m_{\tilde{t}_{LL}}^2$, $m_{\tilde{t}_{RR}}^2$ and $m_{\tilde{t}_{LR}}^2$ are the low energy (33) elements of the squark mass matrices defined in Eq. (2.11). The so-determined μ param-

eter can then be used to calculate the physical Higgs mass. Adopting the approximate formulas of Section 2.4 of [31], we demand that the resulting Higgs mass lies within the interval [110, 135] GeV. Additionally, we impose cuts on the SUSY parameters from direct searches by requiring that the first and the second generation squark masses are larger than 1.4 TeV.

3.2 Estimates of the low energy mass insertion parameters

In this section, we analyse the predictions for the low energy mass insertion parameters δ whose explicit expressions are given in Appendix A. Tables 2-6 provide naive expectations for the individual δ s, where we take into account the λ -suppression and the main effects of the RG running, while setting any order one coefficients to one. Clearly, we still expect to see a spread within a few orders of magnitude due to the variation of the SUSY scale and the order one coefficients. The third columns of Tables 2-6 list existing experimental bounds. The full ranges of our δ s arising from scanning over the input parameters, given in Table 1, are depicted in Figures 1-3.

3.2.1 Up-type quark sector

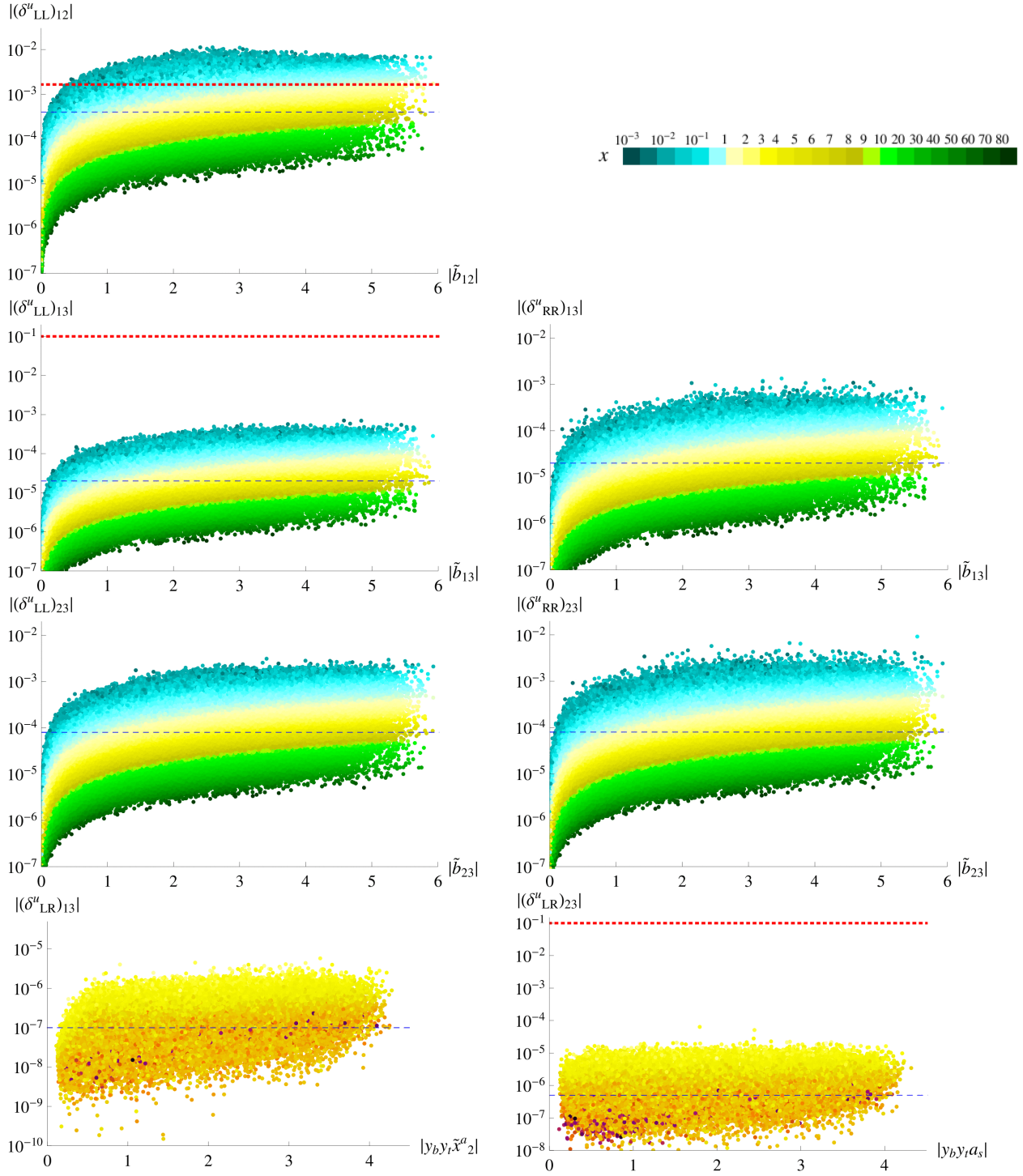
The strongest constraints on the up-type mass insertion parameters involve the (12) sector and stem from $D^0 - \bar{D}^0$ mixing. The SM contribution to this amplitude conserves CP to a good approximation and provides significant constraints on the imaginary parts of $(\delta_{AB}^u)_{12}$, $A, B = L, R$. These limits were derived in [32], assuming equal squark and gluino masses of 1 TeV. We quote them in the third column of Table 2, rescaled to masses of 1.5 TeV. The limits on the RR and RL parameters are identical to the LL and LR ones due to the $L \leftrightarrow R$ symmetric form of the gluino-squark box diagram. The index $LL = RR$ refers to the assumption that $(\delta_{LL}^u)_{12} \approx (\delta_{RR}^u)_{12}$, as is the case in our model. In the second column of Table 2, we give a naive estimate for $\sqrt{|\text{Im}[(\delta_{LL}^u)_{12}^2]|} \approx \sqrt{|\text{Im}[(\delta_{RR}^u)_{12}^2]|} \approx \sqrt{|\text{Im}[(\delta_{LL}^u)_{12}(\delta_{RR}^u)_{12}]|}$. For $\theta_2^d = \pi/2$, as suggested from maximising the Jarlskog invariant of Eq. (2.8), these quantities vanish to LO. Since $\sqrt{|\text{Im}[(\delta_{LL,RR}^u)_{12}^2]|}$ is at most $\sim |(\delta_{LL}^u)_{12}|$, we only show the full range of the absolute value of that parameter in Figure 1, plotted against the corresponding GUT scale coefficient \tilde{b}_{12} , defined in Eq. (A.1). This coefficient quantifies the mismatch between the Kähler metric and the soft mass matrix elements for the $SU(5)$ **10**-plets and can be as large as 6 when the associated parameters contribute constructively and receive their maximum values in the scan. The effects of the RG running are trivial and depend only on $x = (M_{1/2}/m_0)^2$; for $x \approx 1$ and $\tilde{b}_{12} \approx 1$, we estimate a value of around 4×10^{-4} , shown by the blue dashed line in Figure 1. With increasing x , we obtain even smaller values, as the RG suppression is

Parameter	Naive expectation	Exp. bound
$\sqrt{ \text{Im}[(\delta_{LL,RR}^u)_{12}^2] }$	$\mathcal{O}\left(\frac{\sqrt{\sin(2\theta_2^d)}\lambda^4}{1+6.3x} \approx 4 \times 10^{-4} \sqrt{\sin(2\theta_2^d)}\right)$	2.85×10^{-2} [32] $(1.65 \times 10^{-3}) _{LL=RR}$
$\sqrt{ \text{Im}[(\delta_{LR,RL}^u)_{12}^2] }$	0	3.75×10^{-3} [32]
$ (\delta_{LL}^u)_{13} $	$\mathcal{O}\left(\frac{1+\eta\left(\frac{R_q}{1+6.5x}-y_t^2\right)}{1+6.5x}\lambda^6 \approx 2 \times 10^{-5}\right)$	$\mathcal{O}(10^{-1})$ [33]
$ (\delta_{RR}^u)_{13} $	$\mathcal{O}\left(\frac{1+2\eta\left(\frac{R_q}{1+6.15x}-y_t^2\right)}{1+6.15x}\lambda^6 \approx 2 \times 10^{-5}\right)$	
$ (\delta_{LL}^u)_{23} $	$\mathcal{O}\left(\frac{1+\eta\left(\frac{R_q}{1+6.5x}-y_t^2\right)}{1+6.5x}\lambda^5 \approx 8 \times 10^{-5}\right)$	
$ (\delta_{RR}^u)_{23} $	$\mathcal{O}\left(\frac{1+2\eta\left(\frac{R_q}{1+6.15x}-y_t^2\right)}{1+6.15x}\lambda^5 \approx 8 \times 10^{-5}\right)$	
$ (\delta_{LR}^u)_{13} $	$\mathcal{O}\left(\frac{\alpha_0 v_u}{m_0} \frac{2\eta}{(1+6.3x)}\lambda^7 \approx 10^{-7}\right)$	
$ (\delta_{LR}^u)_{23} $	$\mathcal{O}\left(\frac{\alpha_0 v_u}{m_0} \frac{2\eta}{(1+6.3x)}\lambda^6 \approx 5 \times 10^{-7}\right)$	$\mathcal{O}(10^{-1})$ [34]
$ (\delta_{RL}^u)_{13} $	0	
$ (\delta_{RL}^u)_{23} $	$\mathcal{O}\left(\frac{\alpha_0 v_u}{m_0} \frac{1+\eta\left(\frac{46g_U^2}{5}-8y_t^2+\frac{R_q}{1+6.5x}\right)}{1+6.3x}\lambda^7 \approx 5 \times 10^{-7}\right)$	

Table 2: The naive numerical expectations for the low energy up-type mass insertion parameters as extracted from our model (second column), to be compared with experimental bounds in the literature (third column). The full ranges of the δ s are shown in Figure 1. Note that the (12), (21) and (31) δ_{LR}^u parameters remain zero up to order λ^8 .

increased. The red dotted line shows the experimental limit, adapted from [32] and valid for $(\delta_{LL}^u)_{12} \approx (\delta_{RR}^u)_{12}$.

The LL and RR parameters of the $(i3)$ sector ($i = 1, 2$) have GUT scale coefficients with the same range as the parameters of the (12) sector but a different RG suppression due to the milder running of the third generation sfermionic masses. This is represented by the factor ηR_q appearing in Eq. (A.13), where η and R_q are defined in Eqs. (2.15, A.7), respectively. Approximating these δ s as shown in Table 2 and taking $x \approx 1$, $R_q \approx 3y_t^2 + 1$ as well as $y_t \approx 0.5$, we expect $|(\delta_{LL,RR}^u)_{13}| \propto \lambda^6$ and $|(\delta_{LL,RR}^u)_{23}| \propto \lambda^5$ to vary around 2×10^{-5} and 8×10^{-5} , respectively. The existing bounds on these variables from flavour changing effects are very weak, leaving them essentially unconstrained. B_d mixing can place a bound on $|(\delta_{LL}^u)_{13}|$ of the order of 10^{-1} at most, as described in [33].



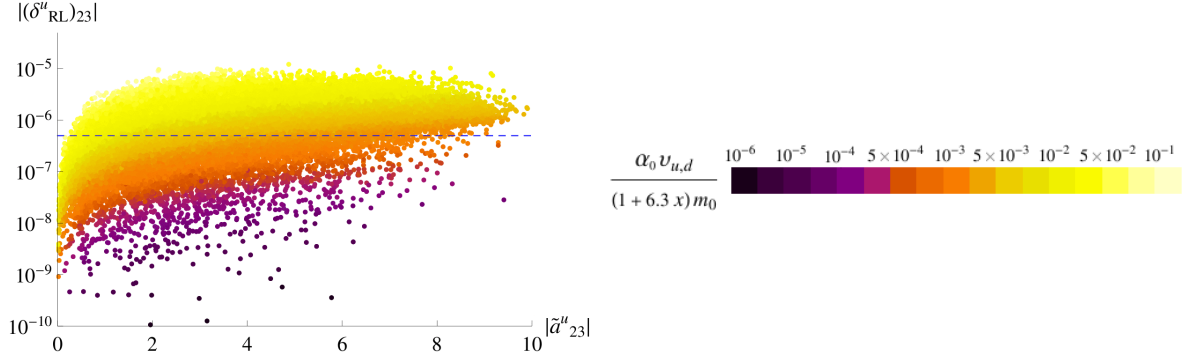


Figure 1: The low energy up-type mass insertion parameters plotted against their GUT scale coefficients, defined in Eqs. (A.1,A.2) [except for $(\delta^u_{LR})_{13,23}$ which are plotted against a coefficient multiplying the RG running contribution, cf. Eqs. (A.26,A.27)]. The blue dashed lines represent our naive numerical expectations according to the second column of Table 2, while the red dotted lines (when available) represent their experimental limits, shown in the third column of Table 2. Since $(\delta^u_{RR})_{12} \approx (\delta^u_{LL})_{12}$, only the LL parameter is plotted. The plots have been produced by scanning over the input parameters listed in Table 1.

The parameters of LR type have a slightly different behaviour. They are proportional to the factor $(\alpha_0 v_u/m_0)$ which, for $|A_0| > 0.5$ TeV, can cause an extra suppression of up to $\mathcal{O}(10^{-3})$. Because of this factor, the LR parameters show a dependence on the mass scale, even at the GUT scale. $(\delta^f_{LR})_{ij}$ are also generally proportional to the mismatch of the ratios of soft trilinear over Yukawa sector coefficients for the i -th and the j -th generation and vanish, barring RG induced corrections, if those are aligned. To estimate the magnitude of these parameters in Table 2, we take $|\alpha_0| v_u/m_0 \approx 10^{-1}$, $x \approx 1$, $y_t \approx 0.5$ and $R_q \approx 1.75$, while their full ranges are shown in Figure 1. The $(\delta^u_{LR})_{13}$ parameter was zero at the GUT scale but receives a contribution through the RG running of the order of $\eta \lambda^7$. Similarly, $(\delta^u_{LR})_{23}$, which was suppressed by λ^7 at the GUT scale, receives a similar running contribution which comes in at an even lower order, namely $\eta \lambda^6$. Such an effect is not found in any other δ parameter. Finally, we remark that $(\delta^u_{LR,RL})_{12}$ as well as $(\delta^u_{RL})_{13}$ are zero up to order λ^8 , where we truncate our expansion.

The limits on the LR parameters of the $(i3)$ sector ($i = 1, 2$) originate mainly from the requirement that the potential be bounded from below with a vacuum that does not break charge or colour [28]. We have already constrained the trilinear parameters accordingly and do not comment on those effects any further. Other bounds on the LR off-diagonal parameters can be deduced by demanding that the supersymmetric radiative corrections to the CKM matrix elements do not exceed their experimental values [35]. The limit for $|(\delta^u_{LR})_{23}|$ quoted in Table 2 has been obtained in [34] by considering chargino loop

Parameter	Naive expectation	Exp. bound
$\sqrt{ \text{Re}[(\delta_{LL}^d)_{12}^2] }$	$\mathcal{O}\left(\frac{1}{1+6.5x}\lambda^3 \approx 2 \times 10^{-3}\right)$	$[6.6 \times 10^{-2}, 3.3 \times 10^{-1}]$
$\sqrt{ \text{Re}[(\delta_{RR}^d)_{12}^2] }$	$\mathcal{O}\left(\frac{\sqrt{\cos(2\theta_2^d)}}{1+6.1x}\lambda^4 \approx 4 \times 10^{-4}\sqrt{\cos(2\theta_2^d)}\right)$	
$\sqrt{ \text{Im}[(\delta_{LL}^d)_{12}^2] }$	$\mathcal{O}\left(\frac{\sqrt{\sin(\theta_2^d)}}{1+6.5x}\lambda^{7/2} \approx 7 \times 10^{-4}\sqrt{\sin(\theta_2^d)}\right)$	$[8.7 \times 10^{-3}, 4.2 \times 10^{-2}]$
$\sqrt{ \text{Im}[(\delta_{RR}^d)_{12}^2] }$	$\mathcal{O}\left(\frac{\sqrt{\sin(2\theta_2^d)}}{1+6.1x}\lambda^4 \approx 4 \times 10^{-4}\sqrt{\sin(2\theta_2^d)}\right)$	
$\sqrt{ \text{Re}[(\delta_{LR(RL)}^d)_{12}^2] }$	$\mathcal{O}\left(\frac{\alpha_0 v_d}{m_0} \frac{1+\eta \frac{44 g_{\tilde{t}l}^2}{5}}{1+6.3x}\lambda^5 \times\right.$	$[7.8, 12] \times 10^{-3}$
$ \text{Im}[(\delta_{LR(RL)}^d)_{12}] $	$\text{Re(Im)}[f(\theta_2^{\tilde{x}a} - \theta_2^{\tilde{x}}, \theta_s^a - \theta_s^y)] \approx 7 \times 10^{-7}$	$[1, 5.7] \times 10^{-4}$

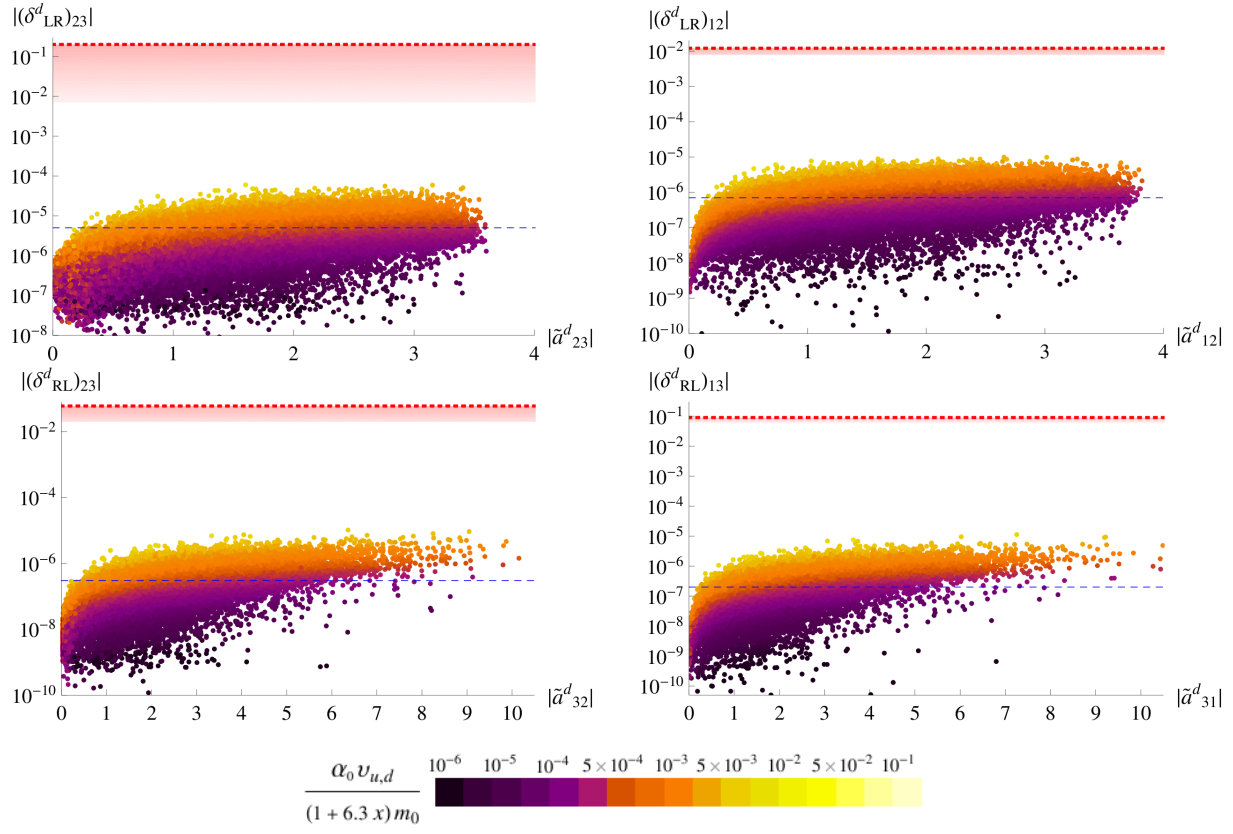
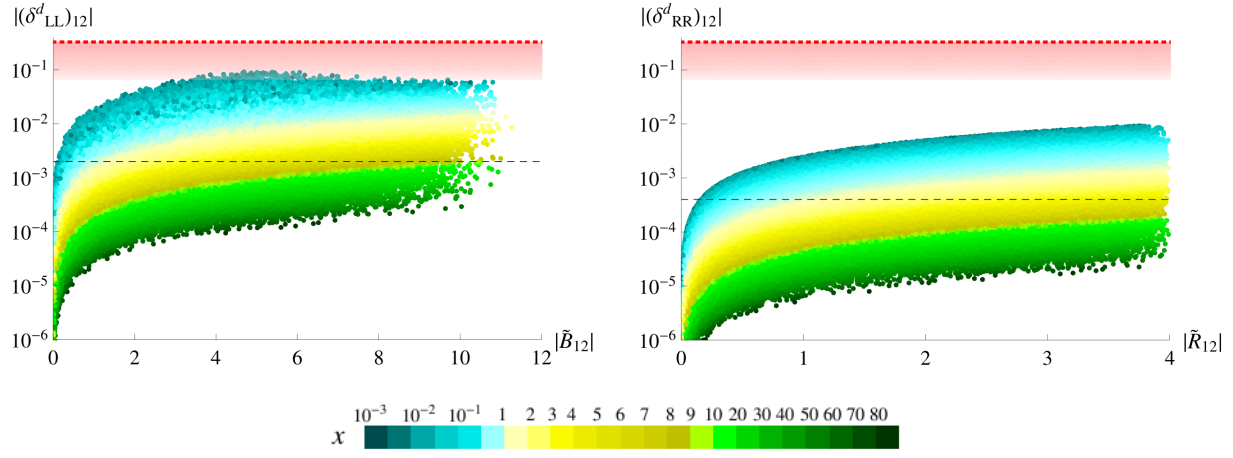
Table 3: The naive expectation for the ranges of $(\delta_{AB}^d)_{12}$, $A, B = L, R$, as extracted from our model (second column), to be compared with experimental bounds from [36] for $m_{\tilde{q}} \approx 1.5$ TeV and $(m_{\tilde{g}}/m_{\tilde{q}})^2 \in [0.3, 4]$ (third column). The full ranges of these δ s as produced in our scan are shown in Figure 2.

contributions to $b \rightarrow sl^+l^-$. In our model, all up-type mass insertion parameters of the LR type turn out to be safely below any current bound.

3.2.2 Down-type quark sector

We first consider the (12) elements of the down-type mass insertion parameters $(\delta_{AB}^d)_{12}$, where $A, B = L, R$. The corresponding bounds are derived from the results of [36] which we have rescaled to $m_{\tilde{q}} \approx 1.5$ TeV and $(m_{\tilde{g}}/m_{\tilde{q}})^2 \in [0.3, 4]$. These bounds are summarised in the third column of Table 3 and have been extracted using observables related to Kaon mixing. They are given separately for the real and imaginary parts due to a relative difference of an order of magnitude.

In our model, $(\delta_{LL}^d)_{12} \sim \lambda^3$ is real at LO, while the next-to-leading order (NLO) contribution is a linear combination of $e^{-i\theta_2^d}$ and $\cos(4\theta_2^d + \theta_3^d)$. Therefore, $\sqrt{|\text{Im}[(\delta_{LL}^d)_{12\text{NLO}}^2]|}$ is proportional to $\sqrt{\sin(\theta_2^d)}\lambda^{7/2}$. Setting $\theta_2^d = \pi/2$, i.e. the value preferred by the Jarlskog invariant J_{CP}^q , we expect $\text{Im}[(\delta_{LL}^d)_{12\text{NLO}}^2]$ to take its maximum value. In Figure 2 we only plot the absolute value of this mass insertion parameter versus its GUT scale coefficient \tilde{B}_{12} , see Eq. (A.1), which can take values between zero and twelve. Our naive numerical estimate of $|(\delta_{LL}^d)_{12}|$, approximated as shown in the second column of Table 3, is of the order of 10^{-3} for $x \approx 1$, visualised by the blue dashed line in Figure 2. Since the experimental limits are given as ranges, we depict them by the red shaded region.



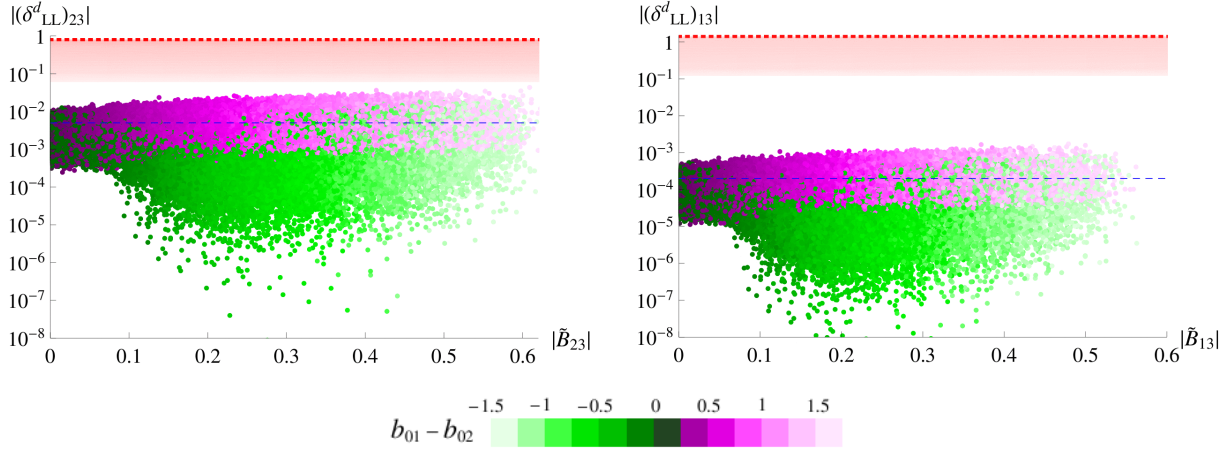


Figure 2: The low energy down-type mass insertion parameters $(\delta_{AB}^d)_{ij}$, $A, B = L, R$, $i = 1, 2, 3$ plotted against their GUT scale coefficients, defined in Eqs. (A.1,A.2). The blue dashed lines represent our naive numerical expectation according to the second columns of Tables 3-5. The red shaded areas cover the parameter space bounded by the limits shown in the third column of the corresponding tables, with the red dotted lines denoting the weakest limit in each case. The absolute values of δ_{RR}^d are equal in the (12),(23) and (13) sectors and also $|(\delta_{LR}^d)_{12}| = |(\delta_{RL}^d)_{12}| = |(\delta_{LR}^d)_{13}|$. We therefore only show the bounds stemming from the (12) sector as they are the strongest ones. All plots have been produced by scanning over the input parameters shown in Table 1.

The parameter $(\delta_{RR}^d)_{12}$ is proportional to $e^{i\theta_2^d}$, so that $\sqrt{|\text{Im}[(\delta_{RR}^d)_{12}^2]|}$ vanishes for $\theta_2^d = \pi/2$, while the corresponding real part is maximised. The RG suppression is again trivial, only depending on x , while the GUT scale δ parameter is proportional to $\tilde{R}_{12} = (B_3 - K_3)$, see Eq. (A.1). When $B_3 = -K_3 = 2$ and $x \ll 1$, the absolute value of the mass insertion reaches its maximum of 10^{-2} , as can be seen in the associated plot in Figure 2. On the other hand, for $B_3 = 0.5$, $K_3 = 1$ and $x \gg 1$, it can scale down to about 10^{-6} . Note that $|(\delta_{RR}^d)_{12}| = |(\delta_{RR}^d)_{23}| = |(\delta_{RR}^d)_{13}|$, as can be seen in Eqs. (A.32,A.33).

The mass insertion parameters $(\delta_{LR}^d)_{12} = -(\delta_{RL}^d)_{12} = (\delta_{LR}^d)_{13}$ receive an extra suppression from the factor $\alpha_0 v_d/m_0$, for which we use the value of 5×10^{-3} in our naive numerical estimates. Then, for $x \approx 1$, we expect these δ parameters to vary around 7×10^{-7} , see the last two rows of Table 3. As can be seen in Figure 2, our model predictions lie well below the limits. Furthermore, if the Yukawa and soft trilinear phase structures are aligned, the phases within \tilde{a}_{12}^d cancel and $(\delta_{LR}^d)_{12}$ becomes real at the given order in λ .

As parts of our parameter space place the down-type mass insertion parameter $|(\delta_{LL}^d)_{12}|$ within a region possibly excluded by Kaon mixing observables, we study the relevant contributions in Section 4 in more detail. Due to additional strong constraints on the

Parameter	Naive expectation	Exp. bound
$ (\delta_{LL}^d)_{23} $	$\mathcal{O}\left(\frac{2\eta R_q}{1+6.5x}\lambda^2 _{b_{01}=b_{02}} \approx 5 \times 10^{-3}\right)$	$[6 \times 10^{-2}, 8 \times 10^{-1}]$
$ (\delta_{RR}^d)_{23} $	$\mathcal{O}\left(\frac{1}{1+6.1x}\lambda^4 \approx 4 \times 10^{-4}\right)$	$[6.3, 9.7] \times 10^{-1}$
$ (\delta_{LR}^d)_{23} $	$\mathcal{O}\left(\frac{\alpha_0 v_d}{m_0} \frac{1+\eta\left(\frac{44 g_U^2}{5} + 2a_t y_t\right)}{1+6.3x} \lambda^4 \approx 5 \times 10^{-6}\right)$	$[7 \times 10^{-3}, 2 \times 10^{-1}]$
$ (\delta_{RL}^d)_{23} $	$\mathcal{O}\left(\frac{\alpha_0 v_d}{m_0} \frac{1+\eta\left(\frac{44 g_U^2}{5} + 2a_t y_t + \frac{R_q}{1+6.5x}\right)}{1+6.3x} \lambda^6 \approx 3 \times 10^{-7}\right)$	$[2, 6] \times 10^{-2}$

Table 4: The naive expectation for the ranges of $(\delta_{AB}^d)_{23}$, $A, B = L, R$, as extracted from our model (second column), to be compared with experimental bounds from [37] (third column). The full ranges of each δ parameter, produced by scanning over the input parameters as shown in Table 1, are plotted in Figure 2.

product of LL and RR mass insertion parameters, we see that actually a large fraction of the parameter space is excluded.

The bounds on $(\delta_{AB}^d)_{23}$, $A, B = L, R$ are related to $b \rightarrow s$ transitions. They are taken from [37] and were derived by demanding that the contribution of each individual mass insertion parameter to the flavour observables $\text{BR}(B \rightarrow X_s \gamma)$, $\text{BR}(B_s \rightarrow \mu^+ \mu^-)$ and ΔM_{B_s} does not exceed the current experimental limits. The analysis was performed for six representative points of the MSSM parameter space which are compatible with LHC SUSY and Higgs searches as well as an explanation of the discrepancy of $(g-2)_\mu$ from its SM value in terms of one-loop SUSY contributions from charginos and neutralinos. We present the extracted bounds in the third column of Table 4, where the intervals arise due to the dependence on the SUSY spectra. We note that, for simplicity, all δ s were assumed to be real in [37].

At the GUT scale, the parameter $(\delta_{LL}^d)_{23} \sim \lambda^2$ is proportional to $(b_{01} - b_{02})$; it can therefore vanish at that order if $b_{02} \rightarrow b_{01}$. In that case, it would still receive a non-zero contribution through the running, as can be seen in Eq. (A.31), through the factor R_q , defined in Eq. (A.7). To see this effect, we expand $(\delta_{LL}^d)_{23}$ to first order in the running parameter η , defined in Eq. (2.15), taking the limit $b_{02} \rightarrow b_{01}$. Then, for $R_q \approx 3y_t^2 + 1$, $y_t \approx 0.5$ and $x \approx 1$, we expect the absolute value of $(\delta_{LL}^d)_{23}$ to vary around 5×10^{-3} for $\tilde{B}_{23} \propto b_{01} - b_{02} \rightarrow 0$, as shown by the blue dashed line in Figure 2. The spread towards smaller values of $(\delta_{LL}^d)_{23}$ as \tilde{B}_{23} deviates from zero, is mainly due to the parameter space where $b_{01} - b_{02}$ is negative, thereby partly cancelling the R_q contribution. As can be seen in Figure 2, all generated points lie below the limits of the corresponding (23) sector.

Parameter	Naive expectation	Exp. bound
$ (\delta_{LL}^d)_{13} $	$\mathcal{O}\left(\frac{2\eta R_q}{1+6.5x}\lambda^4 _{b_{01}=b_{02}} \approx 2 \times 10^{-4}\right)$	$[1.2, 14] \times 10^{-1}$
$ (\delta_{RR}^d)_{13} $	$\mathcal{O}\left(\frac{1}{1+6.1x}\lambda^4 \approx 4 \times 10^{-4}\right)$	
$ (\delta_{LR}^d)_{13} $	$\mathcal{O}\left(\frac{\alpha_0 v_d}{m_0} \frac{1+\eta \frac{44 g_U^2}{5}}{1+6.3x} \lambda^5 \approx 7 \times 10^{-7}\right)$	$[6, 9] \times 10^{-2}$
$ (\delta_{RL}^d)_{13} $	$\mathcal{O}\left(\frac{\alpha_0 v_d}{m_0} \frac{1+\eta \left(\frac{44 g_U^2}{5} + \frac{R_q}{1+6.5x} - y_t^2\right)}{1+6.3x} \lambda^6 \approx 2 \times 10^{-7}\right)$	

Table 5: The naive expectation for the ranges of $(\delta_{AB}^d)_{13}$, $A, B = L, R$, as extracted from our model (second column), to be compared with experimental bounds from [36] for $m_{\tilde{q}} \approx 1$ TeV and $(m_{\tilde{g}}/m_{\tilde{q}})^2 \in [0.25, 4]$ (third column). The full ranges of the δ s as produced in our scan are shown in Figure 2.

The experimental bounds for $(\delta_{AB}^d)_{13}$ are taken from [36], where they were extracted from B_d mixing related observables and given in terms of $|\text{Re}[\delta_{AB}^d]|$ and $|\text{Im}[\delta_{AB}^d]|$. Their orders of magnitude are at most of the same order as $|\delta_{AB}^d|$, and for $m_{\tilde{q}} \approx 1$ TeV and $(m_{\tilde{g}}/m_{\tilde{q}})^2 \in [0.25, 4]$ they are summarised in the third column of Table 5. The limits for the RR and RL type δ s are equal to the LL and LR type ones, respectively, as the gluino contribution to the box diagram for meson mixing is symmetric under $L \leftrightarrow R$.

In our model, we expect $|(\delta_{LL}^d)_{13}|$ to have a similar behaviour as $|(\delta_{LL}^d)_{23}|$ but with an extra suppression of λ^2 . Furthermore, $|(\delta_{LR}^d)_{23}|$ mimics $|(\delta_{LR}^d)_{12}| = |(\delta_{RL}^d)_{12}| = |(\delta_{LR}^d)_{13}|$ with an extra enhancement factor of λ^{-1} . The RL parameters (13) and (23) sectors are of the same order in λ and should therefore have a similar numerical range. All (13) sector mass insertion parameters δ_{AB}^d lie below the limits set by B_d mixing, as can be seen in Figure 2.

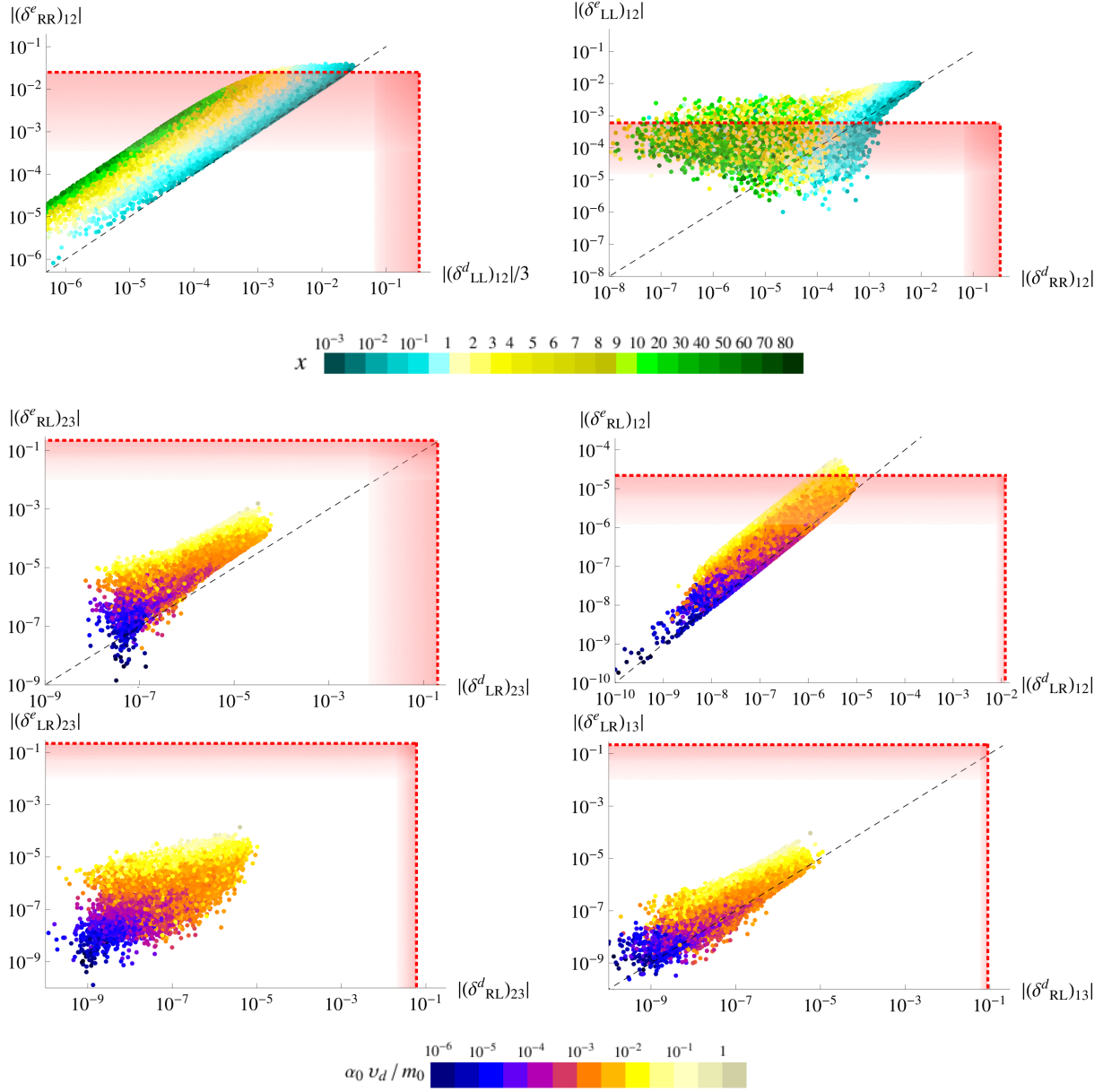
3.2.3 Charged lepton sector

The bounds on the mass insertion parameters $(\delta_{AB}^e)_{ij}$, $A, B = L, R$, of the charged lepton sector are taken from [38]. They were derived by studying radiative, leptonic and semileptonic LFV decays as well as $\mu \rightarrow e$ conversion in heavy nuclei. The analysis was performed for six representative points in the MSSM parameter space, which are in agreement with LHC SUSY and Higgs searches as well as data on $(g-2)_\mu$. Moreover, four additional, more general two-dimensional scenarios, characterised by universal squark and slepton mass scales, were considered in [38]. The derived limits vary within an order of magnitude in all cases and are summarised in the third column of Table 6. We note that all δ s were assumed to be real in [38] for simplicity.

Parameter	Naive expectation	Exp. bound
$ (\delta_{LL}^e)_{12} $	$\mathcal{O}\left(\frac{2R_l\eta_N}{1+0.5x}\lambda^4 _{B_3=K_3}\approx 2\times 10^{-4}\right)$	$[1.5, 60]\times 10^{-5}$
$ (\delta_{LL}^e)_{23,13} $		$[0.7, 35]\times 10^{-2}$
$ (\delta_{RR}^e)_{12} $	$\mathcal{O}\left(\frac{\lambda^3}{1+0.15x}\approx 10^{-2}\right)$	$[0.35, 25]\times 10^{-3}$
$ (\delta_{RR}^e)_{23} $	$\mathcal{O}\left(\frac{\lambda^2}{1+0.15x}\approx 4\times 10^{-2}\right)$	$[2, 10]\times 10^{-1}$
$ (\delta_{RR}^e)_{13} $		
$ (\delta_{LR(RL)}^e)_{12} $	$\mathcal{O}\left(\frac{\alpha_0 v_d}{m_0}\frac{1+\eta\frac{24g_U^2}{5}+\eta_N\left(\frac{R_l}{1+0.5x}-y_D^2\right)}{1+0.3x}\lambda^5\approx 3\times 10^{-6}\right)$	$[1.2, 22]\times 10^{-6}$
$ (\delta_{RL}^e)_{13} $		$[1, 22]\times 10^{-2}$
$ (\delta_{LR}^e)_{13} $	$\mathcal{O}\left(\frac{\alpha_0 v_d}{m_0}\frac{1+\eta\frac{24g_U^2}{5}+\eta_N\left(\frac{R_l}{1+0.5x}-y_D^2\right)}{1+0.3x}\lambda^6\approx 8\times 10^{-7}\right)$	
$ (\delta_{LR}^e)_{23} $		
$ (\delta_{RL}^e)_{23} $	$\mathcal{O}\left(\frac{\alpha_0 v_d}{m_0}\frac{1+\eta\frac{24g_U^2}{5}+\eta_N\left(\frac{R_l}{1+0.5x}-y_D^2\right)}{1+0.3x}\lambda^4\approx 10^{-5}\right)$	

Table 6: The naive expectation for the ranges of $(\delta_{AB}^e)_{ij}$, $A, B = L, R$, as extracted from our model (second column), to be compared with experimental bounds from [38] (third column). The full ranges of the δ parameters produced in our scan are shown in Figure 3.

At the GUT scale, the mass insertion parameter $(\delta_{LL}^e)_{12} \sim \lambda^4$ is proportional to $\tilde{R}_{12} = B_3 - K_3$. Its absolute value is equal to $|(\delta_{RR}^d)_{12}|$ due to the $SU(5)$ framework. However, the parameter of the lepton sector, given in Eq. (A.41), receives large RG corrections which encode seesaw effects. At the low energy scale, it is non-zero even for $B_3 = K_3$, due to the term proportional to the small parameter η_N which is defined in Eq. (2.15) and originates from the running between the GUT scale and the scale of the right-handed neutrinos. In the second column of Table 6, we estimate this effect by considering $B_3 = K_3$. We then expand to first order in η_N and consider $R_l \approx R'_l$, where R_l and R'_l are defined in Eqs. (A.8,A.9). For $x \approx 1$, $R_l \approx 3y_D^2 + 1$ and $y_D \approx 0.5$, we expect the low energy $|(\delta_{LL}^e)_{12}|$ to vary around 2×10^{-4} . However, the non-trivial expression of \tilde{E}_{12} , cf. Eqs. (A.41,A.54), creates a spread of about two orders of magnitude around this value. As $|\tilde{R}_{12}|$ increases, the mass insertion parameter lies above the limits given in Table 6. As can be seen from Figure 3, the non-observation of $\mu \rightarrow e\gamma$ places stronger constraints on the down-type quark δ s than the direct bounds from the quark sector. Analogous to the down-type RR parameters, the absolute values of the (12), (23) and (13) lepton LL parameters are identical, see Eqs. (A.41,A.42).



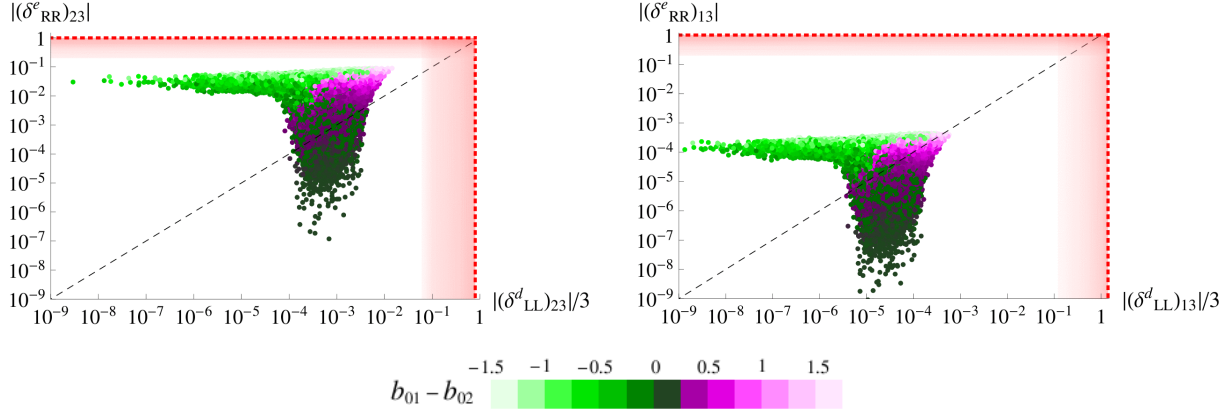


Figure 3: The low energy lepton mass insertion parameters $(\delta^e_{AB})_{ij}$, $A, B = L, R$, plotted against the down-type δ s to which they are related via the $SU(5)$ framework. The dashed lines represent their GUT scale relations, while the red shaded areas denote experimental limits on the parameter space according to the third column of Tables 3-6. Scanning over the input parameters within the ranges shown in Table 1, we observe that in particular $|(\delta^e_{LL})_{12}|$ exceeds its limit for much of our parameter space. Note that $|(\delta^e_{LL})_{12}| = |(\delta^e_{LL})_{23}| = |(\delta^e_{LL})_{13}|$ and $|(\delta^e_{RL})_{12}| = |(\delta^e_{LR})_{12}| = |(\delta^e_{RL})_{13}|$.

Similarly, at the GUT scale, the absolute values of the RR parameters in the lepton sector are equal to the LL ones of the down-type sector times the Georgi-Jarlskog factor of $1/3$. For the (12) δ s, the RG running effects are trivial, consisting only of a suppression through x , which is milder in the lepton sector where the numerical prefactor of x is 0.15, as compared to a factor of 6.5 in the quark one. For the (13) and (23) parameters, the non-trivial running effects in the quark sector are obvious in Figure 3, where we see that even though $|(\delta^d_{LL})_{23,13}|$ can get very small for negative $b_{01} - b_{02}$, $|(\delta^e_{RR})_{23,13}|$ can only receive such small values when $b_{01} \rightarrow b_{02}$, see e.g. Eqs. (A.30, A.44).

Finally, the variation of the LR parameters can be understood in an analogous way to the one described in the quark sector. $|(\delta^e_{LR})_{ij\text{GUT}}| = |(\delta^d_{RL})_{ij\text{GUT}}|$, with the exception of the (23) parameters which are not equal due to a term which involves a H_{45} , thereby receiving an extra factor of 9 for the leptons, see Eqs. (A.40, A.52) together with Eq. (A.2). As in the down-type sector, $|(\delta^e_{RL})_{12}| = |(\delta^e_{LR})_{12}| = |(\delta^e_{RL})_{13}|$ and we only show the (12) parameter in Figure 3 which features the strongest experimental constraint.

4 Phenomenological implications

In the preceding section, we found that parts of the parameter space spanned by the (12) mass insertion parameters of the down-type and charged lepton sector are excluded

due to experimental limits set by $\mu \rightarrow e\gamma$ and Kaon mixing observables. The corresponding bounds are available in the literature and their derivation is highly dependent on the assumed SUSY mass spectra. Possible interference effects between contributions from multiple δ parameters to a given observable can additionally have significant effects. These are usually ignored when setting “model independent” limits on mass insertion parameters.

In this section, we therefore investigate the phenomenological implications of the deviations of our model from MFV. In particular, we focus on the predictions for $BR(\mu \rightarrow e\gamma)$ and ϵ_K . We also scrutinise whether the phase structure of our model can survive the strong limits set by electric dipole moments. Since the analysis in [37], which provides the limits on $(\delta_{AB}^d)_{23}$, assumes real parameters throughout, we also study how our model contributes to the time-dependent CP asymmetry associated with the decay $B_s \rightarrow J/\psi\phi$. For completeness, we check that the limits set by the decay $B_d \rightarrow J/\psi K_S$ and the mass differences $\Delta M_{B_{s,d}}$ are satisfied. Finally, we also consider the branching ratios of $b \rightarrow s\gamma$ and $B_{s,d} \rightarrow \mu^+\mu^-$.

Adopting the leading logarithmic approximation, the low energy gaugino masses [39]

$$M_i = \frac{g_i^2}{g_U^2} M_{1/2} \approx \frac{M_{1/2}}{1 + 2\eta g_U^2 \beta_i}, \quad i = 1, 2, 3, \quad (4.1)$$

with $\beta_1 = 33/5$, $\beta_2 = 1$ and $\beta_3 = -3$, are given by

$$M_1 \approx 0.43 M_{1/2}, \quad M_2 \approx 0.83 M_{1/2}, \quad M_3 \approx 2.53 M_{1/2}. \quad (4.2)$$

4.1 Electron EDM

The current experimental limit for the electric dipole moment of the electron stems from the ACME collaboration [40] and is given by

$$|d_e/e| \lesssim 8.7 \times 10^{-29} \text{ cm} \approx 4.41 \times 10^{-15} \text{ GeV}^{-1}. \quad (4.3)$$

This tiny value poses a strong constraint on the phases of any model. The supersymmetric contributions depend on the mass insertion parameters as follows [41]⁵

⁵The corresponding expression in [15] also includes triple mass insertions of type $(LR)(RR)(RR)$ and $(LL)(LL)(LR)$. In our model, these give suppressed contributions to d_e/e of order λ^{11} and λ^{13} , respectively, which can be safely neglected.

$$\begin{aligned}
\frac{d_e}{e} = & \frac{\alpha}{8\pi \cos^2 \theta_W} 0.43 \frac{\sqrt{x}}{m_0^3} m_{\tilde{e}_{LL}} \text{Im} \left[-(\delta_{LR}^e)_{11} C_B m_{\tilde{e}_{RR}} + \right. \\
& + \left\{ (\delta_{LL}^e)_{1i} (\delta_{LR}^e)_{i1} C'_{B,L} + (\delta_{LR}^e)_{1i} (\delta_{RR}^e)_{i1} C'_{B,R} \right\} m_{R_{ii}} - \\
& \left. - \left\{ (\delta_{LL}^e)_{1i} (\delta_{LR}^e)_{ij} (\delta_{RR}^e)_{j1} + (\delta_{LR}^e)_{1j} (\delta_{RL}^e)_{ji} (\delta_{LR}^e)_{i1} \right\} C''_B m_{R_{jj}} \right], \quad (4.4)
\end{aligned}$$

where $m_{\tilde{e}_{LL}}$ and $m_{\tilde{e}_{RR}}$ are given in Eq. (A.12). Moreover $m_{R_{ii}} = m_{\tilde{e}_{RR}}$ for $i = 1, 2$ and $m_{R_{33}} = m_{\tilde{\tau}_{RR}}$ with the latter being defined in Eq. (A.12). The expression of Eq. (4.4) is actually proportional to the bino mass M_1 , which we have approximated by Eq. (4.2) using $x = (M_{1/2}/m_0)^2$. The dimensionless loop functions C_i , whose expressions can be found in Appendix B encode the contributions from the pure bino ($i = B$) and the bino-higgsino with left- ($i = B, L$) and right-handed ($i = B, R$) slepton diagrams. For $x \ll 1$, all ratios of different C_i functions are close to one. With increasing x , C_B takes slightly larger values than the rest of the functions, reaching up to twice the value of $C'_{B,L(R)}$ and three times the value of C''_B . This can be seen in the limit where the left- and right-type slepton masses are not very different, such that the loop functions take the form [41]

$$\begin{aligned}
C_B & \approx \frac{m_0^4}{m_{\tilde{e}}^4} h_1(\bar{x}), \quad C''_B \approx \frac{m_0^4}{3m_{\tilde{e}}^4} (h_1(\bar{x}) + 2k_1(\bar{x})), \\
C'_{B,L} & \approx C'_{B,R} \approx \frac{m_0^4}{2m_{\tilde{e}}^4} (h_1(\bar{x}) + k_1(\bar{x})), \quad (4.5)
\end{aligned}$$

where we consider $m_{\tilde{e}} = \sqrt{m_{\tilde{e}_{LL}} m_{\tilde{e}_{RR}}}$ as the average slepton mass⁶ and $\bar{x} = (M_1/m_{\tilde{e}})^2$. The function h_1 is given in Appendix B while k_1 denotes the derivative $k_1(\bar{x}) \equiv d(\bar{x}h_1(\bar{x}))/d\bar{x}$. Their behaviour is shown in the right panel of Figure 4.

The dominant contribution to the electron EDM comes from the single chirality flipping diagonal mass insertion $(\delta_{LR}^e)_{11} \propto \lambda^6$, such that we can make the approximation

$$|d_e/e| \approx \frac{\alpha}{8\pi \cos^2 \theta_W} 0.43 \sqrt{x} \frac{|\alpha_0| v_d}{m_0^2} (1 + R_e^y) \frac{1}{3} |\text{Im}[\tilde{a}_{11}^d]| \lambda^6 C_B, \quad (4.6)$$

where R_e^y is an RG running factor defined in Eq. (3.9) and $\tilde{a}_{11}^d/3$, defined in Eq. (A.2),

⁶ $m_{\tilde{e}_{RR}}$ and $m_{\tilde{\tau}_{RR}}$ only differ in the order one coefficients b_{01} and b_{02} which take values in the same range. Since the dominant term in Eq. (4.4) involves the first generation masses, we use $m_{\tilde{e}} = \sqrt{m_{\tilde{e}_{LL}} m_{\tilde{e}_{RR}}}$ rather than $m_{\tilde{e}} = \sqrt{m_{\tilde{e}_{LL}} \sqrt{m_{\tilde{e}_{RR}} m_{\tilde{\tau}_{RR}}}}$ as the average slepton mass.

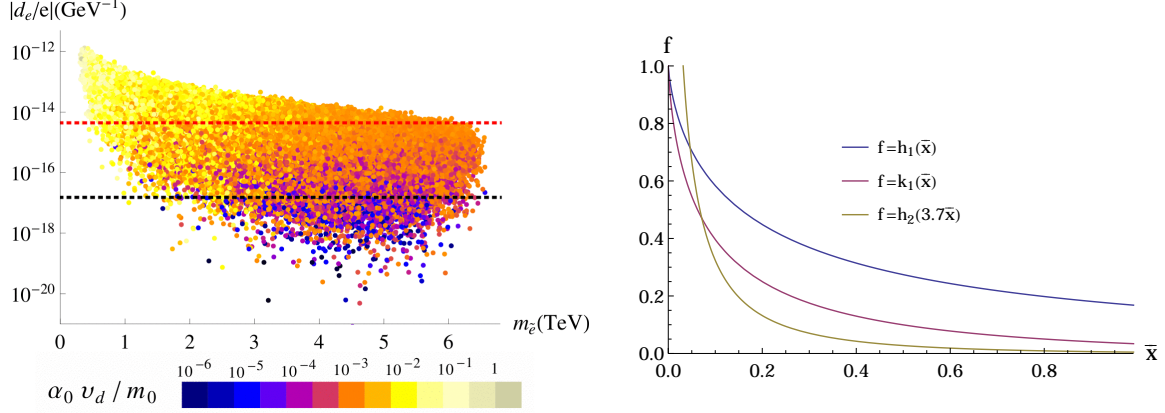


Figure 4: Left panel: the prediction for the SUSY contribution to the electron EDM versus $m_{\tilde{e}} = \sqrt{m_{\tilde{e}LL} m_{\tilde{e}RR}}$. The red dotted line represents the current experimental limit of Eq. (4.3), while the black dotted line corresponds to the expected future limit of $|d_e/e| \lesssim 3 \times 10^{-31} \text{ cm} \approx 1.52 \times 10^{-17} \text{ GeV}^{-1}$ [42]. Right panel: the behaviour of the functions h_1 , k_1 and (in anticipation of the discussion in Section 4.2) h_2 .

is the (11) element of $\tilde{A}_{\text{GUT}}^e/A_0$, with \tilde{A}_{GUT}^e denoting the GUT scale soft trilinear matrix in the SCKM basis. Its imaginary part is non-zero when allowing the phases of the soft trilinear sector to be different from the phases of the corresponding Yukawa sector. Then, for $|\alpha_0 v_d/m_0| \approx 10^{-2}$, $m_0 \approx 1 \text{ TeV}$ and $x \approx 1$, we expect $|d_e/e|$ to vary around $10^{-13} \text{ GeV}^{-1}$.

As can be seen in the left panel of Figure 4, which was produced using the full expression in Eq. (4.4), the numerical choice for the suppression factor $|\alpha_0 v_d/m_0|$ corresponds to the yellow points and brings our prediction for the EDM above its current experimental limit, represented by the red dotted line.

In the case where the phases of the soft trilinear and Yukawa sectors are equal, \tilde{a}_{11}^d and all factors in Eq. (A.2) become real. In that case, the dominant imaginary part originates from the NLO contribution⁷ to $(\delta_{LR}^e)_{11}$ and is proportional to $\sin(4\theta_2^d + \theta_3^d)$. Setting $\theta_2^d = \pi/2$, as is preferred by the Jarlskog invariant J_{CP}^q , given in Eq. (2.8), we see that also the NLO contribution vanishes for $\theta_3^d = 0$, such that $|d_e/e|$ would only arise at order λ^8 .

Concerning the terms of Eq. (4.4) with double mass insertions, they enter at orders $(\delta_{LR}^e)_{12}(\delta_{RR}^e)_{21} \sim \lambda^8$, $(\delta_{LR}^e)_{13}(\delta_{RR}^e)_{31} \sim \lambda^{10}$ and $(\delta_{LL}^e)_{12}(\delta_{LR}^e)_{21} \sim (\delta_{LL}^e)_{13}(\delta_{LR}^e)_{31} \sim \lambda^9$ in our model. In the situation described in the preceding paragraph, the first two terms are real, while the contributions of the latter two cancel against each other. Finally, the

⁷The SCKM rotation which renders the Yukawa sector diagonal and real does not do the same to the A -terms beyond leading order.

contributions of the triple mass insertions are further suppressed, with the largest one, $(\delta_{LL}^e)_{13}(\delta_{LR}^e)_{33}(\delta_{RR}^e)_{31} \sim \lambda^{10}$, being real in the case at hand, while all other triple insertions entail contributions which lie below the experimental limit.

4.2 $BR(\mu \rightarrow e\gamma)$

According to Figure 3, a large part of our parameter space in the (12) charged lepton sector appears to be excluded by the experimental limit set by the non-observation of $\mu \rightarrow e\gamma$. In this section, we therefore study in detail the contributions to this LFV process within our model. The current experimental limit for the branching ratio

$$BR(\mu \rightarrow e\gamma) \lesssim 5.7 \times 10^{-13}, \quad (4.7)$$

is set by the MEG collaboration [43]. The expression for the corresponding SUSY contribution is given by [41]

$$\begin{aligned} BR(\mu \rightarrow e\gamma) = & 3.4 \times 10^{-4} \times 0.43^2 M_W^4 x \frac{\mu^2 t_\beta^2}{m_0^6} \times \\ & \times \left(\left| (\delta_{LL}^e)_{12} \left(-(\delta_{LR}^e)_{22} \frac{m_{\tilde{e}_{LL}} m_{\tilde{e}_{RR}}}{\mu t_\beta m_\mu} C'_{B,L} + \frac{1}{2} C'_L + C'_2 \right) + (\delta_{LR}^e)_{12} \frac{m_{\tilde{e}_{LL}} m_{\tilde{e}_{RR}}}{\mu t_\beta m_\mu} C_B \right|^2 \right. \\ & \left. + \left| (\delta_{RR}^e)_{12} \left(-(\delta_{LR}^e)^*_{22} \frac{m_{\tilde{e}_{LL}} m_{\tilde{e}_{RR}}}{\mu t_\beta m_\mu} C'_{B,R} - C'_R \right) + (\delta_{LR}^e)^*_{21} \frac{m_{\tilde{e}_{LL}} m_{\tilde{e}_{RR}}}{\mu t_\beta m_\mu} C_B \right|^2 \right). \end{aligned} \quad (4.8)$$

It is proportional to the bino mass squared, that has been approximated by Eq. (4.2) and expressed as $M_1^2 = 0.43^2 x m_0^2$, where $x = (M_{1/2}/m_0)^2$. The loop function C'_2 encodes the wino-higgsino contribution and is defined in Appendix B, along with the rest of the functions C_i .

In our model, $(\delta_{LL}^e)_{12} \sim \lambda^4$, $(\delta_{RR}^e)_{12} \sim \lambda^3$, $(\delta_{LR}^e)_{12(21)} \sim \lambda^5$ and $(\delta_{LR}^e)_{22} \sim \lambda^4$. To get an estimate of the dominant δ s in Eq. (4.8), we first compare the $SU(2)$ ($\propto C'_2$) and the $U(1)$ ($\propto C'_{B,L}, C'_L$) contributions to the $(\delta_{LL}^e)_{12}$ term by studying the ratio

$$R = \left| C'_2 / \left(\left(1 - \frac{A_0}{\mu t_\beta} \frac{\tilde{a}_{22}^d}{y_s} \right) C'_{B,L} + \frac{1}{2} C'_L \right) \right|, \quad (4.9)$$

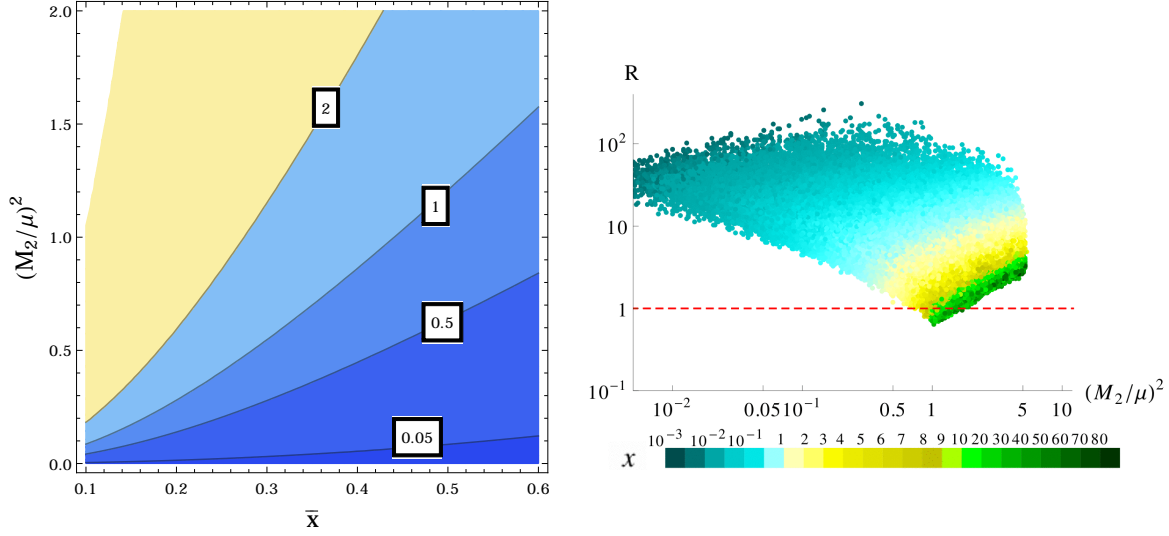


Figure 5: Left panel: the contour lines for \bar{R} , the approximate ratio of the $SU(2)$ over the $U(1)$ contributions to the $(\delta_{LL}^e)_{12}$ term in Eq. (4.8), as defined in Eq. (4.10). For the average slepton mass $m_{\tilde{e}} = \sqrt{m_{\tilde{e}LL} m_{\tilde{e}RR}}$, $\bar{x} = (M_1/m_{\tilde{e}})^2 \approx 0.43^2 x / (1 + 0.3x)$, with $x = (M_{1/2}/m_0)^2$. Right panel: the ratio R (without approximation), as defined in Eq. (4.9) and produced in our scan. The dependence of $(M_2/\mu)^2$ and \bar{x} on x is such that the $SU(2)$ contributions dominate for most of the parameter space.

which, in the limit where $m_{\tilde{e}RR}$ and $m_{\tilde{e}LL}$ are not very different, can be written as

$$R \approx \bar{R} = 2 \frac{M_2}{M_1} \cot^2 \theta_W \left| \frac{\frac{1}{\bar{y}-\bar{x}'} (h_2(\bar{x}') - h_2(\bar{y}))}{h_1(\bar{x}) + k_1(\bar{x}) + \frac{1}{\bar{y}-\bar{x}} (h_1(\bar{x}) - h_1(\bar{y}))} \right|. \quad (4.10)$$

The behaviour of the loop functions h_1 and h_2 , which are defined in Appendix B, as well as $k_1(\bar{x}) \equiv d(\bar{x}h_1(\bar{x}))/d\bar{x}$ is shown in the right panel of Figure 4, and $\bar{x} = (M_1/m_{\tilde{e}})^2$, $\bar{x}' = (M_2/m_{\tilde{e}})^2$, $\bar{y} = (\mu/m_{\tilde{e}})^2$, with $m_{\tilde{e}} = \sqrt{m_{\tilde{e}LL} m_{\tilde{e}RR}}$. The contours in the left panel of Figure 5 show the dependence of \bar{R} , as defined in Eq. (4.10), on $(M_2/\mu)^2$ and \bar{x} . We see that for $(M_2/\mu)^2 \gtrsim 1.5$, \bar{R} is larger than one for all $\bar{x} \approx 0.43^2 x / (1 + 0.3x) \lesssim 0.6$, while for $(M_2/\mu)^2 \sim \mathcal{O}(1)$ and smaller, the $U(1)$ contributions can dominate if \bar{x} does not decrease faster than $(M_2/\mu)^2$. The right panel in Figure 5 is based on our scan and shows that the correlation of $(M_2/\mu)^2$ and \bar{x} through x is such that R , as defined in Eq. (4.9), stays larger than one in most of our parameter space, making the $SU(2)$ contribution to the $(\delta_{LL}^e)_{12}$ term in Eq. (4.8) the most important one.

Similarly, one can show that the RR contribution to $\mu \rightarrow e\gamma$ in Eq. (4.8) is comparable to the LL one only when $|(\delta_{RR}^e)_{12}\lambda|/|(\delta_{LL}^e)_{12}| \gtrsim 1$, although $(\delta_{LL}^e)_{12}$ is suppressed by an order of λ with respect to $(\delta_{RR}^e)_{12}$. This happens because the RR parameter has only

two $U(1)$ contributions which come in with opposite signs, allowing even for a complete cancellation.

Finally, we study the relative size of the LL and LR contributions by considering the ratio

$$R' = \left| \frac{\mu t_\beta m_\mu (\delta_{LL}^e)_{12} C_2'}{m_{\tilde{e}_{LL}} m_{\tilde{e}_{RR}} (\delta_{LR}^e)_{12} C_B} \right| = \lambda^3 \kappa \left| \frac{\mu t_\beta C_2'}{A_0 C_B} \right|, \quad (4.11)$$

where $\kappa = \left| 3 y_s (\tilde{R}_{12} - 2\eta_N \tilde{E}_{12}) / (\tilde{a}_{12}^d (p_L^e)^2) \right|$, with \tilde{R}_{12} , \tilde{a}_{12}^d , p_L^e , \tilde{E}_{12} and η_N defined in Eqs. (A.1,A.2,A.15,A.54,2.15), respectively. The absolute value of the right-hand side of Eq. (4.11) exhibits a similar behaviour as the ratio R , defined in Eq. (4.9) and shown in the right panel of Figure 5. Taking into account the λ -suppression ($\lambda^3 \sim 10^{-2}$) and the range of κ which can vary within two orders of magnitude, we find that the $(\delta_{LR}^e)_{12}$ contribution to the branching ratio can be comparable to the $(\delta_{LL}^e)_{12}$ one when $(M_2/\mu)^2 \sim 1$.

Considering situations in which the $(\delta_{LR}^e)_{12}$ contribution to Eq. (4.8) dominates, we obtain the approximate expression

$$BR(\mu \rightarrow e\gamma)|_{(\delta_{LR}^e)_{12}} \approx \mathcal{O} \left(10^2 \alpha_0^2 \frac{m_0^4}{m_{\tilde{e}}^8} h_1^2(\bar{x}) \right) \left(\frac{|\tilde{a}_{12}^d|}{3 y_s} \right)^2. \quad (4.12)$$

In the case where $(\delta_{LL}^e)_{12}$ is more important, e.g. when $(M_2/\mu)^2 \ll 1$, cf. right panel of Figure 5, we obtain

$$BR(\mu \rightarrow e\gamma)|_{(\delta_{LL}^e)_{12}} \approx \mathcal{O} \left(\frac{x t_\beta^2}{\mu^2} \frac{m_0^6}{m_{\tilde{e}_{LL}}^8} h_2^2(3.7 x_L) \right) \left| \tilde{R}_{12} - 2\eta_N \tilde{E}_{12} \right|^2. \quad (4.13)$$

For $x_L \equiv (M_1/m_{\tilde{e}_{LL}})^2 \approx \bar{x} \approx 0.1$, $x \approx 1$, $\alpha_0 \approx 1$, $t_\beta \approx 10$, $\mu \approx m_0 \approx 1$ TeV and $m_{\tilde{e}_{LL}} \approx 750$ GeV, the approximations of Eqs. (4.12,4.13) both produce a value of the order of 10^{-10} times the relevant order one coefficients squared. In order to gain an extra suppression of at least an order of magnitude, the latter are preferred to be smaller than one.

The total supersymmetric contribution to the branching ratio of $\mu \rightarrow e\gamma$ of Eq. (4.8) as produced in our scan is shown in Figure 6. There it is plotted against the average slepton mass (left panel) as well as $|d_e/e|$ (right panel). From the left panel we observe that our model requires rather heavy sleptons, in the TeV range, in order to survive the current experimental limit in Eq. (4.7), which is denoted by the red dotted line. As can be seen in Eqs. (4.8,4.13), there is also a strong μ dependence, with a preference for large values. The right panel of Figure 6 shows that the $\mu \rightarrow e\gamma$ branching ratio is correlated with the electron EDM, mainly through the slepton masses and the bino-slepton mass

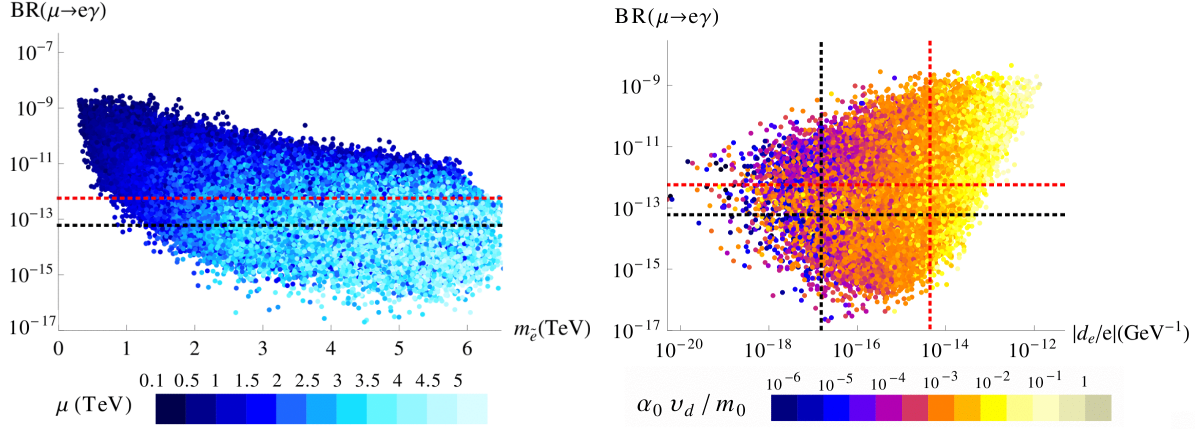


Figure 6: The supersymmetric contribution to the branching ratio of $\mu \rightarrow e \gamma$ versus the average slepton mass $m_{\tilde{e}} = \sqrt{m_{\tilde{e}_{LL}} m_{\tilde{e}_{RR}}}$ (left panel) as well as $|d_e/e|$ (right panel). The red dotted lines represent the current experimental limits given in Eqs. (4.3,4.7) while the black dotted lines show the expected future limits, that is $BR(\mu \rightarrow e \gamma) \lesssim 6 \times 10^{-14}$ [44] and $|d_e/e| \lesssim 1.52 \times 10^{-17} \text{ GeV}^{-1}$ [42].

ratio. The combination of the current limits on both observables highly restricts our parameter space. Reaching the expected future limits, denoted by the black dotted lines, would nearly exclude our model.

In Figure 7 we show our predictions for $BR(\mu \rightarrow e \gamma)$ in the plane of two (12) mass insertion parameters as produced in our scan. Comparing this to the discussion of Section 3.2.3 reveals that, with the present MEG bound, $|(\delta_{LL}^e)_{12}| \lesssim 5 \times 10^{-3}$ and $|(\delta_{LR}^e)_{12}| \lesssim 5 \times 10^{-6}$ are not excluded as it was suggested by the limits in Figure 3. On the other hand, $|(\delta_{RR}^e)_{12}|$ can take its maximum values produced by the scan. The reason for these weaker bounds is twofold. Firstly, the analysis in [38] sets the limits on the mass insertion parameters by choosing t_β as large as 60, whereas we only allow for maximum values of 25. Secondly, the derivation in [38] requires that the discrepancy of $(g-2)_\mu$ from its SM value is explained by SUSY contributions.

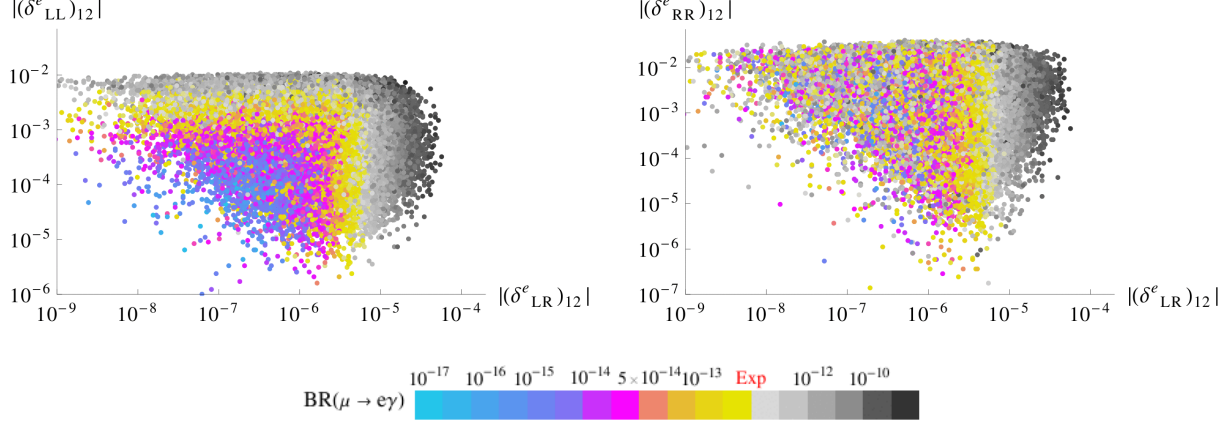


Figure 7: The range of the (12) lepton mass insertion parameters as produced in our scan, together with the resulting prediction for the branching ratio of $\mu \rightarrow e\gamma$. The grey points do not satisfy the current experimental limit given in Eq. (4.3).

4.3 Meson mixing

Turning to $\Delta F = 2$ transitions, we study the SUSY contributions to meson mixing. The dispersive part of the mixing for a meson P can be parametrised as [45]

$$M_{12}^P = M_{12}^{P,\text{SM}} + M_{12}^{P,\text{NP}} = M_{12}^{P,\text{SM}} (1 + h_P e^{2i\sigma_P}), \quad (4.14)$$

and the corresponding mass difference is given by

$$\Delta M_P = 2|M_{12}^P|. \quad (4.15)$$

We express the SM contribution as $M_{12}^{P,\text{SM}} = |M_{12}^{P,\text{SM}}| e^{2i\phi_P^{\text{SM}}}$. The New Physics (NP) contribution, $M_{12}^{P,\text{NP}} = |M_{12}^{P,\text{NP}}| e^{2i\theta_P}$, is encoded in the real parameters

$$h_P = \frac{|M_{12}^{P,\text{NP}}|}{|M_{12}^{P,\text{SM}}|}, \quad \sigma_P = \theta_P - \phi_P^{\text{SM}}. \quad (4.16)$$

The contributions of the gluino-squark box diagram in terms of mass insertion parameters read [11, 15]

$$M_{12}^{P,(\tilde{g})} = A_1^{P,(\tilde{g})} \left(A_2^{P,(\tilde{g})} [(\delta_{LL}^d)_{ji}^2 + (\delta_{RR}^d)_{ji}^2] + A_3^{P,(\tilde{g})} (\delta_{LL}^d)_{ji} (\delta_{RR}^d)_{ji} \right. \\ \left. + A_4^{P,(\tilde{g})} [(\delta_{LR}^d)_{ji}^2 + (\delta_{RL}^d)_{ji}^2] + A_5^{P,(\tilde{g})} (\delta_{LR}^d)_{ji} (\delta_{RL}^d)_{ji} \right), \quad (4.17)$$

where

$$A_1^{P,(\tilde{g})} = -\frac{\alpha_s^2}{216 m_{\tilde{q}}^2} \frac{1}{3} M_P f_P^2, \quad A_2^{P,(\tilde{g})} = 24 y f_6(y) + 66 \tilde{f}_6(y), \quad (4.18)$$

$$A_3^{P,(\tilde{g})} = \left(384 \left(\frac{M_P}{m_j + m_i} \right)^2 + 72 \right) y f_6(y) + \left(-24 \left(\frac{M_P}{m_j + m_i} \right)^2 + 36 \right) \tilde{f}_6(y),$$

$$A_4^{P,(\tilde{g})} = -132 \left(\frac{M_P}{m_j + m_i} \right)^2 y f_6(y), \quad A_5^{P,(\tilde{g})} = \left(-144 \left(\frac{M_P}{m_j + m_i} \right)^2 - 84 \right) \tilde{f}_6(y).$$

M_P denotes the mass of the meson under consideration and f_P is the associated decay constant. m_i and m_j are the masses of the meson's constituent quarks while $m_{\tilde{q}}$ is an average squark mass which we define as

$$m_{\tilde{q}} = \begin{cases} \sqrt{m_{\tilde{d}_{LL}} m_{\tilde{d}_{RR}}}, & P = K, \\ \sqrt{\sqrt{m_{\tilde{d}_{LL}} m_{\tilde{b}_{LL}}} m_{\tilde{d}_{RR}}}, & P = B_{s,d}, \end{cases} \quad (4.19)$$

with $m_{\tilde{d}_{LL}}$, $m_{\tilde{b}_{LL}}$ and $m_{\tilde{d}_{RR}}$ defined in Eq. (A.11). The loop functions $f_6(y)$ and $\tilde{f}_6(y)$, where $y = (m_{\tilde{g}}/m_{\tilde{q}})^2$, are given in Appendix B and the gluino mass has been approximated by Eq. (4.2).

4.3.1 $B_q - \bar{B}_q$ mixing

The SM contribution to B_q , $q = s, d$ meson mixing given by [46]

$$M_{12}^{B_q, \text{SM}} = \frac{G_F^2 M_{B_q}}{12\pi^2} M_W^2 (V_{tb} V_{tq}^*)^2 \eta_B S_0(x_t) f_{B_q}^2 \hat{B}_{B_q}, \quad (4.20)$$

with

$$V_{ts} = -|V_{ts}| e^{i\beta_s}, \quad V_{td} = |V_{td}| e^{-i\beta}, \quad (4.21)$$

$$\phi_{B_s}^{\text{SM}} = -\beta_s, \quad \phi_{B_d}^{\text{SM}} = \beta. \quad (4.22)$$

Here η_B is a QCD factor, \hat{B}_{B_q} a perturbative parameter related to hadronic matrix elements and $S_0(x_t \equiv \bar{m}_t^2(\bar{m}_t)/M_W^2)$ is the Inami-Lim loop function [47]. The calculation of the pure SM contribution to the B_s mass difference gives [48]

$$\Delta M_{B_s}^{(\text{SM})} = 125.2_{-12.7}^{+13.8} \times 10^{-13} \text{ GeV}, \quad (4.23)$$

with the largest uncertainty stemming from the non-perturbative factor $f_{B_s}\sqrt{\hat{B}_{B_s}}$, for which the value 275 ± 13 MeV [49] has been used.⁸ The SM prediction for ΔM_{B_d} can be deduced from the ratio [48]

$$\frac{\Delta M_{B_d}^{(\text{SM})}}{\Delta M_{B_s}^{(\text{SM})}} = 0.02835 \pm 0.00187, \quad (4.24)$$

which is less sensitive to theoretical uncertainties. On the other hand, the associated experimental averages as of summer 2014, provided by the HFAG group, read [51]

$$\Delta M_{B_s}^{(\text{exp})} = (116.9 \pm 0.1) \times 10^{-13} \text{ GeV} , \quad (4.25)$$

$$\Delta M_{B_d}^{(\text{exp})} = (3.357 \pm 0.020) \times 10^{-13} \text{ GeV} , \quad (4.26)$$

$$\frac{\Delta M_{B_d}^{(\text{exp})}}{\Delta M_{B_s}^{(\text{exp})}} = 0.02879 \pm 0.0002. \quad (4.27)$$

Comparing Eq. (4.23) with Eq. (4.25) leads to a negative central value for the experimentally allowed NP contribution to ΔM_{B_s} , with a similar result being obtained for ΔM_{B_d} . The main source for the errors are the uncertainties of the SM calculation.⁹ In view of Eqs. (4.23-4.27), and in anticipation of reduced theoretical uncertainties, we conclude that the largest NP effects that could still be allowed should be consistent with

$$|\Delta M_{B_s}^{(\text{NP})}| \leq 2 \times 10^{-12} \text{ GeV} , \quad |\Delta M_{B_d}^{(\text{NP})}| \leq 1 \times 10^{-13} \text{ GeV} . \quad (4.28)$$

Using Eqs. (4.15,4.17), we can estimate the effects of the gluino-squark box diagrams. Taking into account the λ -suppression of each δ parameter entering Eq. (4.17), we can write $\Delta M_{B_{s,d}}^{(\tilde{g})}$ in the schematic form

$$\begin{aligned} \Delta M_{B_s}^{(\tilde{g})} &\propto \lambda^4 \left(A_2^{B_s,(\tilde{g})} + A_3^{B_s,(\tilde{g})} \lambda^2 + A_4^{B_s,(\tilde{g})} \lambda^4 + A_5^{B_s,(\tilde{g})} \lambda^6 \right) , \\ \Delta M_{B_d}^{(\tilde{g})} &\propto \lambda^8 \left(A_2^{B_d,(\tilde{g})} + A_3^{B_d,(\tilde{g})} + A_4^{B_d,(\tilde{g})} \lambda^2 + A_5^{B_d,(\tilde{g})} \lambda^3 \right) . \end{aligned} \quad (4.29)$$

Figure 8 shows the individual contributions as a function of $y = (m_{\tilde{g}}/m_{\tilde{q}})^2$. The largest

⁸We note that the 2014 average of the FLAG collaboration [50] corresponds to a lower central value but with a larger error: $f_{B_s}\sqrt{\hat{B}_{B_s}} \Big|_{\text{FLAG}} = 266 \pm 18$ MeV.

⁹For a recent discussion on theoretical uncertainties and comparison with experimental results, see [52].

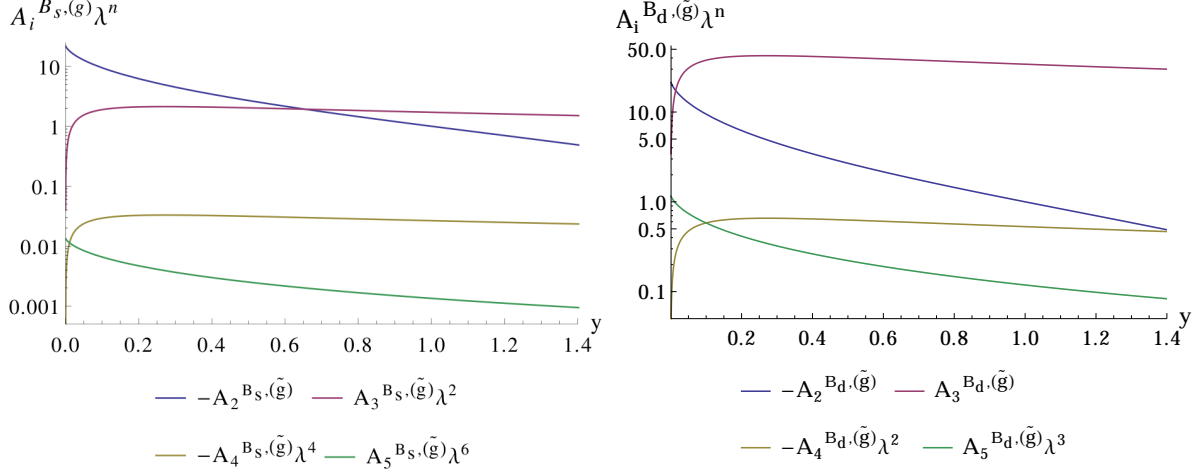


Figure 8: The dependence of the individual contributions in Eq. (4.29) on $y = (m_{\tilde{g}}/m_{\tilde{q}})^2$. The average squark mass $m_{\tilde{q}}$ is defined in Eq. (4.19) while the functions $A_i^{B_{s,d},(\tilde{g})}$ can be found in Eq. (4.18).

contributions originate from the terms proportional to $A_2^{B_{s,d},(\tilde{g})}$ and $A_3^{B_{s,d},(\tilde{g})}$, i.e. the terms associated with the δ_{LL}^d and δ_{RR}^d , cf. Eq. (4.17). The contributions from the LR -type mass insertion parameters, proportional to $A_{4,5}^{B_{s,d},(\tilde{g})}$, are negligible. The maximum effect of the gluino-squark box diagrams is obtained when $x = (M_{1/2}/m_0)^2$ and y are smaller than one, with the $(\delta_{LL(RR)}^d)_{i3}^2$ and $(\delta_{LL}^d)_{i3}(\delta_{RR}^d)_{i3}$ terms interfering constructively. For relatively light $m_{\tilde{q}}$ around 2 TeV, $|A_1^{B_{s,d},(\tilde{g})}|_{\max} \sim \mathcal{O}(10^{-12})$ GeV. Assuming furthermore $|(\delta_{LL}^d)_{13}| \approx 10^{-3}$, $|(\delta_{LL}^d)_{23}| \approx 2 \times 10^{-2}$ and $|(\delta_{RR}^d)_{13}| = |(\delta_{RR}^d)_{23}| \approx 10^{-2}$ (cf. Figure 2) as well as $y \approx 0.3$, we can use Eqs. (4.15,4.17) together with Figure 8 to estimate the maximum gluino effects as $|\Delta M_{B_s}^{(\tilde{g})}|_{\max} \sim \mathcal{O}(10^{-14})$ GeV and $|\Delta M_{B_d}^{(\tilde{g})}|_{\max} \sim \mathcal{O}(10^{-15})$ GeV. This is about two orders of magnitude smaller than the corresponding SM and experimental values.

For relatively large values of t_β and a light CP-odd Higgs mass M_A , the contributions of the double penguin (DP) diagrams, which scale as $t_\beta^4 \mu^2/M_A^2$, become important. Considering diagrams with (i) two gluino, (ii) one gluino and one Higgsino and (iii) one gluino and one Wino loops, the associated part of $M_{12}^{B_q}$ can be approximated by [15]

$$M_{12}^{B_q,(\text{DP})} = A_1^{B_q,(\text{DP})}(\delta_{RR}^d)_{3i} t_\beta^4 \frac{\mu^2}{M_A^2} \left\{ A_2^{B_q,(\text{DP})} + (\delta_{LL}^d)_{3i} A_3^{B_q,(\text{DP})} \right\}, \quad (4.30)$$

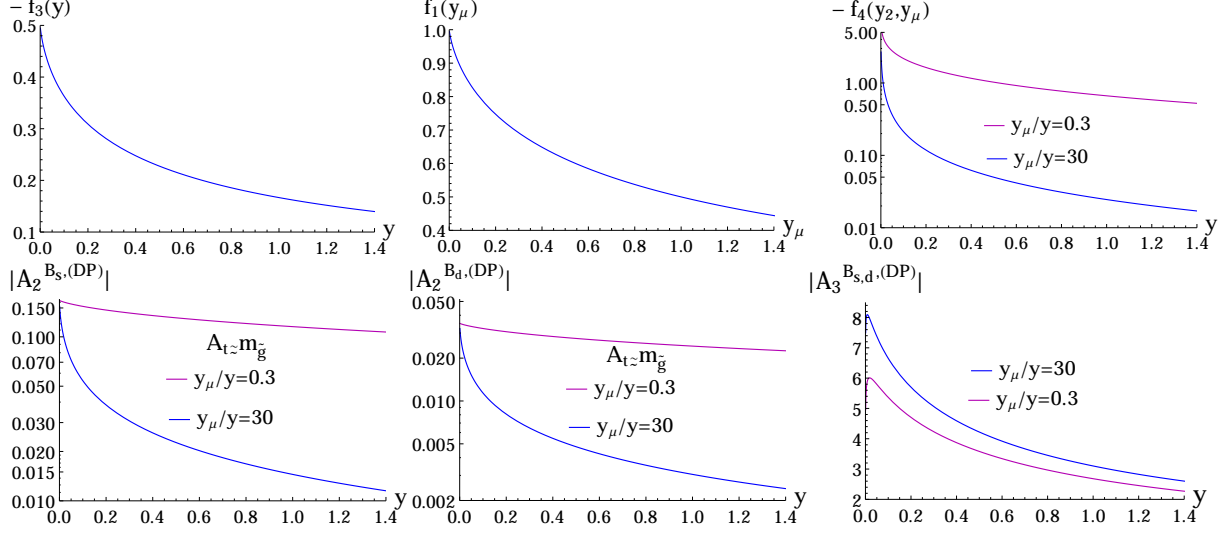


Figure 9: The dependence of the loop functions as well as $|A_{2,3}^{B_{q,(DP)}}|$ appearing in Eq. (4.30) on $y = (m_{\tilde{g}}/m_{\tilde{q}})^2$, $y_\mu = (\mu/m_{\tilde{q}})^2$ and $y_2 = (M_2/m_{\tilde{q}})^2 \approx 0.11 y$. The blue lines correspond to $y_\mu/y = 30$ and the magenta ones to $y_\mu/y = 0.3$. In the plots for $|A_2^{B_{q,(DP)}}|$, we have assumed that $A_t \approx m_{\tilde{q}}$.

where $i = 1(2)$ for $q = d(s)$ and

$$\begin{aligned}
A_1^{B_{q,(DP)}} &= \frac{\alpha_s \alpha_2^2 M_{B_q} f_{B_q}^2}{16\pi m_{\tilde{q}}^2} \left(\frac{M_{B_q}}{m_b + m_q} \right)^2 \frac{2m_b^2}{3M_W^2} y f_3(y), \\
A_2^{B_{q,(DP)}} &= \frac{A_t}{m_{\tilde{g}}} \frac{m_t^2}{M_W^2} V_{tb} V_{tq}^* f_1(y_\mu), \\
A_3^{B_{q,(DP)}} &= 2 \left(\frac{M_2}{m_{\tilde{g}}} f_4(y_2, y_\mu) - \frac{8}{3} \frac{\alpha_s}{\alpha_2} f_3(y) \right). \tag{4.31}
\end{aligned}$$

$y_\mu = (\mu/m_{\tilde{q}})^2$ and $y_2 = (M_2/m_{\tilde{q}})^2$ where the latter is related to $y = (m_{\tilde{g}}/m_{\tilde{q}})^2$ via the approximations of Eq. (4.2). The loop functions $f_3(y)$, $f_1(y_\mu)$, $f_4(y_2, y_\mu)$ are given in Appendix B. Their behaviour is sketched in Figure 9, along with that of $|A_{2,3}^{B_{q,(DP)}}|$. For $|A_t| > 500$ GeV, the dominant contribution to Eq. (4.30) comes from $A_2^{B_{d,(DP)}}$ in the B_d sector, even for our maximum values of $|(\delta_{LL}^d)_{13}|$, while for B_s , where $|(\delta_{LL}^d)_{23}|$ assumes larger values (cf. Figure 2), the two terms in the curly brackets are comparable. For light average squark masses $m_{\tilde{q}}$ around 2 TeV, $A_1^{B_{q,(DP)}}$ can reach values up to $\mathcal{O}(10^{-16})$ GeV, while $|(\delta_{RR}^d)_{i3}|_{\max} \approx 10^{-2}$ (cf. Figure 2). Then, for $A_t \gtrsim m_{\tilde{g}}$ and $\mu \ll m_{\tilde{q}}$, $|A_2^{B_{s(d),(DP)}}| \approx \mathcal{O}(10^{-1(-2)})$, such that $|\Delta M_{12}^{B_{s(d),(DP)}}| \approx 2 \times 10^{-19(-20)} \times t_\beta^4 \mu^2 / M_A^2$ GeV,

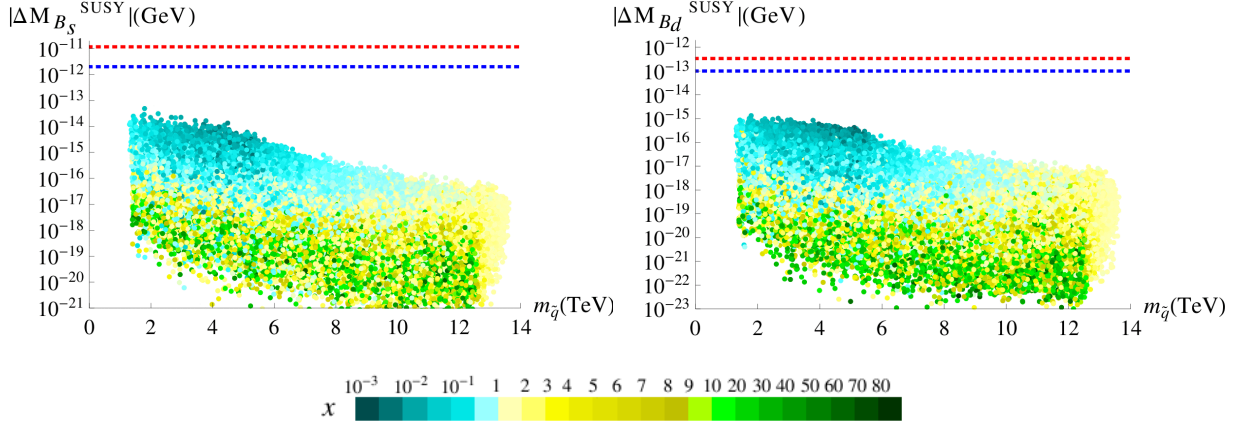


Figure 10: The absolute value of the gluino and double penguin contributions to $\Delta M_{B_{s(d)}}$ versus the average squark mass as defined in Eq. (4.19). The colour coding corresponds to different values of $x = (M_{1/2}/m_0)^2$. The red dotted lines denote the experimental central values of Eqs. (4.25,4.26), while the blue dotted lines indicate the maximum allowed NP contributions according to Eq. (4.28).

barring contributions from the $A_3^{B_q,(\text{DP})}$ term. When t_β takes its maximum value of 25 and $\mu \sim M_A$, the double penguin contributions to ΔM_{B_q} increase to about an order of magnitude above the gluino-box contributions, which is however still significantly below the SM and experimental values.

Figure 10 shows the predicted SUSY contributions to the B_q meson mixings as produced in our scan. They are plotted against the average squark mass defined in Eq. (4.19) and lie below both the experimental measurements (red dotted lines) and the NP limits (blue dotted lines) by at least an order of magnitude. This result is in agreement with the findings in Section 3.2.2, where we have compared our predictions for the mass insertion parameters with existing limits in the literature.

The effects of the complex down-type mass insertion parameters of the (23) and (13) sectors can be studied through the time dependent CP asymmetries associated with the decays $B_s \rightarrow J/\psi \phi$ and $B_d \rightarrow J/\psi K_S$. Focusing on the mixing-induced CP asymmetries, we have [53]

$$S_f = \frac{2 \text{Im}(\lambda_f)}{1 + |\lambda_f|^2}, \quad (4.32)$$

with

$$\lambda_f = \frac{q}{p} \frac{\bar{\mathcal{A}}(\bar{B}_q \rightarrow f)}{\mathcal{A}(B_q \rightarrow f)}, \quad \frac{q}{p} = \sqrt{\frac{M_{12}^{B_q^*} - \frac{i}{2}\Gamma_{12}^{B_q^*}}{M_{12}^{B_q} - \frac{i}{2}\Gamma_{12}^{B_q}}}, \quad (4.33)$$

where f denotes the final state of the decay and \mathcal{A} is the corresponding amplitude. As the absorptive part $\Gamma_{12}^{B_q}$ of the B_q meson mixing is much smaller than the dispersive one $M_{12}^{B_q}$, i.e. $\Gamma_{12}^{B_q} \ll M_{12}^{B_q}$, we can approximate $q/p \approx \sqrt{M_{12}^{B_q^*}/M_{12}^{B_q}}$. Then, the λ_f factors associated with the decays $B_s \rightarrow J/\psi \phi$ and $B_d \rightarrow J/\psi K_S$ take the form

$$\begin{aligned} \lambda_{J/\psi \phi} &= e^{-i\phi_s}, & \phi_s &= -2\beta_s + \arg(1 + h_{B_s} e^{2i\sigma_{B_s}}), \\ \lambda_{J/\psi K_S} &= -e^{-i\phi_d}, & \phi_d &= 2\beta + \arg(1 + h_{B_d} e^{2i\sigma_{B_d}}), \end{aligned} \quad (4.34)$$

where the parameters h_{B_q} and σ_{B_q} are defined in Eq. (4.16), while the SM phases β_s and β can be found in Eqs. (4.21,4.22). The mixing-induced time dependent asymmetries can then be simply written as

$$S_{J/\psi \phi} = -\sin(\phi_s), \quad S_{J/\psi K_S} = \sin(\phi_d). \quad (4.35)$$

The current measurements are [51]¹⁰

$$S_{J/\psi \phi} = 0.015 \pm 0.035, \quad S_{J/\psi K_S} = 0.682 \pm 0.019, \quad (4.36)$$

while the SM expectations read [55]

$$S_{J/\psi \phi}^{\text{SM}} = \sin(2\beta_s) = 0.0365_{-0.0013}^{+0.0012}, \quad S_{J/\psi K_S}^{\text{SM}} = \sin(2\beta) = 0.771_{-0.041}^{+0.017}. \quad (4.37)$$

$S_{J/\psi \phi}^{\text{SM}}$ comes with a relatively small error, whereas $S_{J/\psi K_S}^{\text{SM}}$ depends strongly on the value of $|V_{ub}|$, which differs significantly when extracted via inclusive or exclusive decays, see e.g. [46], with the above data preferring the lower exclusive result. The value of $S_{J/\psi K_S}^{\text{SM}}$ quoted in Eq. (4.37) has been derived by averaging over inclusive and exclusive semileptonic determinations of the relevant CKM elements and using the value of the CP-violating parameter ϵ_K , see Eq. (4.45), amongst the input parameters but not the measurement of $\sin(2\beta)$ itself.

¹⁰LHCb recently published their first measurements of $S_{J/\psi K_S} = 0.746 \pm 0.030$ [54] in the limit of a vanishing direct CP asymmetry, i.e. $\frac{1-|\bar{\mathcal{A}}(\bar{B}_q \rightarrow J/\psi K_S)/\mathcal{A}(B_q \rightarrow J/\psi K_S)|^2}{1+|\bar{\mathcal{A}}(\bar{B}_q \rightarrow J/\psi K_S)/\mathcal{A}(B_q \rightarrow J/\psi K_S)|^2} = 0$, thereby improving consistency with the SM expectation.

Comparing Eq. (4.36) and Eq. (4.37), we observe that the NP contributions to $S_{J/\psi\phi}$ and $S_{J/\psi K_S}$ can be as large as $\sim 100\%$ and $\sim 10\%$ of the respective SM values. In order to reach 10% deviations, h_{B_s} and h_{B_d} should be larger than $\sim 4 \times 10^{-3}$ and ~ 0.14 respectively, corresponding to $|\Delta M_{B_{s,d}}^{(\text{NP})}| \gtrsim 5 \times 10^{-14}$. Here we have assumed NP phases which maximise the effect. In view of Figure 10, we would expect a non-negligible contribution to $S_{J/\psi\phi}$ in a small part of the parameter space. However, at leading order, $(\delta_{LL}^d)_{23}$ and $(\delta_{RR}^d)_{23}$ are real, cf. Eqs. (A.31,A.33). They only receive non-trivial phase factors at order λ^5 , suppressing the imaginary part of $\Delta M_{B_s}^{\text{SUSY}}$ by one power of $\lambda \approx 10^{-1}$ with respect to the real part. As a result, any deviation from $S_{J/\psi\phi}^{\text{SM}}$ is only of the order of 1%. In the B_d sector, $(\delta_{LL}^d)_{13}$ and $(\delta_{RR}^d)_{13}$ are already complex at leading order in λ , cf. Eqs. (A.30,A.32). But as can be seen from Figure 10, $|\Delta M_{B_d}^{\text{SUSY}}|_{\text{max}} \approx 10^{-15}$ is too small to be relevant. Even for $|\Delta M_{B_d}^{\text{SUSY}}| \approx 10^{-14}$, the maximum deviation from $S_{J/\psi K_S}^{\text{SM}}$ would be $\sim 3\%$ at most.

In conclusion, our model would not be able to explain any persistent deviations from SM expectations in observables related to B meson mixing.

4.3.2 $K - \bar{K}$ mixing

The SM contribution to the Kaon mixing reads [46]

$$M_{12}^{K,\text{SM}} = \frac{G_F^2 M_K}{12\pi^2} M_W^2 \left((V_{cs} V_{cd}^*)^2 \eta_{cc} S_0(x_c) + (V_{ts} V_{td}^*)^2 \eta_{tt} S_0(x_t) + \right. \\ \left. + 2V_{cs} V_{cd}^* V_{ts} V_{td}^* \eta_{ct} S_0(x_c, x_t) \right) f_K^2 \hat{B}_K, \quad (4.38)$$

where η_i are QCD factors, \hat{B}_K denotes a perturbative parameter and $S_0(x_i \equiv \bar{m}_i^2(\bar{m}_i)/M_W^2)$ are the Inami-Lim loop functions [47]. From this, the SM value for the Kaon mass difference is numerically given by [56]

$$\Delta M_K^{(\text{SM})} = 3.30(34) \times 10^{-15} \text{ GeV}, \quad (4.39)$$

while the experimental measurement yields [57]

$$\Delta M_K^{(\text{exp})} = 3.484(6) \times 10^{-15} \text{ GeV}. \quad (4.40)$$

We therefore impose the constraint that the maximum allowed NP contribution should be limited by

$$\Delta M_K^{(\text{NP})} \leq 5 \times 10^{-16} \text{ GeV}. \quad (4.41)$$

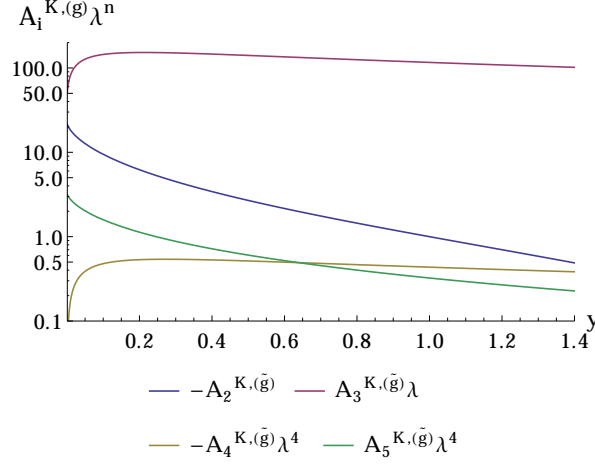


Figure 11: The dependence of the individual contributions in Eq. (4.42) on $y = (m_{\tilde{g}}/m_{\tilde{q}})^2$. The average squark mass $m_{\tilde{q}}$ is defined in Eq. (4.19) while the functions $A_i^{K,(\tilde{g})}$ can be found in Eq. (4.18).

For Kaon mixing, the relevant mass insertion parameters are those of the (12) sector. Taking into account their λ -suppression, we can write the gluino-box contribution to the mixing amplitude, given in Eq. (4.17), in the schematic form

$$\Delta M_K^{(\tilde{g})} \propto \lambda^6 \left(A_2^{K,(\tilde{g})} + A_3^{K,(\tilde{g})} \lambda + A_4^{K,(\tilde{g})} \lambda^4 + A_5^{K,(\tilde{g})} \lambda^4 \right). \quad (4.42)$$

Figure 11 depicts the individual contributions as a function of $y = (m_{\tilde{g}}/m_{\tilde{q}})^2$. It shows that the dominant contribution originates from the term proportional to $A_3^{K,(\tilde{g})}$, i.e. the term proportional to $(\delta_{LL}^d)_{21}(\delta_{RR}^d)_{21}$, see Eq. (4.17). The effects of the LR -type δ s, proportional to $A_{4,5}^{K,(\tilde{g})}$, are negligible. Using Eqs. (4.15,4.17) together with Figure 11, we can estimate the maximum gluino contributions to $|\Delta M_K|$. Assuming $y \approx 0.3$, $A_1^{K,(\tilde{g})} \approx 10^{-13}$ GeV and $(\delta_{LL}^d)_{21} \approx 5 \times 10^{-2}$, $(\delta_{RR}^d)_{21} \approx 7 \times 10^{-3}$ (cf. Figure 2), we expect that $|\Delta M_K^{(\tilde{g})}|_{\max} \approx 5 \times 10^{-14}$ GeV, which is about one order of magnitude larger than the experimental result of Eq. (4.40).

The double penguin (DP) contributions to ΔM_K arise at the level of four mass insertions, by effectively generating the $(s \rightarrow d)$ transitions through $(s \rightarrow b)$ followed by $(b \rightarrow d)$. The relevant part of the mixing amplitude takes the form [15]

$$M_{12}^{K,(\text{DP})} = \frac{\alpha_s^2 \alpha_2}{16\pi} M_K f_K^2 \left(\frac{M_K}{m_s + m_d} \right)^2 \frac{32m_b^2}{9M_W^2} \frac{t_\beta^2 \mu^2}{M_A^2 m_{\tilde{q}}^2} y (f_5(y))^2 \times \quad (4.43)$$

$$\times (\delta_{LL}^d)_{23}(\delta_{LL}^d)_{31}(\delta_{RR}^d)_{23}(\delta_{RR}^d)_{31}, \quad (4.44)$$

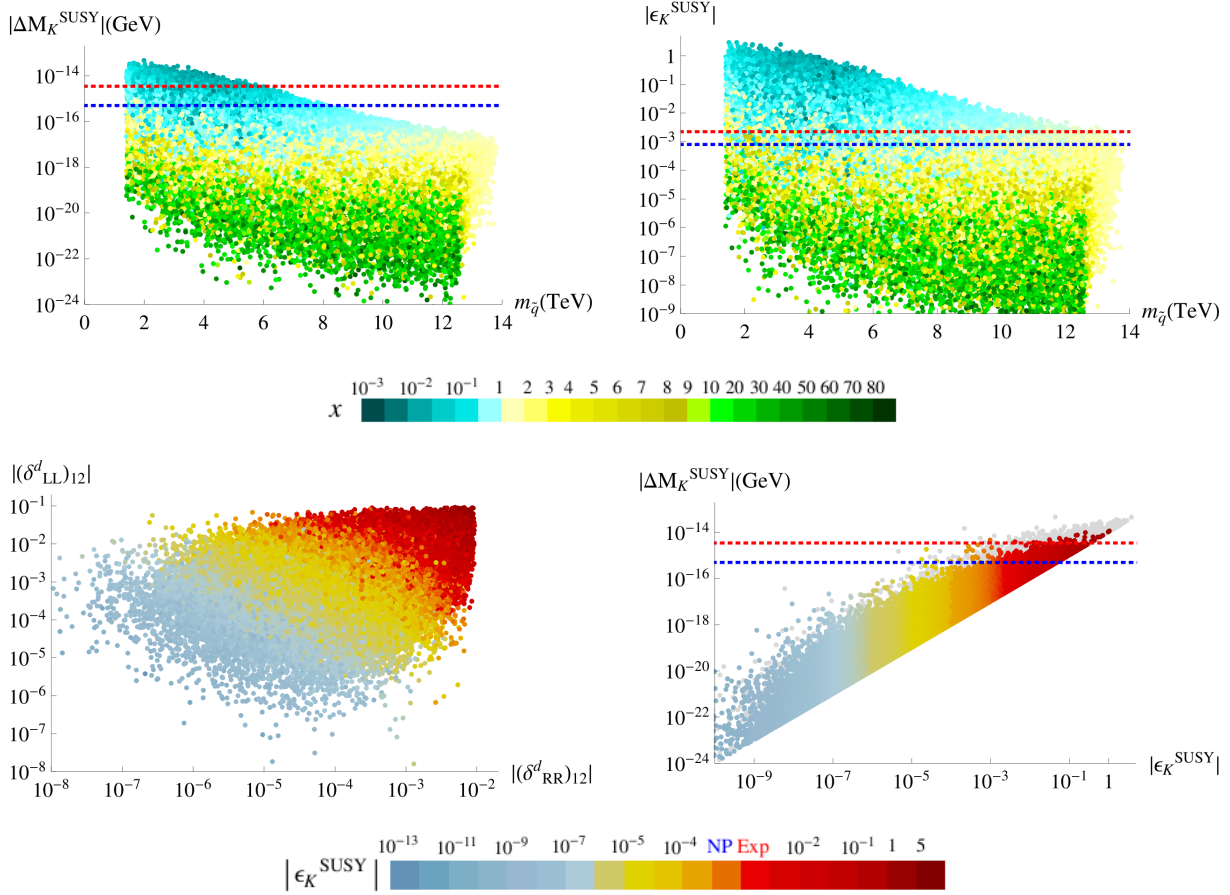


Figure 12: Upper panels: the absolute value of SUSY contributions to ΔM_K (left) and ϵ_K (right) plotted against the average squark mass defined in Eq. (4.19), with the different colours corresponding to different values of $x = (M_{1/2}/m_0)^2$. Lower panels: the most important mass insertion parameters, relevant for K mixing (left) with different colours representing the produced value of $|\epsilon_K^{\text{SUSY}}|$; $|\Delta M_K^{\text{SUSY}}|$ versus $|\epsilon_K^{\text{SUSY}}|$ (right), with the grey shaded points being excluded by $BR(\mu \rightarrow e\gamma)$. The red dotted lines indicate the experimentally observed values, while the blue dotted lines show the limits on NP contributions.

with the loop function $f_5(y)$ given in Appendix B. We find that this contribution is completely negligible, as it is proportional to λ^{14} . The upper left panel of Figure 12 shows the combined gluino and DP SUSY contribution to ΔM_K , as produced in our scan. It can exceed the NP limit quoted in Eq. (4.41) (blue dotted line) for small values of x , even shooting above the experimental value of Eq. (4.40) (red dotted line) for $x \ll 1$.

We now turn to the CP-violating parameter ϵ_K , defined as [46]

$$\epsilon_K = \frac{\kappa_\epsilon e^{i\varphi_\epsilon}}{\sqrt{2}\Delta M_K^{\text{exp.}}} \left(\text{Im}(M_{12}^{K,\text{SM}}) + \text{Im}(M_{12}^{K,\text{SUSY}}) \right), \quad (4.45)$$

where the superweak phase¹¹ $\varphi_\epsilon = \arctan(2\Delta M_K/\Delta\Gamma) = (43.52 \pm 0.05)^\circ$ [57], and the factor $\kappa_\epsilon = 0.94 \pm 0.02$ [58] takes into account that $\varphi_\epsilon \neq \pi/4$ and includes long distance contributions. The experimentally measured value of ϵ_K is [57]

$$\epsilon_K^{(\text{exp})} = (2.228 \pm 0.011) \times 10^{-3} \times e^{i\varphi_\epsilon}, \quad (4.46)$$

while the SM prediction depends highly on the value of V_{cb} [46]. According to [59] and for the input set from the angle-only fit [60], where the Wolfenstein parameters do not show an unwanted correlation with ϵ_K and \hat{B}_K , one finds

$$\begin{aligned} |\epsilon_K^{(\text{SM})}| &= 2.17(24) \times 10^{-3} \text{ (inclusive } V_{cb}), \\ |\epsilon_K^{(\text{SM})}| &= 1.58(18) \times 10^{-3} \text{ (exclusive } V_{cb}). \end{aligned} \quad (4.47)$$

We therefore demand that

$$|\epsilon_K^{(\text{NP})}| \leq 0.8 \times 10^{-3}. \quad (4.48)$$

The upper right panel of Figure 12 shows the absolute value of our predicted SUSY contribution to ϵ_K , plotted against the average squark mass. We find that it can exceed the limit of Eq. (4.48) by more than three orders of magnitude when $x < 1$. In view of Figure 2, we would not have expected such a big effect. However, the limits on the mass insertion parameters used in Section 3.2.2, only take into account one non-zero mass insertion at a time. As we have seen in this section, the dominant contribution to the Kaon mixing amplitude stems from the multiple δ term $A_3^{K,(\tilde{g})}(\delta_{LL}^d)_{21}(\delta_{RR}^d)_{21}$ (cf. Figure 11). The non-zero phase of the RR parameter is the source of our prediction of a large $|\epsilon_K^{\text{SUSY}}|$.

The lower left panel of Figure 12 shows $|\epsilon_K^{\text{SUSY}}|$ in the $|(\delta_{LL}^d)_{12}| - |(\delta_{RR}^d)_{12}|$ plane. It indicates that for $|(\delta_{LL}^d)_{12}| \sim 5 \times 10^{-2}$, i.e. towards the largest possible value according to Figure 2, $|(\delta_{RR}^d)_{12}| \lesssim 10^{-5}$ is required. When $|(\delta_{RR}^d)_{12}|$ takes its maximum value of $\sim 10^{-2}$, $|(\delta_{LL}^d)_{12}|$ should stay below $\sim 10^{-4}$.

Finally, from the lower right panel of Figure 12 we observe that ϵ_K places stronger bounds on the mass insertion parameters than ΔM_K . Due to the $SU(5)$ framework of our model there is a correlation between the δ parameters relevant in Kaon mixing and

¹¹ $\Delta\Gamma$ denotes the difference of the widths.

the ones that enter the branching ratio of $(\mu \rightarrow e\gamma)$. Denoting the points excluded by $BR(\mu \rightarrow e\gamma)$ with a grey shade reveals that there still remains a small area of parameter space which is excluded by ϵ_K .

4.4 $BR(b \rightarrow s\gamma)$

We now consider the gluino contribution to the branching ratio of $b \rightarrow s\gamma$. In terms of the relevant mass insertion parameters it is given by [11]

$$BR(b \rightarrow s\gamma) = \frac{\alpha_s^2 \alpha}{81\pi^2 m_{\tilde{q}}^4} m_b^3 \tau_B \left(|m_b M_3(y)(\delta_{LL}^d)_{23} + m_{\tilde{g}} M_1(y)(\delta_{LR}^d)_{23}|^2 + L \leftrightarrow R \right), \quad (4.49)$$

where the loop functions $M_1(y)$, $M_3(y)$ are defined in Appendix B, τ_B denotes the mean life of the B meson and $y = (m_{\tilde{g}}/m_{\tilde{q}})^2$. This observable does not constrain our parameter space. Even for squark masses as low as 100 GeV and $y = 1$, the LL and RR mass insertion parameters would only need to be smaller than 0.4 to be consistent with the current experimental value of [51]

$$BR(B \rightarrow X_s \gamma) = (3.43 \pm 0.21 \pm 0.07) \times 10^{-4}, \quad (4.50)$$

which is in good agreement with the SM prediction [61]. Similarly, the chirality flipping mass insertion parameters would need to be smaller than 3×10^{-3} . In our scan we find, cf. Figure 2, $(\delta_{LL}^d)_{23} \lesssim 10^{-2}$, $(\delta_{RR}^d)_{23} \lesssim 10^{-2}$, $(\delta_{LR}^d)_{23} \lesssim 10^{-5}$ and $(\delta_{RL}^d)_{23} \lesssim 10^{-6}$. Taking into account the squark mass dependence and the fact that our scan excludes such light squarks, we have found that our model predicts a contribution to $BR(b \rightarrow s\gamma)$ which is at least three orders of magnitude below the experimental measurement.

4.5 $BR(B_{s,d} \rightarrow \mu^+ \mu^-)$

The most recent SM predictions for the branching ratios of $B_{s,d} \rightarrow \mu^+ \mu^-$ are given by [62]

$$\begin{aligned} BR(B_s \rightarrow \mu^+ \mu^-)^{(\text{SM})} &= (3.65 \pm 0.23) \times 10^{-9}, \\ BR(B_d \rightarrow \mu^+ \mu^-)^{(\text{SM})} &= (1.06 \pm 0.09) \times 10^{-10}, \end{aligned} \quad (4.51)$$

while the averages of the CMS and LHCb collaborations read [63]

$$\begin{aligned} BR(B_s \rightarrow \mu^+ \mu^-)^{(\text{exp.})} &= 2.8_{-0.6}^{+0.7} \times 10^{-9}, \\ BR(B_d \rightarrow \mu^+ \mu^-)^{(\text{exp.})} &= 3.9_{-1.4}^{+1.6} \times 10^{-10}. \end{aligned} \quad (4.52)$$

The B_d sector therefore still allows for rather large relative deviations from the SM expectations. In the case of B_s the experimental measurement yields a value which is slightly lower than the SM prediction.¹² We therefore quote the allowed room for contributions from new physics as

$$\begin{aligned} BR(B_s \rightarrow \mu^+ \mu^-)^{(\text{NP})} &\leq 1.68 \times 10^{-9}, \\ BR(B_d \rightarrow \mu^+ \mu^-)^{(\text{NP})} &\leq 4.53 \times 10^{-10}. \end{aligned} \quad (4.53)$$

The chargino and gluino contributions to the branching ratio of $B_{s,d} \rightarrow \mu^+ \mu^-$ can be expressed as [15]

$$\begin{aligned} BR(B_q \rightarrow \mu^+ \mu^-) &= \frac{\tau_{B_q} f_{B_q}^2 M_{B_q}^3}{32\pi} \sqrt{1 - 4 \frac{m_\mu^2}{M_{B_q}^2}} \times \\ &\times \left\{ \left| \mathcal{A}_1^{B_q} \left[\mathcal{A}_2^{B_q} - \frac{\alpha_s}{\alpha_2} f_3(y) ((\delta_{LL}^d)_{i3} - (\delta_{RR}^d)_{i3}) \right] \right|^2 \left(1 - 4 \frac{m_\mu^2}{M_{B_q}^2} \right) \right. \\ &\left. + \left| 2 \frac{m_\mu}{M_{B_q}} C_{10}^{\text{SM}} + \mathcal{A}_1^{B_q} \left[\mathcal{A}_2^{B_q} - \frac{\alpha_s}{\alpha_2} f_3(y) ((\delta_{LL}^d)_{i3} + (\delta_{RR}^d)_{i3}) \right] \right|^2 \right\}, \end{aligned} \quad (4.54)$$

where

$$\begin{aligned} \mathcal{A}_1^{B_q} &= \alpha_2^2 t_\beta^3 \frac{M_{B_q} m_\mu}{4M_W^2} \frac{m_{\tilde{g}} \mu}{M_A^2 m_{\tilde{q}}^2}, \quad \mathcal{A}_2^{B_q} = \frac{m_t^2}{M_W^2} \frac{A_t}{m_{\tilde{g}}} V_{tb} V_{tq}^* f_1(y_\mu) + \frac{M_2}{m_{\tilde{g}}} (\delta_{LL}^u)_{i3} f_4(y_2, y_\mu), \\ C_{10}^{\text{SM}} &= \frac{\alpha_2}{4\pi} \frac{4G_F}{\sqrt{2}} V_{tb} V_{tq}^* Y_0(x_t), \quad Y_0(x) = \frac{x}{8} \left(\frac{x-4}{x-1} + \frac{3x}{(x-1)^2} \ln(x) \right), \end{aligned} \quad (4.55)$$

with $x_t = m_t^2/M_W^2$ and $i = 1(2)$ for $q = d(s)$. The loop functions $f_1(y_\mu)$, $f_3(y)$ and $f_4(y_2, y_\mu)$ are the ones which appear in the double penguin contributions to B_q mixing in Section 4.3.1. With $C_{10}^{\text{SM}} = 0$ and $A_t \gtrsim 100$ GeV, the dominant contribution to Eq. (4.54) originates from the flavour blind term of $\mathcal{A}_2^{B_q}$, such that we can make the approximation

$$BR(B_{s(d)} \rightarrow \mu^+ \mu^-) \approx \mathcal{O} \left(\frac{6 \times 10^{-6} (1 \times 10^{-7}) \text{GeV}^4}{m_{\tilde{q}}^4} t_\beta^6 \frac{A_t^2 \mu^2}{M_A^4} f_1^2(y_\mu) \right). \quad (4.56)$$

¹²The calculations in [62] have been performed using the inclusive value of $|V_{cb}|$. Working with the exclusive one would result in a lower central value of $BR(B_s \rightarrow \mu^+ \mu^-)^{(\text{SM})} = 3.1 \times 10^{-9}$ which fully agrees with the data [64].

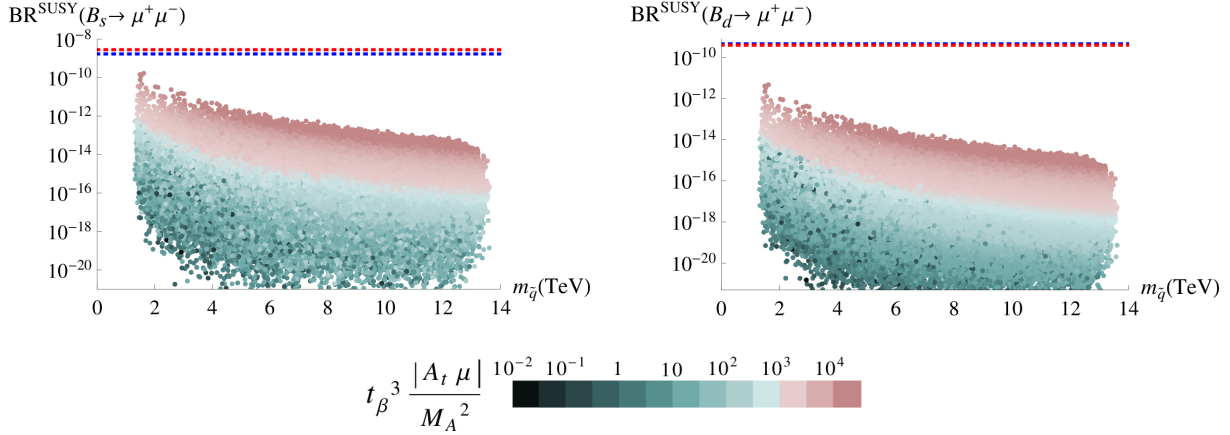


Figure 13: The SUSY contributions to the branching ratios of $B_q \rightarrow \mu^+ \mu^-$ versus the average squark mass $m_{\tilde{q}}$, defined in Eq. (4.19). The red dotted lines denote the experimental measurements, while the blue dotted lines indicate the maximum NP contributions.

Then, for $|A_t \mu|/M_A^2 \approx \mathcal{O}(1)$, $m_{\tilde{q}} \approx 2$ TeV, $t_\beta \approx 25$ and $f_1(y_\mu)$ receiving its maximum value of order one (cf. Figure 9), we expect $BR(B_{s(d)} \rightarrow \mu^+ \mu^-) \approx \mathcal{O}(10^{-10(-12)})$.

In Figure 13, we plot our predicted SUSY contributions to the branching ratios of $B_q \rightarrow \mu^+ \mu^-$ against the average squark mass $m_{\tilde{q}}$, defined in Eq. (4.19). The red dotted lines denote the experimental measurements, while the blue ones correspond to the limits for the NP contributions as given in Eq. (4.53). In both sectors, B_s and B_d , our maximum predictions fall about an order of magnitude below these limits.¹³

4.6 Neutron and ^{199}Hg EDMs

CP-violating effects in the quark sector can manifest themselves through the quark EDMs as well as the quark Chromo Electric Dipole Moments (CEDMs). The gluino contributions read [15, 67, 68]

$$\left\{ \frac{d_{q_i}}{e}, d_{q_i}^C \right\} = \frac{\alpha_s}{4\pi} \frac{m_{\tilde{g}}}{m_{\tilde{q}}^2} \text{Im} [(\delta_{LL}^q)_{ik} (\delta_{LR}^q)_{kj} (\delta_{RR}^q)_{ji}] \{Q_q \mathcal{F}_q(y), \mathcal{F}_q^C(y)\}, \quad (4.57)$$

¹³As discussed in [65] and also in [66], the theory prediction in Eq. (4.54) should take into account the large width difference between the mass eigenstates of the B_s system. This correction enhances the corresponding branching ratio by about 10%. Given the smallness of the new physics contribution in our model, it does, however, not change our results significantly.

with

$$\mathcal{F}_q(y) = -\frac{8}{3}N_1(y), \quad \mathcal{F}_q^C(y) = \left(\frac{1}{3}N_1(y) + 3N_2(y)\right), \quad (4.58)$$

where Q_q denotes the electric charge of quark q and the loop functions $N_1(y)$, $N_2(y)$, with $y = (m_{\tilde{g}}/m_{\tilde{q}})^2$, are given in Appendix B. As the first generation squarks dominate Eq. (4.57), we use the average squark masses

$$m_{\tilde{u}} = \sqrt{m_{\tilde{u}_{LL}} m_{\tilde{u}_{RR}}}, \quad m_{\tilde{d}} = \sqrt{m_{\tilde{d}_{LL}} m_{\tilde{d}_{RR}}}, \quad (4.59)$$

with $m_{\tilde{q}_{LL(RR)}}$ given in Eqs. (A.10,A.11).

Similar to the case of the electron EDM, we consider the most general scenario where the phases of the soft trilinear sector are different from the corresponding Yukawa ones. Then the dominant contributions of Eq. (4.57) arise from the single mass insertions with $i = j = k = 1$,

$$\text{Im}[(\delta_{LR}^u)_{11}] \propto \text{Im}[\tilde{a}_{11}^u] \lambda^8, \quad \text{Im}[(\delta_{LR}^d)_{11}] \propto \text{Im}[\tilde{a}_{11}^d] \lambda^6, \quad (4.60)$$

where \tilde{a}_{ij}^f is defined in Eq. (A.2). The double and triple mass insertions start contributing at orders λ^{12} and λ^8 for the up and down quark (C)EDMs, respectively.

If, however, the phases of the soft trilinear and Yukawa sectors are aligned, \tilde{a}_{ij}^f is real. In the case of the up quark sector, one should then check¹⁴ whether the NLO corrections to $\text{Im}[(\delta_{LR}^u)_{11}]$ also vanish, before assuming that the term $\text{Im}[(\delta_{LL}^u)_{13}(\delta_{LR}^u)_{33}(\delta_{RR}^u)_{31}] \propto \sin(4\theta_2^d - \theta_3^d)\lambda^{12}$ dominates. The situation in the down sector is such that the NLO correction to $(\delta_{LR}^d)_{11}$ gives a non-vanishing contribution to the (C)EDMs. Explicitly, we find $\text{Im}[(\delta_{LR}^d)_{11}]_{\text{NLO}} \propto \sin(4\theta_2^d + \theta_3^d)\lambda^7$, while the smallest contribution from multiple mass insertions is $\text{Im}[(\delta_{LL}^d)_{12\text{NLO}}(\delta_{LR}^d)_{21}] \propto \sin(\theta_2^d)\lambda^9$.

In order to compare the gluino contributions of our model according to Eq. (4.57) with the experimental limits, we take into account the RG running from the SUSY scale down to the hadronic scale, using the LO results of [69], for $\alpha_s(\mu_S \approx 1\text{TeV}) \approx 0.089$ and $\alpha_s(\mu_H \approx 1\text{GeV}) \approx 0.358$ [70]. Then,

$$\begin{aligned} d_{q_i}^C(\mu_H) &\approx 0.87 d_{q_i}^C(\mu_S), \\ \frac{d_{q_i}}{e}(\mu_H) &\approx 0.38 \frac{d_{q_i}}{e}(\mu_S) - 0.39 Q_q d_{q_i}^C(\mu_S), \end{aligned} \quad (4.61)$$

with $d_{q_i}^{(C)}(\mu_S)$ as given in Eq. (4.57).

¹⁴We have truncated our expansion at the order of λ^8 .

With these preparations, we can study the predictions for the neutron and the ^{199}Hg EDMs. Adopting the QCD sum rules approach, the neutron EDM at the renormalisation scale $\mu = 1 \text{ GeV}$ is given in terms of the QCD $\bar{\theta}$ -term and the quark (C)EDMs by [42]

$$\frac{d_n}{e} = 8.2 \times 10^{-17} \text{ cm } \bar{\theta} - 0.12 \frac{d_u}{e} + 0.78 \frac{d_d}{e} + (-0.3 d_u^C + 0.3 d_d^C - 0.014 d_s^C), \quad (4.62)$$

while the current experimental limit is [71]

$$|d_n/e| \leq 2.9 \times 10^{-26} \text{ cm} \approx 1.47 \times 10^{-12} \text{ GeV}^{-1}. \quad (4.63)$$

The quark (C)EDMs can also be probed through measurements of the EDMs of atomic systems, where ^{199}Hg provides the best upper limit amongst the diamagnetic systems [72]

$$|d_{\text{Hg}}/e| \leq 3.1 \times 10^{-29} \text{ cm} \approx 1.57 \times 10^{-15} \text{ GeV}^{-1}. \quad (4.64)$$

However, large theoretical uncertainties in the atomic and in particular the nuclear calculations prevent the extraction of bounds on $d_{q_i}^{(C)}$. Eq. (4.64) limits the nuclear Schiff moment as [73]

$$S_{\text{Hg}} \leq 1.45 \times 10^{-12} |e| \text{ fm}^3, \quad (4.65)$$

which, assuming it is dominated by pion-nucleon interactions, can be expressed as [74]

$$S_{\text{Hg}} = 13.5 \left(0.01 \bar{g}_{\pi NN}^{(0)} + (\pm) 0.02 \bar{g}_{\pi NN}^{(1)} + 0.02 \bar{g}_{\pi NN}^{(2)} \right). \quad (4.66)$$

In this equation, the $\bar{g}_{\pi NN}^{(i)}$ denote the pion-nucleon couplings. Their coefficients in Eq. (4.66) are the best fit values taken from the review article [74], which assesses the strengths and weaknesses of different, sometimes contradictory, nuclear calculations provided in the literature. Combining Eqs. (4.65,4.66) with the relation

$$\bar{g}_{\pi NN}^{(1)} = 2 \times 10^{-12} (d_u^C - d_d^C), \quad (4.67)$$

which was derived in [75], it can be inferred that [73]

$$|(d_u^C - d_d^C)/e| \leq 2.8 \times 10^{-26} \text{ cm} \approx 1.42 \times 10^{-12} \text{ GeV}^{-1}. \quad (4.68)$$

However, this bound only applies if the coefficient of $\bar{g}_{\pi NN}^{(1)}$ in Eq. (4.66) takes its best fit value. In principle, it could also be zero, in which case no bound on $|(d_u^C - d_d^C)/e|$ could be extracted.

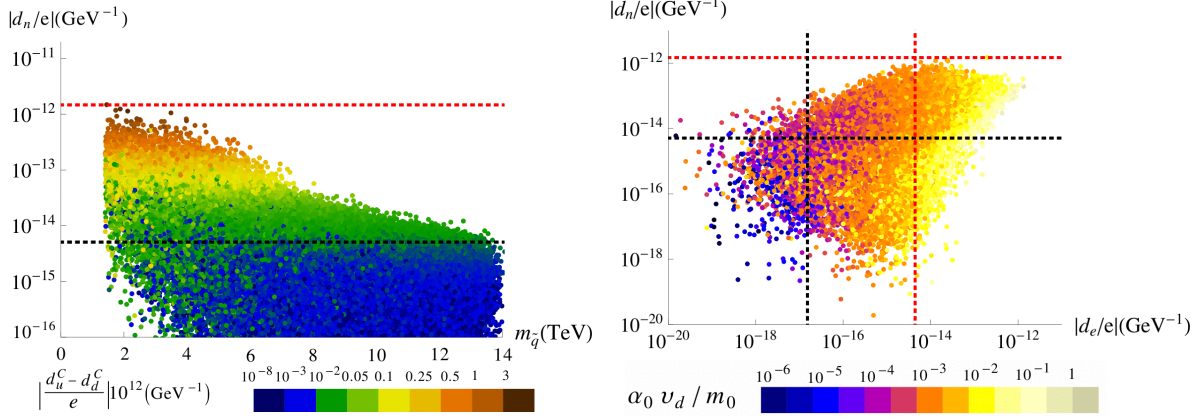


Figure 14: The neutron EDM versus the average squark mass $m_{\bar{q}} = \sqrt{m_{\bar{u}} m_{\bar{d}}}$, with $m_{\bar{u}}$ and $m_{\bar{d}}$ as defined in Eq. (4.59) (left panel) and versus the electron EDM (right panel). The red dotted lines denote the current experimental limits as given in Eqs. (4.63,4.3) and the black dotted lines the future limits $|d_n/e| \lesssim 10^{-28} \text{ cm} \approx 5 \times 10^{-15} \text{ GeV}^{-1}$ and $|d_e/e| \lesssim 3 \times 10^{-31} \text{ cm} \approx 1.52 \times 10^{-17} \text{ GeV}^{-1}$ [42].

In the left panel of Figure 14, we show our prediction for the neutron EDM versus the average first generation squark mass $m_{\bar{q}} = \sqrt{m_{\bar{u}} m_{\bar{d}}}$. For squark masses less than about 6 TeV, it lies just below the red line denoting the experimental limit in Eq. (4.63). For heavier squarks it stays below the limit by at least one order of magnitude. The colour coding corresponds to the predicted value of $|(d_u^C - d_d^C)/e| \times 10^{12} \text{ GeV}^{-1}$, which can also reach the limit in Eq. (4.68) for large $|d_n/e|$ values. In the right panel of Figure 14, the neutron and electron EDMs are plotted against each other. They are of the same order of magnitude, but it is the current electron EDM limit that constrains our parameter space. When the future experimental limits are reached, only the small part lying in the lower left corner bounded by the black dotted lines will survive.

5 Conclusions

In a recent paper we showed how MFV can emerge approximately from an $SU(5)$ SUSY GUT whose flavour structure is controlled by the family symmetry $S_4 \times U(1)$ [1], providing a good description of all quark and lepton masses, mixings as well as CP violation. We showed that the model leads to mass insertion parameters in Eqs. (2.16,2.17,2.18) which very closely resemble the MFV forms, where $\delta_{LL,RR}^{u,d,e}$ are unit matrices and $\delta_{LR}^{u,d,e}$ are proportional to the Yukawa matrices.

Whereas in [1] we focused on the similarity to MFV, here we highlight the differences, which we do by considering the predictions for electric dipole moments, lepton flavour

d_e	$\mu \rightarrow e\gamma$	$\Delta M_{B_{s,d}}$	$S_{J/\psi\phi}$	$S_{J/\psi K_S}$	ΔM_K	ϵ_K	$B_{s,d} \rightarrow \mu^+\mu^-$	d_n
★ ★ ★	★ ★ ★	★	★	★	★★	★ ★ ★	★	★★

Table 7: The flavour “DNA” of our $SU(5) \times S_4 \times U(1)$ SUSY GUT model following the labelling proposed in [15]. The predicted contributions to the various flavour observables are classified into three categories: ★ ★ ★ indicates large observable effects while visible but small effects are marked by ★★. The absence of sizable effects is shown by ★.

violation, B and K meson mixing as well as rare B decays. As expected, many of the new physics contributions fall well below current limits. This is the case for example in B physics observables, where deviations are negligible (at the 1% level). Thus, our model would be unable to explain any discrepancies between SM expectations and measurements in $\Delta M_{B_{s,d}}$ or in the time dependent asymmetries $S_{J/\psi\phi}$ and $S_{J/\psi K_S}$. This is in marked contrast to the $SU(3)$ family symmetry models previously studied, where large effects were expected in these observables. Thus, neutrino physics which led to $S_4 \times U(1)$, appears to lead us towards models with small such deviations.

On the other hand there are observable effects which would distinguish the $SU(5) \times S_4 \times U(1)$ SUSY GUT model from MFV. The most significant effects of the departure from MFV appear in the (12) down-type quark and charged lepton sectors, related to Kaon mixing observables and the branching ratio of $\mu \rightarrow e\gamma$. We find that $(\delta_{LL}^e)_{12}$ provides the dominant contribution to $\text{BR}(\mu \rightarrow e\gamma)$ and that our model requires rather heavy sleptons, exceeding about 1 TeV, in order to satisfy the experimental bound. Another important area where our model gives observable deviations from MFV is CP violation, in particular the electron EDM, where again large (TeV scale) slepton masses are required for compatibility with current bounds to be achieved. The model therefore predicts that a signal should be observed in both $\mu \rightarrow e\gamma$ and the electron EDM within the expected future sensitivity of these experiments.

Turning to CP violation in the Kaon system, the model contributes significantly to ϵ_K due to the phase of $(\delta_{RR}^d)_{12}$. The SM prediction for this observable depends sensitively on $|V_{cb}|$, which differs when considering inclusive or exclusive decays, leading to a lower central value in the latter case. However, even for inclusive values of $|V_{cb}|$, the SM expectation for ϵ_K is about 10% below the measurement. Our model is capable of providing sufficient enhancement to explain the experimentally observed value of ϵ_K .

We collect our findings in Table 7, where we classify various flavour observables according to the expected size of our model’s predictions. Large observable effects are indicated by ★ ★ ★, while visible but small effects are labelled by ★★. A single star ★ shows the absence of sizable effects on a particular flavour observable. This classification, which was first suggested in [15], is undoubtedly somewhat vague by nature and therefore limited in

its scope. Yet, it has proved to be a useful tool in comparing characteristic predictions of various models of flavour. Table 8 of [15] shows the expected predictions of a selection of different models. Comparing this table with our model’s DNA, see Table 7, demonstrates the specific signatures of our $SU(5) \times S_4 \times U(1)$ SUSY GUT of flavour. According to the phenomenological study in [15], all of the discussed models which predict large effects on ϵ_K also predict large contributions to $S_{J/\psi\phi}$. In contrast, our model features large contributions to ϵ_K in conjunction with negligible effects on $S_{J/\psi\phi}$. Furthermore, all SUSY models in [15] entail large contributions to $B_s \rightarrow \mu^+\mu^-$ while such contributions are tiny in our model. Those models in [15] which lead to a large electron EDM (d_e) also predict a large neutron EDM (d_n). Again, our model differs from this pattern by predicting large observable d_e together with only small d_n . Concerning $\mu \rightarrow e\gamma$ we observe that sizable effects are expected for our model as well as all flavour models scrutinised in [15]. This comparison illustrates that the phenomenological signatures of our $SU(5) \times S_4 \times U(1)$ SUSY GUT are indeed quite different from those of previously discussed flavour models.

In summary, theories with discrete flavour symmetries such as the $SU(5) \times S_4 \times U(1)$ SUSY GUT model, motivated by neutrino physics, seem to lead to MFV-like flavour changing expectations, but with some important exceptions. This study shows that, while observable deviations in B physics are generally not expected to show up, departures from MFV are expected in both $\mu \rightarrow e\gamma$ and the electron EDM within the foreseeable future sensitivity of these experiments. CP violating effects may also be observed in ϵ_K , perhaps resolving some possible SM discrepancies.

Acknowledgements

We thank Claudia Hagedorn for helpful discussions throughout this project. MD and SFK acknowledge partial support from the STFC Consolidated ST/J000396/1 grant and the European Union FP7 ITN-INVISIBLES (Marie Curie Actions, PITN-GA-2011-289442). CL is supported by the Deutsche Forschungsgemeinschaft (DFG) within the Research Unit FOR 1873 “Quark Flavour Physics and Effective Field Theories”.

Appendix

A Low energy mass insertion parameters

In this appendix, we show explicitly the full expressions of the low energy mass insertion parameters used in our numerical analysis. They are given in terms of the high energy

order one coefficients introduced in Section 2. Performing the transformation to the SCKM basis, it is useful to define the corresponding GUT scale parameters

$$\tilde{b}_{12} = (b_2 - b_{01}k_2), \quad \tilde{b}_{13} = -(b_4 - b_{01}k_4), \quad \tilde{b}_{23} = -(b_3 - b_{01}k_3), \quad (\text{A.1})$$

$$\tilde{B}_{12} = 2\frac{\tilde{x}_2}{y_s}(b_1 - b_{01}k_1), \quad \tilde{B}_{13} = \frac{\tilde{x}_2^2}{y_b y_s}(b_{01} - b_{02}), \quad \tilde{B}_{23} = \frac{y_s}{y_b}(b_{01} - b_{02}), \quad \tilde{R}_{12} = B_3 - K_3,$$

and

$$\begin{aligned} \tilde{a}_{11}^u &= a_u e^{i(\theta_u^a - \theta_u^y)}, \quad \tilde{a}_{22}^u = a_c e^{i(\theta_c^a - \theta_u^y)}, \quad \tilde{a}_{33}^u = a_t, \quad \tilde{a}_{23}^u = z_2^u \left(\frac{a_t}{y_t} - e^{i(\theta_2^{z_{ua}} - \theta_2^{z_u})} \frac{z_2^{u_a}}{z_2^u} \right), \\ \tilde{a}_{11}^d &= \frac{\tilde{x}_2^2}{y_s} \left(2\frac{\tilde{x}_2^a}{\tilde{x}_2} e^{i(\theta_2^{\tilde{x}_a} - \theta_2^{\tilde{x}})} - \frac{a_s}{y_s} e^{i(\theta_s^a - \theta_s^y)} \right), \quad \tilde{a}_{22}^d = a_s e^{i(\theta_s^a - \theta_s^y)}, \quad \tilde{a}_{33}^d = a_b e^{i(\theta_b^a - \theta_b^y)}, \\ \tilde{a}_{12}^d &= \tilde{x}_2 \left(\frac{\tilde{x}_2^a}{\tilde{x}_2} e^{i(\theta_2^{\tilde{x}_a} - \theta_2^{\tilde{x}})} - \frac{a_s}{y_s} e^{i(\theta_s^a - \theta_s^y)} \right), \quad \tilde{a}_{23}^d = y_s \left(\frac{a_s}{y_s} e^{i(\theta_s^a - \theta_s^y)} - \frac{a_b}{y_b} e^{i(\theta_b^a - \theta_b^y)} \right), \\ \tilde{a}_{31}^d &= z_3^d \left(\frac{a_b}{y_b} e^{i(\theta_b^a - \theta_b^y)} - \frac{z_3^{d_a}}{z_3^d} e^{i(\theta_3^{z_{da}} - \theta_3^{z_d})} \right), \\ \tilde{a}_{32}^d &= \frac{y_s^2}{y_b} \left(\frac{a_s}{y_s} e^{i(\theta_s^a - \theta_s^y)} - \frac{a_b}{y_b} e^{i(\theta_b^a - \theta_b^y)} \right) + z_2^d \left(\frac{a_b}{y_b} e^{i(\theta_b^a - \theta_b^y)} - \frac{z_2^{d_a}}{z_2^d} e^{i(\theta_2^{z_{da}} - \theta_2^{z_d})} \right), \\ \tilde{a}_{23}^e &= 9\frac{y_s^2}{y_b} \left(\frac{a_s}{y_s} e^{i(\theta_s^a - \theta_s^y)} - \frac{a_b}{y_b} e^{i(\theta_b^a - \theta_b^y)} \right) + z_2^d \left(\frac{a_b}{y_b} e^{i(\theta_b^a - \theta_b^y)} - \frac{z_2^{d_a}}{z_2^d} e^{i(\theta_2^{z_{da}} - \theta_2^{z_d})} \right). \end{aligned} \quad (\text{A.2})$$

Here, z_2^u parameterises the (23) and (32) entries of the up-type quark Yukawa matrix of order λ^7 before canonical normalisation; the associated phase is given by $\theta_2^{z_u} = 3\theta_2^d + 2\theta_3^d$. They become subdominant contributions to the (23) and (32) elements of Y_{GUT}^u in Eq. (2.1). The parameter of the corresponding soft trilinear contribution is denoted by $z_2^{u_a}$ with phase $\theta_2^{z_{ua}}$. In addition to z_2^u we also need z_4^d which parameterises a subdominant contribution to the (22) and (23) elements of Y_{GUT}^d in Eq. (2.2) of order λ^5 . For the phase we have $\theta_4^{z_d} = 6\theta_2^d + 4\theta_3^d$, and the corresponding parameters of the A -terms are $z_4^{d_a}$ and $\theta_4^{z_{da}}$. It is worth mentioning that all \tilde{a}_{ij}^f become real in the limit where the Yukawa and trilinear phase structures are aligned such that the relation $\theta_f^y = \theta_f^a$ holds.

In order to describe the renormalisation group running from the GUT scale down to

low energies, we introduce the parameters in Eqs. (3.8,3.9) as well as

$$R_u^a = \eta \left(\frac{46}{5} g_U^2 \frac{M_{1/2}}{A_0} + 3a_t y_t \right) + 3\eta_N y_D \alpha_D, \quad R_t^a = R_u^a + 3\eta a_t y_t, \quad (\text{A.3})$$

$$R_d^a = \eta \frac{44}{5} g_U^2 \frac{M_{1/2}}{A_0}, \quad R_b^a = R_d^a + \eta a_t y_t, \quad R_e^a = \eta \frac{24}{5} g_U^2 \frac{M_{1/2}}{A_0} + \eta_N y_D \alpha_D, \quad (\text{A.4})$$

$$R_\nu = z_1^D - y_D(K_3 + K_3^N), \quad R_\nu^a = z_1^{D_a} e^{i\theta_1^{z_{D_a}}} - \alpha_D(K_3 + K_3^N), \quad (\text{A.5})$$

and

$$R_\mu = 4\eta \left(0.9 g_U^2 - \frac{3}{4} y_t^2 \right) - 3\eta_N y_D^2, \quad (\text{A.6})$$

$$R_q = (2b_{02} + c_{H_u}) y_t^2 + \alpha_0^2 a_t^2, \quad (\text{A.7})$$

$$R_l = (1 + B_0^N + c_{H_u}) y_D^2 + \alpha_0^2 \alpha_D^2, \quad (\text{A.8})$$

$$R_l' = (1 + B_0^N + c_{H_u}) y_D z_1^D + \alpha_0^2 \alpha_D z_1^{D_a} e^{i\theta_1^{z_{D_a}}}. \quad (\text{A.9})$$

In these expressions, $g_U \approx \sqrt{0.52}$ denotes the universal gauge coupling constant at the GUT scale, $M_{1/2}$ is the universal gaugino mass parameter and A_0 is the scale of the soft trilinear terms. Using the SUSY breaking mass m_0 , we have also introduced $\alpha_0 = A_0/m_0$, see Eq. (3.13). η and η_N have been defined in Eq. (2.15), while c_{H_u} is given in Eq. (3.12).

With these definitions, the μ parameter at the low energy scale can be approximated by $\mu \approx \mu_{\text{GUT}} (1 + R_\mu)$, and the low energy sfermion masses, whose GUT scale definitions are given in Eq. (2.11), take the form

$$m_{\tilde{u}_{LL}} \approx m_{\tilde{c}_{LL}} \approx m_0 p_{L^{1G}}^u, \quad m_{\tilde{t}_{LL}} \approx m_0 p_{L^{3G}}^u, \\ m_{\tilde{u}_{RR}} \approx m_{\tilde{c}_{RR}} \approx m_0 p_{R^{1G}}^u, \quad m_{\tilde{t}_{RR}} \approx m_0 p_{R^{3G}}^u, \quad (\text{A.10})$$

$$m_{\tilde{d}_{LL}} \approx m_{\tilde{s}_{LL}} \approx m_0 p_{L^{1G}}^d, \quad m_{\tilde{b}_{LL}} \approx m_0 p_{L^{3G}}^d, \\ m_{\tilde{d}_{RR}} \approx m_{\tilde{s}_{RR}} \approx m_{\tilde{b}_{RR}} \approx m_0 p_R^d, \quad (\text{A.11})$$

$$m_{\tilde{e}_{LL}} \approx m_{\tilde{\mu}_{LL}} \approx m_{\tilde{\tau}_{LL}} \approx m_0 p_L^e, \\ m_{\tilde{e}_{RR}} \approx m_{\tilde{\mu}_{RR}} \approx m_0 p_{R^{1G}}^e, \quad m_{\tilde{\tau}_{RR}} \approx m_0 p_{R^{3G}}^e, \quad (\text{A.12})$$

with

$$p_{L1G}^u = \sqrt{b_{01} + 6.5x}, \quad p_{L3G}^u = \sqrt{b_{02} + 6.5x - 2\eta R_q + \frac{v_u^2}{m_0^2} y_t^2 (1 + R_t^y)^2},$$

$$p_{R1G}^u = \sqrt{b_{01} + 6.15x}, \quad p_{R3G}^u = \sqrt{b_{02} + 6.15x - 4\eta R_q + \frac{v_u^2}{m_0^2} y_t^2 (1 + R_t^y)^2}, \quad (\text{A.13})$$

$$p_{L1G}^d = \sqrt{b_{01} + 6.5x}, \quad p_{L3G}^d = \sqrt{b_{02} + 6.5x - 4\eta R_q}, \quad p_R^d = \sqrt{1 + 6.1x}, \quad (\text{A.14})$$

$$p_{R1G}^e = \sqrt{b_{01} + 0.15x}, \quad p_{R3G}^e = \sqrt{b_{02} + 0.15x}, \quad p_L^e = \sqrt{1 + 0.5x - 2\eta_N R_l}. \quad (\text{A.15})$$

Here, $x = (M_{1/2}/m_0)^2$ as defined in Eqs. (3.13). With these definitions at hand, we can write the mass insertion parameters at the low energy as follows.

Up-type quark sector:

$$(\delta_{LL}^u)_{12} = \frac{1}{(p_{L1G}^u)^2} e^{-i\theta_2^d} \tilde{b}_{12} \lambda^4, \quad (\text{A.16})$$

$$(\delta_{LL}^u)_{13} = \frac{1}{p_{L1G}^u p_{L3G}^u} e^{-i(4\theta_2^d + \theta_3^d)} (1 - \eta y_t^2) \tilde{b}_{13} \lambda^6, \quad (\text{A.17})$$

$$(\delta_{LL}^u)_{23} = \frac{1}{p_{L1G}^u p_{L3G}^u} e^{-i(7\theta_2^d + 2\theta_3^d)} (1 - \eta y_t^2) \tilde{b}_{23} \lambda^5, \quad (\text{A.18})$$

$$(\delta_{RR}^u)_{12} = \frac{1}{(p_{R1G}^u)^2} e^{-i\theta_2^d} \tilde{b}_{12} \lambda^4, \quad (\text{A.19})$$

$$(\delta_{RR}^u)_{13} = \frac{1}{p_{R1G}^u p_{R3G}^u} (1 - 2\eta y_t^2) \tilde{b}_{13} \lambda^6, \quad (\text{A.20})$$

$$(\delta_{RR}^u)_{23} = \frac{1}{p_{R1G}^u p_{R3G}^u} e^{i(5\theta_2^d + \theta_3^d)} (1 - 2\eta y_t^2) \tilde{b}_{23} \lambda^5, \quad (\text{A.21})$$

$$(\delta_{LR}^u)_{11} = \frac{\alpha_0 v_u}{m_0 p_{L1G}^u p_{R1G}^u} y_u (1 + R_u^y) \left(\frac{\tilde{a}_{11}^u}{y_u} - \frac{\mu(1 + R_\mu)}{A_0 t_\beta} - 2 \frac{R_u^a}{1 + R_u^y} \right) \lambda^8, \quad (\text{A.22})$$

$$(\delta_{LR}^u)_{22} = \frac{\alpha_0 v_u}{m_0 p_{L1G}^u p_{R1G}^u} y_c (1 + R_u^y) \left(\frac{\tilde{a}_{22}^u}{y_c} - \frac{\mu(1 + R_\mu)}{A_0 t_\beta} - 2 \frac{R_u^a}{1 + R_u^y} \right) \lambda^4, \quad (\text{A.23})$$

$$(\delta_{LR}^u)_{33} = \frac{\alpha_0 v_u}{m_0 p_{L3G}^u p_{R3G}^u} y_t (1 + R_t^y) \left(\frac{\tilde{a}_{33}^u}{y_t} - \frac{\mu(1 + R_\mu)}{A_0 t_\beta} - 2 \frac{R_t^a}{1 + R_t^y} \right), \quad (\text{A.24})$$

$$(\delta_{LR}^u)_{12} = (\delta_{LR}^u)_{21} = (\delta_{LR}^u)_{31} = 0, \quad (\text{A.25})$$

$$(\delta_{LR}^u)_{13} = -\frac{\alpha_0 v_u}{m_0 p_{L1G}^u p_{R3G}^u} \tilde{x}_2 y_b y_t \left(\frac{\tilde{x}_2^a}{\tilde{x}_2} e^{i(\theta_2^a - \theta_2^y)} + \frac{R_t^a}{1 + R_t^y} \right) 2\eta \lambda^7, \quad (\text{A.26})$$

$$\begin{aligned} (\delta_{LR}^u)_{23} = & \frac{\alpha_0 v_u}{m_0 p_{L1G}^u p_{R3G}^u} \left\{ -y_s y_b y_t \left(\frac{a_s}{y_s} e^{i(\theta_s^a - \theta_s^y)} + \frac{R_t^a}{1 + R_t^y} \right) 2\eta \lambda^6 + \right. \\ & + \lambda^7 \left[e^{i\theta_2^d} \tilde{a}_{23}^u (1 + R_t^y - \eta y_t^2) + 2\eta y_b y_t \left(e^{i\theta_2^d} \tilde{a}_{12}^d + \left(\frac{a_s}{y_s} e^{i(\theta_s^a - \theta_s^y)} + \frac{R_t^a}{1 + R_t^y} \right) \times \right. \right. \\ & \left. \left. \times (\tilde{x}_2 \cos(\theta_2^d) - z_4^d \cos(4\theta_2^d + \theta_3^d)) + z_4^d e^{i(4\theta_2^d + \theta_3^d)} \left(e^{i(\theta_s^a - \theta_s^y)} - \frac{z_4^{d_a}}{z_4^d} e^{i(\theta_4^{z_{d_a}} - \theta_4^{z_d})} \right) \right) \right] \right\}, \quad (\text{A.27}) \end{aligned}$$

$$(\delta_{LR}^u)_{32} = \frac{\alpha_0 v_u}{m_0 p_{L3G}^u p_{R1G}^u} (1 + R_t^y - 2\eta y_t^2) e^{i(3\theta_2^d + \theta_3^d)} \tilde{a}_{23}^u \lambda^7. \quad (\text{A.28})$$

At the GUT scale, $(\delta_{LR}^u)_{13}$ is zero up to the order λ^8 where we truncate our expansion. The non-zero value in Eq. (A.26) is purely generated via the RG evolution. Similarly, a term proportional to $\eta \lambda^6$ is generated in $(\delta_{LR}^u)_{23}$, which was of order λ^7 at the GUT scale. The λ -suppression of all other low energy mass insertion parameters $(\delta_{LL,RR,LR}^f)_{ij}$ remains unaffected by the running, such that the corresponding RG effects can simply be absorbed into new order one coefficients.

Down-type quark sector:

$$(\delta_{LL}^d)_{12} = \frac{1}{(p_{L1G}^d)^2} \tilde{B}_{12} \lambda^3, \quad (\text{A.29})$$

$$(\delta_{LL}^d)_{13} = \frac{1}{p_{L1G}^d p_{L13}^d} e^{i\theta_2^d} \frac{\tilde{x}_2^2}{y_b y_s} (b_{01} - b_{02} + 2\eta R_q) \left(1 + \frac{\eta y_t^2}{1 + R_b^y}\right) \lambda^4, \quad (\text{A.30})$$

$$(\delta_{LL}^d)_{23} = \frac{1}{p_{L1G}^d p_{L13}^d} \frac{y_s}{y_b} (b_{01} - b_{02} + 2\eta R_q) \left(1 + \frac{\eta y_t^2}{1 + R_b^y}\right) \lambda^2, \quad (\text{A.31})$$

$$(\delta_{RR}^d)_{12} = -(\delta_{RR}^d)_{13} = \frac{1}{(p_R^d)^2} e^{i\theta_2^d} \tilde{R}_{12} \lambda^4, \quad (\text{A.32})$$

$$(\delta_{RR}^d)_{23} = -\frac{1}{(p_R^d)^2} \tilde{R}_{12} \lambda^4, \quad (\text{A.33})$$

$$(\delta_{LR}^d)_{11} = \frac{\alpha_0 v_d}{m_0 p_{L1G}^d p_R^d} \frac{\tilde{x}_2^2}{y_s} (1 + R_d^y) \left(\frac{\tilde{a}_{11}^d}{\tilde{x}_2^2/y_s} - \frac{\mu t_\beta (1 + R_\mu)}{A_0} - 2 \frac{R_d^a}{1 + R_d^y} \right) \lambda^6, \quad (\text{A.34})$$

$$(\delta_{LR}^d)_{22} = \frac{\alpha_0 v_d}{m_0 p_{L1G}^d p_R^d} y_s (1 + R_d^y) \left(\frac{\tilde{a}_{22}^d}{y_s} - \frac{\mu t_\beta (1 + R_\mu)}{A_0} - 2 \frac{R_d^a}{1 + R_d^y} \right) \lambda^4, \quad (\text{A.35})$$

$$(\delta_{LR}^d)_{33} = \frac{\alpha_0 v_d}{m_0 p_{L3G}^d p_R^d} y_b (1 + R_b^y) \left(\frac{\tilde{a}_{33}^d}{y_b} - \frac{\mu t_\beta (1 + R_\mu)}{A_0} - 2 \frac{R_b^a}{1 + R_b^y} \right) \lambda^2, \quad (\text{A.36})$$

$$(\delta_{LR}^d)_{12} = -(\delta_{LR}^d)_{21} = (\delta_{LR}^d)_{13} = \frac{\alpha_0 v_d}{m_0 p_{L1G}^d p_R^d} (1 + R_d^y) \tilde{a}_{12}^d \lambda^5, \quad (\text{A.37})$$

$$(\delta_{LR}^d)_{23} = \frac{\alpha_0 v_d}{m_0 p_{L1G}^d p_R^d} y_s (1 + R_d^y) \left(\frac{\tilde{a}_{23}^d}{y_s} + 2 \frac{\eta y_t^2}{1 + R_b^y} \left(\frac{a_t}{y_t} + \frac{R_d^a}{1 + R_d^y} \right) \right) \lambda^4, \quad (\text{A.38})$$

$$(\delta_{LR}^d)_{31} = \frac{\alpha_0 v_d}{m_0 p_{L3G}^d p_R^d} e^{-i\theta_2^d} (1 + R_b^y) \tilde{a}_{31}^d \lambda^6, \quad (\text{A.39})$$

$$\begin{aligned} (\delta_{LR}^d)_{32} = & \frac{\alpha_0 v_d}{m_0 p_{L3G}^d p_R^d} (1 + R_b^y) y_b \left(\frac{\tilde{a}_{32}^d}{y_b} + 2\eta y_t^2 \frac{y_s^2}{y_b^2} \left[\frac{2(1 + R_b^y) + \eta y_t^2}{2(1 + R_b^y)^2} \frac{\tilde{a}_{23}^d}{y_s} \right. \right. \\ & \left. \left. + \left(\frac{a_t}{y_t} + \frac{R_d^a}{1 + R_d^y} \right) \frac{(1 + R_d^y)^2}{(1 + R_b^y)^3} \right] \right) \lambda^6. \end{aligned} \quad (\text{A.40})$$

Charged lepton sector:

$$(\delta_{LL}^e)_{12} = -(\delta_{LL}^e)_{23} = \frac{1}{(p_L^e)^2} \left(\tilde{R}_{12} - 2\eta_N \tilde{E}_{12} \right) \lambda^4, \quad (\text{A.41})$$

$$(\delta_{LL}^e)_{13} = -\frac{1}{(p_L^e)^2} \left(\tilde{R}_{12} - 2\eta_N \tilde{E}_{12}^* \right) \lambda^4, \quad (\text{A.42})$$

$$(\delta_{RR}^e)_{12} = -\frac{1}{(p_{R^{1G}}^e)^2} e^{i\theta_2^d} \frac{\tilde{B}_{12}}{3} \lambda^3, \quad (\text{A.43})$$

$$(\delta_{RR}^e)_{13} = \frac{1}{p_{R^{1G}}^e p_{R^{3G}}^e} \frac{\tilde{B}_{13}}{3} \lambda^4, \quad (\text{A.44})$$

$$(\delta_{RR}^e)_{23} = \frac{1}{p_{R^{1G}}^e p_{R^{3G}}^e} 3\tilde{B}_{23} \lambda^2, \quad (\text{A.45})$$

$$(\delta_{LR}^e)_{11} = \frac{1}{p_L^e p_{R^{1G}}^e} \frac{v_d \alpha_0}{m_0} \frac{\tilde{x}_2^2}{3 y_s} (1 + R_e^y) \left(\frac{y_s \tilde{a}_{11}^d}{\tilde{x}_2^2} - \frac{\mu t_\beta}{A_0} (1 + R_\mu) - 2 \frac{R_e^a}{1 + R_e^y} \right) \lambda^6, \quad (\text{A.46})$$

$$(\delta_{LR}^e)_{22} = \frac{1}{p_L^e p_{R^{1G}}^e} \frac{v_d \alpha_0}{m_0} 3 y_s (1 + R_e^y) \left(\frac{\tilde{a}_{22}^d}{y_s} - \frac{\mu t_\beta}{A_0} (1 + R_\mu) - 2 \frac{R_e^a}{1 + R_e^y} \right) \lambda^4, \quad (\text{A.47})$$

$$(\delta_{LR}^e)_{33} = \frac{1}{p_L^e p_{R^{3G}}^e} \frac{v_d \alpha_0}{m_0} y_b (1 + R_e^y) \left(\frac{\tilde{a}_{33}^d}{y_b} - \frac{\mu t_\beta}{A_0} (1 + R_\mu) - 2 \frac{R_e^a}{1 + R_e^y} \right) \lambda^2, \quad (\text{A.48})$$

$$(\delta_{LR}^e)_{12} = \frac{1}{p_L^e p_{R^{1G}}^e} \frac{v_d \alpha_0}{m_0} (1 + R_e^y) e^{i\theta_2^d} \tilde{a}_{12}^d \lambda^5, \quad (\text{A.49})$$

$$(\delta_{LR}^e)_{13} = \frac{1}{p_L^e p_{R^{3G}}^e} \frac{v_d \alpha_0}{m_0} \left((1 + R_e^y) \tilde{a}_{31}^d + 2\eta_N y_D R_\nu y_b \left(\frac{\alpha_D}{y_D} + \frac{R_e^a}{1 + R_e^y} \right) \right) \lambda^6, \quad (\text{A.50})$$

$$(\delta_{LR}^e)_{21} = (\delta_{LR}^e)_{31} = -\frac{1}{p_L^e p_{R^{1G}}^e} \frac{v_d \alpha_0}{m_0} (1 + R_e^y) e^{-i\theta_2^d} \tilde{a}_{12}^d \lambda^5, \quad (\text{A.51})$$

$$(\delta_{LR}^e)_{23} = \frac{1}{p_L^e p_{R^{3G}}^e} \frac{v_d \alpha_0}{m_0} \left((1 + R_e^y) \tilde{a}_{23}^e + 2\eta_N y_D R_\nu y_b \left(\frac{R_\nu^a}{R_\nu} + \frac{R_e^a}{1 + R_e^y} \right) \right) \lambda^6, \quad (\text{A.52})$$

$$(\delta_{LR}^e)_{32} = \frac{1}{p_L^e p_{R^{1G}}^e} \frac{v_d \alpha_0}{m_0} (1 + R_e^y) 3 \tilde{a}_{23}^d \lambda^4. \quad (\text{A.53})$$

Here we have additionally introduced \tilde{E}_{12} which parameterises the off-diagonal entries of $(\delta^e)_{LL}$ in Eqs. (A.41,A.42) induced by the RG running. It is defined as

$$\tilde{E}_{12} = y_D^2 \left(\tilde{R}_{12} + B_3^N - K_3^N B_0^N \right) + R'_l - (K_3 + K_3^N) R_l. \quad (\text{A.54})$$

B Loop functions

The dimensionless functions C_B , C'_L , C'_R , C'_2 , $C'_{B,R}$, $C'_{B,L}$ and C''_B which appear in the expressions for the EDM of the electron in Section 4.1 and the branching ratio of $\mu \rightarrow e\gamma$ in Section 4.2 are defined as [41]

$$C_i = \frac{m_0^4}{\mu^2} I_i, \quad (\text{B.1})$$

where

$$I_B(M_1^2, m_L^2, m_R^2) = \frac{1}{m_R^2 - m_L^2} [y_L g_1(x_L) - y_R g_1(x_R)], \quad (\text{B.2})$$

$$I'_L(m_L^2, M_1^2, \mu^2) = \frac{1}{m_L^2} \frac{y_L}{y_L - x_L} [h_1(x_L) - h_1(y_L)], \quad (\text{B.3})$$

$$I'_R(m_R^2, M_1^2, \mu^2) = \frac{1}{m_R^2} \frac{y_R}{y_R - x_R} [h_1(x_R) - h_1(y_R)], \quad (\text{B.4})$$

$$I'_2(m_L^2, M_2^2, \mu^2) = \frac{M_2 \cot^2 \theta_W}{M_1 m_L^2} \frac{y_L}{y_L - x'_L} [h_2(x'_L) - h_2(y_L)], \quad (\text{B.5})$$

$$I'_{B,R}(M_1^2, m_L^2, m_R^2) = -\frac{1}{m_R^2 - m_L^2} (y_R h_1(x_R) - m_R^2 I_B), \quad (\text{B.6})$$

$$I'_{B,L}(M_1^2, m_L^2, m_R^2) = \frac{1}{m_R^2 - m_L^2} (y_L h_1(x_L) - m_L^2 I_B), \quad (\text{B.7})$$

$$I''_B(M_1^2, m_L^2, m_R^2) = \frac{m_L^2 m_R^2}{m_R^2 - m_L^2} \frac{1}{\mu^2} (y_R I'_{B,R} - y_L I'_{B,L}), \quad (\text{B.8})$$

with

$$x_L = \frac{M_1^2}{m_L^2}, \quad x_R = \frac{M_1^2}{m_R^2}, \quad x'_L = \frac{M_2^2}{m_L^2}, \quad y_L = \frac{\mu^2}{m_L^2}, \quad y_R = \frac{\mu^2}{m_R^2}, \quad (\text{B.9})$$

and

$$\begin{aligned}
g_1(y) &= \frac{1 - y^2 + 2y \ln(y)}{(1 - y)^3}, \\
h_1(y) &= \frac{1 + 4y - 5y^2 + (2y^2 + 4y) \ln(y)}{(1 - y)^4}, \\
h_2(y) &= \frac{7y^2 + 4y - 11 - 2(y^2 + 6y + 2) \ln(y)}{2(y - 1)^4}.
\end{aligned} \tag{B.10}$$

Note that we assume real and positive values for M_i and μ^2 .

The loop functions appearing in the meson mixing amplitudes of Section 4.3 as well as the branching ratios of $B_{s,d} \rightarrow \mu^+ \mu^-$ in Section 4.5 read [15]

$$f_6(y) = \frac{6(1 + 3y) \ln(y) + y^3 - 9y^2 - 9y + 17}{6(y - 1)^5}, \tag{B.11}$$

$$\tilde{f}_6(y) = \frac{6y(1 + y) \ln(y) - y^3 - 9y^2 + 9y + 1}{3(y - 1)^5}, \tag{B.12}$$

$$f_1(y) = \frac{1}{1 - y} + \frac{y}{(1 - y)^2} \ln(y), \tag{B.13}$$

$$f_3(y) = -\frac{1 + y}{2(1 - y)^2} - \frac{y}{(1 - y)^3} \ln(y), \tag{B.14}$$

$$f_4(x, y) = -\frac{x \ln(x)}{(1 - x)^2(y - x)} - \frac{y \ln(y)}{(1 - y)^2(x - y)} + \frac{1}{(1 - x)(1 - y)}, \tag{B.15}$$

$$f_5(y) = \frac{2 + 5y - y^2}{6(1 - y)^3} + \frac{y}{(1 - y)^4} \ln(y). \tag{B.16}$$

The relevant functions for the branching ratio of $b \rightarrow s\gamma$ in Section 4.4 are given by [11]

$$M_1(y) = \frac{1 + 4y - 5y^2 + 4y \ln(y) + 2y^2 \ln(y)}{2(1 - y)^4}, \tag{B.17}$$

$$M_3(y) = \frac{-1 + 9y + 9y^2 - 17y^3 + 18y^2 \ln(y) + 6y^3 \ln(y)}{12(y - 1)^5}. \tag{B.18}$$

Finally, the loop functions entering the hadronic EDM expressions in Section 4.6 are [67]

$$N_1(y) = \frac{3 + 44y - 36y^2 - 12y^3 + y^4 + 12y(2 + 3y) \ln(y)}{6(y - 1)^6}, \quad (\text{B.19})$$

$$N_2(y) = -\frac{10 + 9y - 18y^2 - y^3 + 3(1 + 6y + 3y^2) \ln(y)}{3(y - 1)^6}. \quad (\text{B.20})$$

References

- [1] M. Dimou, S. F. King and C. Luhn, JHEP **1602** (2016) 118 [arXiv:1511.07886].
- [2] S. F. King, Rept. Prog. Phys. **67** (2004) 107 [hep-ph/0310204]; G. Altarelli and F. Feruglio, Rev. Mod. Phys. **82** (2010) 2701 [arXiv:1002.0211]; S. F. King and C. Luhn, Rept. Prog. Phys. **76** (2013) 056201 [arXiv:1301.1340]; S. F. King, A. Merle, S. Morisi, Y. Shimizu and M. Tanimoto, New J. Phys. **16** (2014) 045018 [arXiv:1402.4271]; S. F. King, J. Phys. G: Nucl. Part. Phys. **42** (2015) 123001 [arXiv:1510.02091].
- [3] P. Ballett, S. F. King, C. Luhn, S. Pascoli and M. A. Schmidt, Phys. Rev. D **89** (2014) 1, 016016 [arXiv:1308.4314]; D. Meloni, Phys. Lett. B **728** (2014) 118 [arXiv:1308.4578]; P. Ballett, S. F. King, C. Luhn, S. Pascoli and M. A. Schmidt, J. Phys. Conf. Ser. **598** (2015) 1, 012014 [arXiv:1406.0308]; P. Ballett, S. F. King, C. Luhn, S. Pascoli and M. A. Schmidt, JHEP **1412** (2014) 122 [arXiv:1410.7573].
- [4] R. S. Chivukula and H. Georgi, Phys. Lett. B **188** (1987) 99; L. J. Hall and L. Randall, Phys. Rev. Lett. **65** (1990) 2939; A. J. Buras, P. Gambino, M. Gorbahn, S. Jäger and L. Silvestrini, Phys. Lett. B **500** (2001) 161 [hep-ph/0007085].
- [5] H. Georgi and S. L. Glashow, Phys. Rev. Lett. **32** (1974) 438.
- [6] J. C. Pati and A. Salam, Phys. Rev. D **8** (1973) 1240; J. C. Pati and A. Salam, Phys. Rev. D **10** (1974) 275 [Phys. Rev. D **11** (1975) 703].
- [7] T. Feldmann, JHEP **1104** (2011) 043 [arXiv:1010.2116]; T. Feldmann, F. Hartmann, W. Kilian and C. Luhn, JHEP **1510** (2015) 160 [arXiv:1506.00782]; R. Barbieri and F. Senia, arXiv:1506.09201 [hep-ph].
- [8] G. D’Ambrosio, G. F. Giudice, G. Isidori and A. Strumia, Nucl. Phys. B **645** (2002) 155 [hep-ph/0207036]; V. Cirigliano, B. Grinstein, G. Isidori and M. B. Wise, Nucl. Phys. B **728** (2005) 121 [hep-ph/0507001].

- [9] C. Bobeth, T. Ewerth, F. Kruger and J. Urban, Phys. Rev. D **66** (2002) 074021 [hep-ph/0204225].
- [10] D. J. H. Chung, L. L. Everett, G. L. Kane, S. F. King, J. D. Lykken and L. T. Wang, Phys. Rept. **407** (2005) 1 [hep-ph/0312378].
- [11] F. Gabbiani, E. Gabrielli, A. Masiero and L. Silvestrini, Nucl. Phys. B **477** (1996) 321 [hep-ph/9604387]; M. Misiak, S. Pokorski and J. Rosiek, Adv. Ser. Direct. High Energy Phys. **15** (1998) 795 [hep-ph/9703442].
- [12] G. G. Ross and O. Vives, Phys. Rev. D **67** (2003) 095013 [hep-ph/0211279].
- [13] G. G. Ross, L. Velasco-Sevilla and O. Vives, Nucl. Phys. B **692** (2004) 50 [hep-ph/0401064].
- [14] S. Antusch, S. F. King and M. Malinsky, JHEP **0806** (2008) 068 [arXiv:0708.1282]; S. Antusch, S. F. King, M. Malinsky and G. G. Ross, Phys. Lett. B **670** (2009) 383 [arXiv:0807.5047].
- [15] W. Altmannshofer, A. J. Buras, S. Gori, P. Paradisi and D. M. Straub, Nucl. Phys. B **830** (2010) 17 [arXiv:0909.1333].
- [16] A. J. Buras and J. Girrbach, Acta Phys. Polon. B **43** (2012) 1427 [arXiv:1204.5064]; D. M. Straub, arXiv:1205.6094.
- [17] S. F. King and I. N. R. Peddie, Phys. Lett. B **586** (2004) 83 [hep-ph/0312237]; S. F. King, I. N. R. Peddie, G. G. Ross, L. Velasco-Sevilla and O. Vives, JHEP **0507** (2005) 049 [hep-ph/0407012].
- [18] P. Minkowski, Phys. Lett. B **67** (1977) 421; M. Gell-Mann, P. Ramond and R. Slansky, Conf. Proc. C **790927** (1979) 315 [arXiv:1306.4669]; T. Yanagida, Conf. Proc. C **7902131** (1979) 95; R. N. Mohapatra and G. Senjanovic, Phys. Rev. Lett. **44** (1980) 912.
- [19] Y. Yamada, Z. Phys. C **60** (1993) 83; S. Antusch and M. Spinrath, Phys. Rev. D **78** (2008) 075020 [arXiv:0804.0717].
- [20] P. Paradisi, M. Ratz, R. Schieren and C. Simonetto, Phys. Lett. B **668** (2008) 202 [arXiv:0805.3989]; G. Colangelo, E. Nikolidakis and C. Smith, Eur. Phys. J. C **59** (2009) 75 [arXiv:0807.0801].
- [21] L. Wolfenstein, Phys. Rev. Lett. **51** (1983) 1945.

- [22] C. Hagedorn, S. F. King and C. Luhn, JHEP **1006** (2010) 048 [arXiv:1003.4249];
C. Hagedorn, S. F. King and C. Luhn, Phys. Lett. B **717** (2012) 207 [arXiv:1205.3114].
- [23] R. Gatto, G. Sartori and M. Tonin, Phys. Lett. B **28** (1968) 128.
- [24] C. Jarlskog, Phys. Rev. Lett. **55** (1985) 1039.
- [25] S. Antusch and V. Maurer, JHEP **1311** (2013) 115 [arXiv:1306.6879].
- [26] S. Antusch and M. Spinrath, Phys. Rev. D **78** (2008) 075020 [arXiv:0804.0717].
- [27] H. Georgi and C. Jarlskog, Phys. Lett. B **86** (1979) 297.
- [28] J. A. Casas and S. Dimopoulos, Phys. Lett. B **387** (1996) 107 [hep-ph/9606237].
- [29] R. Barbieri and G. F. Giudice, Nucl. Phys. B **306** (1988) 63; G. L. Kane and S. F. King, Phys. Lett. B **451** (1999) 113 [hep-ph/9810374].
- [30] H. Baer, V. Barger, P. Huang, D. Mickelson, A. Mustafayev and X. Tata, Phys. Rev. D **87** (2013) 11, 115028 [arXiv:1212.2655].
- [31] S. Heinemeyer, Int. J. Mod. Phys. A **21** (2006) 2659 [hep-ph/0407244].
- [32] N. Carrasco *et al.*, Phys. Rev. D **90** (2014) 1, 014502 [arXiv:1403.7302].
- [33] E. Gabrielli and S. Khalil, Phys. Rev. D **67** (2003) 015008 [hep-ph/0207288].
- [34] A. Behring, C. Gross, G. Hiller and S. Schacht, JHEP **1208** (2012) 152 [arXiv:1205.1500].
- [35] A. Crivellin and U. Nierste, Phys. Rev. D **79** (2009) 035018 [arXiv:0810.1613].
- [36] A. Masiero, S. K. Vempati and O. Vives, arXiv:0711.2903.
- [37] M. Arana-Catania, S. Heinemeyer and M. J. Herrero, Phys. Rev. D **90** (2014) 7, 075003 [arXiv:1405.6960].
- [38] M. Arana-Catania, S. Heinemeyer and M. J. Herrero, Phys. Rev. D **88** (2013) 1, 015026 [arXiv:1304.2783].
- [39] S. P. Martin, Adv. Ser. Direct. High Energy Phys. **21** (2010) 1 [Adv. Ser. Direct. High Energy Phys. **18** (1998) 1] [hep-ph/9709356].
- [40] J. Baron *et al.* [ACME Collaboration], Science **343** (2014) 269 [arXiv:1310.753].

- [41] I. Masina and C. A. Savoy, Nucl. Phys. B **661** (2003) 365 [hep-ph/0211283].
- [42] J. Hisano, D. Kobayashi, W. Kuramoto and T. Kuwahara, JHEP **1511** (2015) 085 [arXiv:1507.05836].
- [43] J. Adam *et al.* [MEG Collaboration], Phys. Rev. Lett. **110** (2013) 201801 [arXiv:1303.0754].
- [44] A. M. Baldini *et al.*, arXiv:1301.7225.
- [45] Z. Ligeti, M. Papucci and G. Perez, Phys. Rev. Lett. **97** (2006) 101801 [hep-ph/0604112].
- [46] A. J. Buras and J. Girrbach, Rept. Prog. Phys. **77** (2014) 086201 [arXiv:1306.3775].
- [47] T. Inami and C. S. Lim, Prog. Theor. Phys. **65** (1981) 297 [Prog. Theor. Phys. **65** (1981) 1772]; G. Buchalla, A. J. Buras and M. E. Lautenbacher, Rev. Mod. Phys. **68** (1996) 1125 [hep-ph/9512380].
- [48] E. Golowich, J. Hewett, S. Pakvasa, A. A. Petrov and G. K. Yeghiyan, Phys. Rev. D **83** (2011) 114017 [arXiv:1102.0009].
- [49] J. Laiho, E. Lunghi and R. S. Van de Water, Phys. Rev. D **81** (2010) 034503 [arXiv:0910.2928].
- [50] S. Aoki *et al.*, Eur. Phys. J. C **74** (2014) 2890 [arXiv:1310.8555].
- [51] Y. Amhis *et al.* [Heavy Flavor Averaging Group (HFAG) Collaboration], arXiv:1412.7515.
- [52] M. Artuso, G. Borissov and A. Lenz, arXiv:1511.09466.
- [53] T. Aushev *et al.*, arXiv:1002.5012.
- [54] R. Aaij *et al.* [LHCb Collaboration], Phys. Rev. Lett. **115** (2015) 3, 031601 [arXiv:1503.07089].
- [55] J. Charles *et al.*, Phys. Rev. D **91** (2015) 7, 073007 [arXiv:1501.05013].
- [56] J. Yu, PoS LATTICE **2013** (2014) 398 [arXiv:1312.0306].
- [57] K. A. Olive *et al.* [Particle Data Group Collaboration], Chin. Phys. C **38** (2014) 090001.

- [58] A. J. Buras and D. Guadagnoli, Phys. Rev. D **78** (2008) 033005 [arXiv:0805.3887].
- [59] J. J. A. Bailey *et al.* [SWME Collaboration], Phys. Rev. D **92** (2015) 3, 034510 [arXiv:1503.05388].
- [60] A. Bevan *et al.*, Nucl. Phys. Proc. Suppl. **241-242** (2013) 89.
- [61] M. Misiak *et al.*, Phys. Rev. Lett. **98** (2007) 022002 [hep-ph/0609232]; M. Misiak *et al.*, Phys. Rev. Lett. **114** (2015) 22, 221801 [arXiv:1503.01789]; M. Czakon, P. Fiedler, T. Huber, M. Misiak, T. Schutzmeier and M. Steinhauser, JHEP **1504** (2015) 168 [arXiv:1503.01791].
- [62] C. Bobeth, M. Gorbahn, T. Hermann, M. Misiak, E. Stamou and M. Steinhauser, Phys. Rev. Lett. **112** (2014) 101801 [arXiv:1311.0903].
- [63] V. Khachatryan *et al.* [CMS and LHCb Collaborations], Nature **522** (2015) 68 [arXiv:1411.4413].
- [64] A. Buras, PoS FWNP (2015) 003 [arXiv:1505.00618].
- [65] K. De Bruyn, R. Fleischer, R. Kneijens, P. Koppenburg, M. Merk and N. Tuning, Phys. Rev. D **86** (2012) 014027 [arXiv:1204.1735].
- [66] A. J. Buras, J. Girrbach, D. Guadagnoli and G. Isidori, Eur. Phys. J. C **72** (2012) 2172 [arXiv:1208.0934].
- [67] J. Hisano and Y. Shimizu, Phys. Rev. D **70** (2004) 093001 [hep-ph/0406091].
- [68] J. Hisano, M. Nagai and P. Paradisi, Phys. Rev. D **80** (2009) 095014 [arXiv:0812.4283].
- [69] G. Degrossi, E. Franco, S. Marchetti and L. Silvestrini, JHEP **0511** (2005) 044 [hep-ph/0510137].
- [70] W. Dekens and J. de Vries, JHEP **1305** (2013) 149 [arXiv:1303.3156]; V. Khachatryan *et al.* [CMS Collaboration], Eur. Phys. J. C **75** (2015) 5, 186 [arXiv:1412.1633]; G. Dissertori, arXiv:1506.05407.
- [71] C. A. Baker *et al.*, Phys. Rev. Lett. **97** (2006) 131801 [hep-ex/0602020].
- [72] W. C. Griffith, M. D. Swallows, T. H. Loftus, M. V. Romalis, B. R. Heckel and E. N. Fortson, Phys. Rev. Lett. **102** (2009) 101601.

- [73] Y. Singh and B. K. Sahoo, Phys. Rev. A **91** (2015) 3, 030501 [arXiv:1408.4337].
- [74] J. Engel, M. J. Ramsey-Musolf and U. van Kolck, Prog. Part. Nucl. Phys. **71** (2013) 21 [arXiv:1303.2371].
- [75] M. Pospelov, Phys. Lett. B **530** (2002) 123 [hep-ph/0109044].